OFFICE OF CIVILIAN RADIOACTIVE WASTE MANAGEMENT
ANALYSIS/MODEL COVER SHEET
Complete Only Applicable Items

1. QA: __QA__

Page: 1 of: 82

2. ☒ Analysis Check all that apply		
Type of Analysis	☒ Engineering	
	☐ Performance Assessment	
	☐ Scientific	
Intended Use of Analysis	☐ Input to Calculation	
	☐ Input to another Analysis or Model	
	☒ Input to Technical Document	
	☐ Input to other Technical Products	

Describe use:

This analysis/model report will support the development of the Engineered Barrier System Degradation, Flow and Transport Process Model Report

3. ☒ Model Check all that apply		
Type of Model	☒ Conceptual Model	☐ Abstraction Model
	☒ Mathematical Model	☐ System Model
	☐ Process Model	
Intended Use of Model	☐ Input to Calculation	
	☐ Input to another Model or Analysis	
	☒ Input to Technical Document	
	☐ Input to other Technical Products	

Describe use:

This analysis/model report will support the development of the Engineered Barrier System Degradation, Flow and Transport Process Model Report

4. Title:

Water Distribution and Removal Model

5. Document Identifier (including Rev. No. and Change No., if applicable):

ANL-EBS-MD-000032 REV 00 ICN 01

6. Total Attachments:

Nine

7. Attachment Numbers - No. of Pages in Each:

I-4, II-6, III-3, IV-3, V-2, VI-3, VII-4, VIII-4 (plus 1 CD), IX-17

	Printed Name	Signature	Date
8. Originator	Dwayne C. Kicker		7/6/00
9. Checker	Marek J. Mrugala		7/6/00
10. Lead/Supervisor	Ernest L. Hardin		7/6/00
11. Responsible Manager	Ernest L. Hardin		7/6/00

12. Remarks:

John Case was primarily responsible for the development of this analysis/model (Section 6).

Ming Lin and Sean Vincent contributed to the documentation of computer software and analysis/model inputs (Sections 3 and 4).

Mason Pillow developed test cases used for routine qualification (Attachments I, III, IV, and V).

The following support was provided by Lawrence Livermore National Laboratory:

Nina Rosenburg and Charles Carrigan prepared input files and executed NUFT V3.0s.

Kenrick Lee developed and executed the routine Chim_surf_TP V1.1.

James Gansemer developed and executed ColumnInfiltration V1.1, Cover V1.1, and CONVERTCOORDS V1.1. James Gansemer also executed YMESH V1.53.

Mary Gokoffski developed and executed the routine rme6 V1.1.

Veraun Chipman was the technical checker for Revision 0 of this document.

The following TBVs apply to this analysis/model:

TBV-0389, TBV-3471, TBV-3685, TBV-3686, TBV-3695, TBV-3796, TBV-3828.

AP-3.10Q.3

Rev. 05/12/2000

OFFICE OF CIVILIAN RADIOACTIVE WASTE MANAGEMENT
ANALYSIS/MODEL COVER SHEET
Complete Only Applicable Items

1. QA: __QA__

Page: 1 of: 82

2. ☒ Analysis	Check all that apply		3. ☒ Model	Check all that apply	

Type of Analysis	☒ Engineering		Type of Model	☒ Conceptual Model	☐ Abstraction Model
	☐ Performance Assessment			☒ Mathematical Model	☐ System Model
	☐ Scientific			☐ Process Model	
Intended Use of Analysis	☐ Input to Calculation		Intended Use of Model	☐ Input to Calculation	
	☐ Input to another Analysis or Model			☐ Input to another Model or Analysis	
	☒ Input to Technical Document			☒ Input to Technical Document	
	☐ Input to other Technical Products			☐ Input to other Technical Products	

Describe use:

This analysis/model report will support the development of the Engineered Barrier System Degradation, Flow and Transport Process Model Report

Describe use:

This analysis/model report will support the development of the Engineered Barrier System Degradation, Flow and Transport Process Model Report

4. Title:

Water Distribution and Removal Model

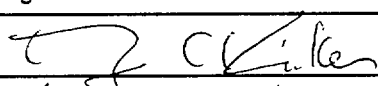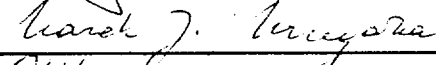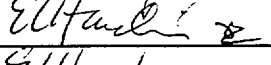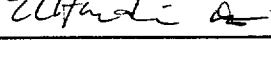5. Document Identifier (including Rev. No. and Change No., if applicable):

ANL-EBS-MD-000032 REV 00 ICN 01

6. Total Attachments:

Nine

7. Attachment Numbers - No. of Pages in Each:

I-4, II-6, III-3, IV-3, V-2, VI-3, VII-4, VIII-4 (plus 1 CD), IX-17

		Printed Name	Signature	Date
8.	Originator	Dwayne C. Kicker		7/6/00
9.	Checker	Marek J. Mrugala		7/6/00
10.	Lead/Supervisor	Ernest L. Hardin		7/6/00
11.	Responsible Manager	Ernest L. Hardin		7/6/00

12. Remarks:

John Case was primarily responsible for the development of this analysis/model (Section 6).

Ming Lin and Sean Vincent contributed to the documentation of computer software and analysis/model inputs (Sections 3 and 4).

Mason Pillow developed test cases used for routine qualification (Attachments I, III, IV, and V).

The following support was provided by Lawrence Livermore National Laboratory:

Nina Rosenburg and Charles Carrigan prepared input files and executed NUFT V3.0s.

Kenrick Lee developed and executed the routine Chim_surf_TP V1.1.

James Gansemer developed and executed ColumnInfiltration V1.1, Cover V1.1, and CONVERTCOORDS V1.1. James Gansemer also executed YMESH V1.53.

Mary Gokoffski developed and executed the routine rme6 V1.1.

Veraun Chipman was the technical checker for Revision 0 of this document.

The following TBVs apply to this analysis/model:

TBV-0389, TBV-3471, TBV-3685, TBV-3686, TBV-3695, TBV-3796, TBV-3828.

INFORMATION COPY

LAS VEGAS DOCUMENT CONTROL

AP-3.10Q.3

Rev. 05/12/2000

OFFICE OF CIVILIAN RADIOACTIVE WASTE MANAGEMENT
ANALYSIS/MODEL REVISION RECORD
Complete Only Applicable Items

1. Page: 2 of: 82

2. Analysis or Model Title:

Water Distribution and Removal Model

3. Document Identifier (including Rev. No. and Change No., if applicable):

ANL-EBS-MD-000032 REV 00 ICN 01

4. Revision/Change No.	5. Description of Revision/Change
00	Initial issue.
00/01	Clarification and editorial changes have been provided in response to DOE's acceptance review. Three references have been added in Section 6.2.3. The technical content and the resulting conclusions of this AMR have not changed. The following pages are affected by this ICN: 13, 15, 21, 38, 39, 44, 45, 49, 69, 72, 73, 77, 79, and 81.

CONTENTS

CONTENTS (Continued)

FIGURES

TABLES

ACRONYMS

ACC	Records Processing Center accession number
AFC	active fracture concept
AMR	analysis/model report
AP	administrative procedure
CRWMS M&O	Civilian Radioactive Waste Management System Management and Operating Contractor
CSNF	commercial spent nuclear fuel
DHLW	defense high-level waste
DKM	dual permeability model
DOE	U.S. Department of Energy
DTN	data tracking number
EBS	Engineered Barrier System
EDA	enhanced design alternative
LADS	License Application Design Selection
LLNL	Lawrence Livermore National Laboratory
NBS	natural barrier system
NUFT	Non-isothermal Unsaturated –saturated Flow and Transport
PMR	process model report
QA	quality assurance
QAP	quality administrative procedure
SAN	software activity number
STN	software tracking number
TBM	tunnel boring machine
TBV	to be verified
THC	Thermal-Hydrological-Chemical
THM	Thermal-Hydrological-Mechanical
TIC	Technical Information Center
Tptpll	Topopah Spring Tuff crystal poor lower lithophysal zone
Tptpmn	Topopah Spring Tuff crystal poor middle nonlithophysal zone
TSw	Topopah Spring welded tuff
UZ	unsaturated zone
WP	waste package

NOMENCLATURE

B	largest aperture that could retain water
b	bulk (equivalent medium)
b,f	fracture bulk
b,m	matrix bulk
c	cross-sectional
cms	cubic meter per second
D_i	diameter of outer cylinder, m
D_0	diameter of inner cylinder, m
eff	effective
f_a	fraction of active fractures (intrinsic)
g	acceleration due to gravity
K	permeability, m^2
k	thermal conductivity, W/m-K
L	$(D_o - D_i)/2.0$
m	van Genuchten parameter (also referred to as λ)
n	van Genuchten beta parameter
Pr	Prandtl number
q'	heat transfer rate per unit length, W/m
R	universal gas constant
Ra	Rayleigh number
w_c	wetted perimeter for the overlapping joint
α_t	thermal diffusivity, m^2/s
α	van Genuchten alpha parameter, 1/Pa
β	volumetric thermal expansion coefficient, K^{-1}
λ	van Genuchten parameter (also referred to as m)
ϕ	porosity
ν	kinematic viscosity, m^2/s
ψ	moisture potential
σ	surface tension of water
*	dimensionless quantity

1. PURPOSE

The purpose of the Engineered Barrier System (EBS) water distribution and removal model is to quantify and evaluate the distribution of liquid water within emplacement drifts and its removal by drainage. The model provides estimates of the principal factor of water seepage into emplacement drifts during the period of compliance for post-closure performance. The model will integrate results from the EBS Water Diversion Model, EBS Water Drainage Model, and the EBS Ventilation Model. This analysis/model report (AMR) is intended to provide input to the EBS Radionuclide Transport Model, the EBS Physical and Chemical Environment Model, and the EBS Features, Events and Processes (FEPs) and Degradation Mode Analysis. The model is comprised of a two-dimensional numerical simulation using the NUFT computer code (Non-isothermal Unsaturated-saturated Flow and Transport) (Nitao 1998). The use of NUFT requires the development of several submodels and several analyses to define hydrologic and thermal properties, initial conditions and boundary conditions.

1.1 BACKGROUND

The water distribution and removal model is one of twenty-three AMRs that support the development of the Engineered Barrier System Degradation and Flow/Transport Process Model Report. The EBS process model report (PMR) is part of a series of PMRs that have the general objective of documenting a synthesis of the necessary and sufficient technical information that the Project will be relying upon to support its site suitability evaluation and the licensing safety case pertaining to a particular process model. The technical information consists of data, analyses, models, software, and supporting documentation used to defend the applicability of the model for its intended purpose of evaluating the post-closure performance of the Yucca Mountain repository system.

Water distribution and removal represents one component of the overall EBS. Under some conditions, liquid water will seep into emplacement drifts through fractures in the host rock and move generally downward, potentially contacting waste packages. After waste packages are breached by corrosion, some of this seepage water will contact the waste, dissolve or suspend radionuclides, and ultimately carry radionuclides through the EBS to the near-field host rock.

Lateral diversion of liquid water within the drift will occur at the inner drift surface, and more significantly from the operation of engineered structures such as drip shields, capillary barriers, and the outer surface of a penetrated waste package. If most of the seepage flux can be diverted laterally and removed from the drifts before contacting waste, the release of radionuclides from the EBS can be controlled, resulting in a proportional reduction in dose release at the accessible environment.

1.2 OBJECTIVES

The specific objectives of this process model include:

- Develop a reasonable representation and bounding estimates for the volume of water that flows through the backfill and into the invert.

- Develop various scenarios for repository performance including:

  - Uniform and focused flow
  - Ambient temperature and elevated heating
  - Plugging of fractures below the EBS
  - Engineered features.

1.3 WORK SCOPE

The scope of work includes developing performance scenarios for various post-closure periods representing the upper range of in-drift flow conditions for the post-closure repository, developing a model for the distribution of liquid water flux within drifts and its removal by flow back into the host rock, and performing analyses for the performance scenarios using the developed model.

1.4 ANALYSIS/MODEL APPLICABILITY

The water distribution and removal results are applicable for the License Application Design Selection (LADS) repository configuration. General guidance on the selection of materials was provided by Wilkins and Heath (1999, Enclosure 2, p. 2) on the basis of thermal, hydrological, and geochemical consequences. The guidance included selection of a ballast material for the invert, a backfill, and a drip shield. Any significant change to these basic parameters would require an assessment of the subsequent impacts to this analysis/model.

2. QUALITY ASSURANCE

This document has been prepared according to AP-3.10Q, *Analyses and Models*. AP-3.10Q is the procedure for planning, developing, validating, and documenting analyses and models. A development plan (CRWMS M&O 1999a) was prepared in accordance with AP-2.13Q, *Technical Product Development Planning*. The plan documents this AMR number as E0090 and the corresponding work package as 1201213EM1. This report has been prepared according to this development plan and applicable quality assurance (QA) controls presented therein.

The applicability of the QA program is documented in an activity evaluation according to QAP-2-0, *Conduct of Activities*. The activity evaluation (CRWMS M&O 1999b) has concluded that this document is quality-affecting and subject to the QA controls of the Quality Assurance Requirements and Description (DOE 2000).

The design analysis, *Classification of the MGR Ex-Container System* (CRWMS M&O 1999c), was performed in accordance with QAP-2-3, *Classification of Permanent Items*. The drip shields and backfill material are part of the Ex-Container System identified on the Q-list (YMP 2000, p. II-11), which is identified as Quality Level 1 (QL1). Water distribution and removal, which is part of the physical and chemical environment, is not specifically addressed by the Q-list but is a characteristic of the ex-container system. For this document, it is assumed that the classification of features affecting the physical and chemical environment is Quality Level 1, important to waste isolation.

Qualified and accepted input data and references have been identified. All electronic data used in the preparation of this AMR was obtained from the Technical Data Management System as appropriate. Electronic data was controlled and managed per the development plan. Unqualified data used in this report are tracked in accordance with AP-3.15Q, *Managing Technical Product Inputs*. AP-3.10Q requires that output resulting from unqualified software be designated as unqualified—to be verified (TBV) in accordance with AP-3.15Q. Computer software and model usage is discussed in Section 3 of this report.

As per Section 5.9 of AP-3.10Q, the results of this analysis/model will be submitted to the Technical Data Management System in accordance with AP-SIII.3Q, *Submittal and Incorporation of Data to the Technical Data Management System*.

3. COMPUTER SOFTWARE AND MODEL USAGE

The computer software and models used in the preparation of this document are identified in this section. Unqualified software was used in parts of the analysis and modeling activities reported in this document. AP-3.10Q, *Analyses and Models*, requires that the resulting output from the unqualified software used in the preparation of this report must be designated as unqualified—TBV in accordance with AP-3.15Q, *Managing Technical Product Inputs*. Further software qualification is required prior to the removal of this TBV designation. All the computer files associated with this document are provided in Attachment VIII. This model is validated as documented in Section 6.4.

Various software packages were used in the development of the inputs to this model. Table 1 shows the sources of inputs and the actual file names of the input and output files for the various routines and software packages used in developing the model inputs. Figure 1 further illustrates the path of data through routines and software packages. Software tracking numbers (STNs) are provided where applicable.

Table 1. Software and Routine Usage

Name/ Number	Description	Software Identifiers (STN) or Validation Location	Input source	Input File name	Output File Name
NUFT V3.0s	Unqualified Software (TBV-3828)	10088-3.0s-00	intermediate file	*.in	*.ext
			supporting input file	vtough.pkg dkm-afc-EBS-Rev10-WDR dkm-afc-NBS-WDR	
rme6 V1.1	Validated Routine	Attachment V	LB99EBS1233129.001 Attachment II	tspa99_primary_mesh UZ99_3.grd	LBL99-YMESH
XTOOL V10.1	Qualified Software Routine	10208-10.1-00	intermediate file	*.ext	*.ps
YMESH V1.53	Qualified Software Routine	10172-1.53-00	intermediate file	LBL99-YMESH I4c4.dat	I4c4.col.units
Chim_Surf_TP V1.1	Validated Routine	Attachment III	LB99EBS1233129.001 LB99EBS1233129.003	tspa99_primary_mesh bcs_99.dat	outpt, outpt_wt
Cover V1.1	Validated Routine	Attachment I	MO9911MWDEBSWD.000	dft1.dat	shape1.dat
CONVERTCOORDS V1.1	Qualified Software Routine	10209-1.1-00	MO9911MWDEBSWD.000	*.inf	*.NV
ColumnInfiltration V1.1	Validated Routine	Attachment IV	intermediate files Table II-3	*.NV column.data	*.out (infiltration rates)

3.1 DESCRIPTION OF SOFTWARE USED

The NUFT V3.0s (NUFT) software code was used in the preparation of this document. NUFT is classified as an unqualified software program (TBV-3828) per AP-SI.1Q, *Software Management*, and is under configuration management (STN: 10088-3.0s-00) with ongoing software qualification activities (Table 1). NUFT was run on a Sun Ultra 10 workstation with SunOS 5.6 operating system.

NUFT, specifically the USNT module of NUFT, is used in this document to model flow through a fractured porous media. NUFT solves the nonisothermal problem by solving a coupled set of balance equations for transported component. NUFT is based on the numerical technique called the integrated finite difference method or the finite volume method. This method allows for arbitrary polyhedral shapes. This method reduces to the standard finite difference method for a standard rectangular mesh. Because of the high of degree of nonlinearity in the van Genuchten constitutive relation for relative permeability for the fluid phase, NUFT uses various weighting approaches. The saturated permeability of a fluid phase between two adjacent cells is harmonically weighted, while the relative permeability is upstream weighted. This approach is used throughout the model domain.

The key options used for the NUFT simulations include the dual permeability model (DKM) and the active fracture concept (AFC). These modeling methods are NUFT options selected in the NUFT input files (see Attachment VIII, files: *.in).

The DKM conceptualizes the fractured rock as having two interacting materials, one representing the matrix and one representing the fractures. The interaction between the fractures and the matrix is explicitly calculated from the local temperature and pressure differences, thus allowing transient behavior to be predicted. The DKM underestimates the fracture-matrix interaction for steep temperature and pressure gradients (Birkholzer and Tsang 1998, p. 2). There are no steep temperature or pressure gradients simulated in this model. Therefore, the DKM is appropriate for the model developed in this document.

The active fracture concept accounts for the contact area between the fracture and the matrix, as well as the frequency of fractures. The AFC is that fracture flow only occurs through some of the fractures. This is more conservative than assuming the influx flows evenly through all fractures (Section 6.2.3). The flux through a fracture is greater when it has higher saturation and, therefore, focusing flow through a portion of the fractures (i.e., to active fractures) maximizes flux and results in fast pathways for flux through the mountain.

The rock properties in DTN: LB990861233129.001 were calibrated using an inverse modeling technique that assumes the properties will only be used in DKM employing AFC. Therefore, the DKM and AFC are appropriate NUFT options. Further discussion is provided in Section 6.2.3.

3.2 DESCRIPTION OF ROUTINES USED

Three routines used in the preparation of this document are qualified through software routine reports in accordance with AP-SI.1Q Section 5.1.2, including XTOOL V10.1, CONVERTCOORDS V1.1, and YMESH V1.53. All other routines used in the preparation of
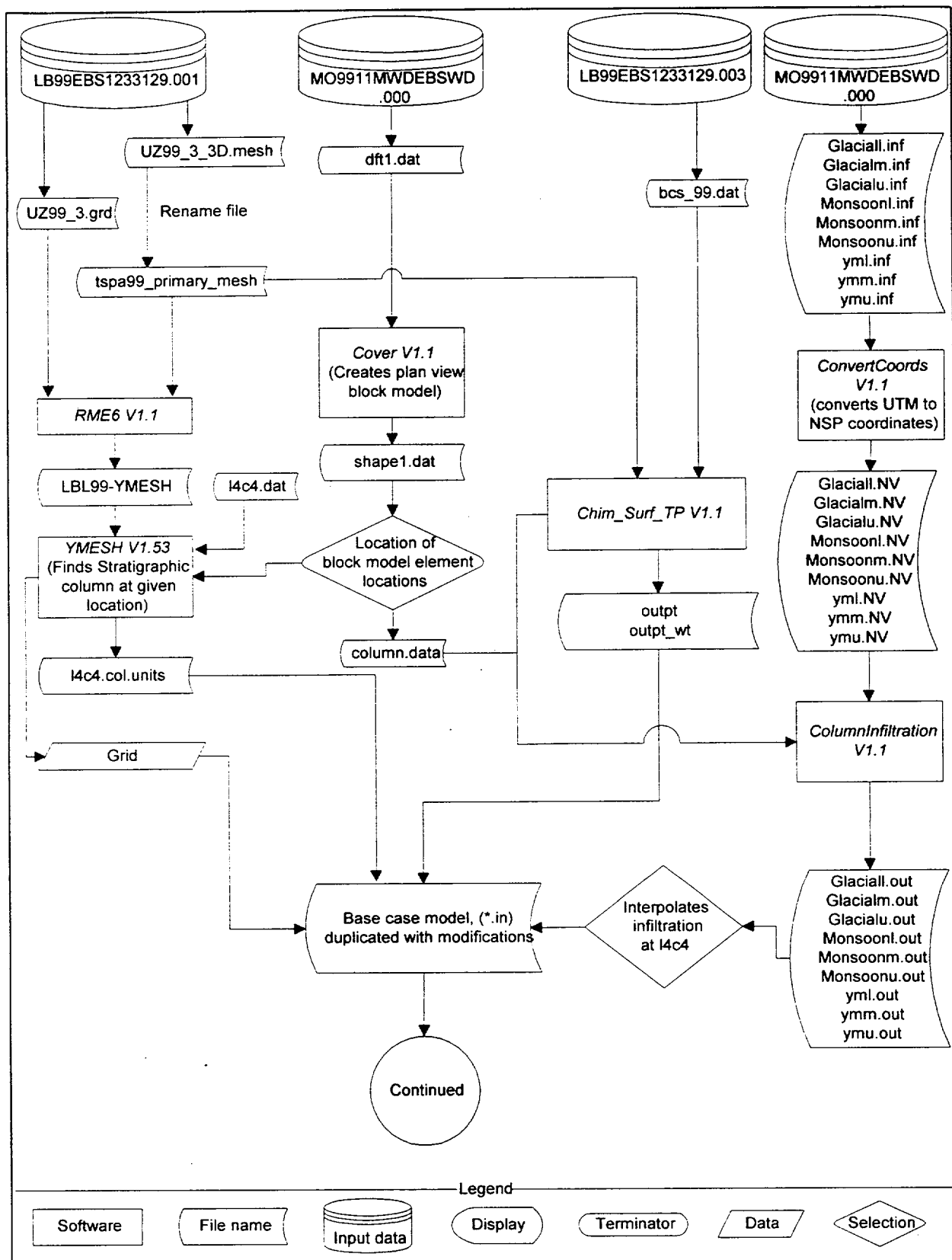
Figure 1. Input Data Manipulation Flowchart
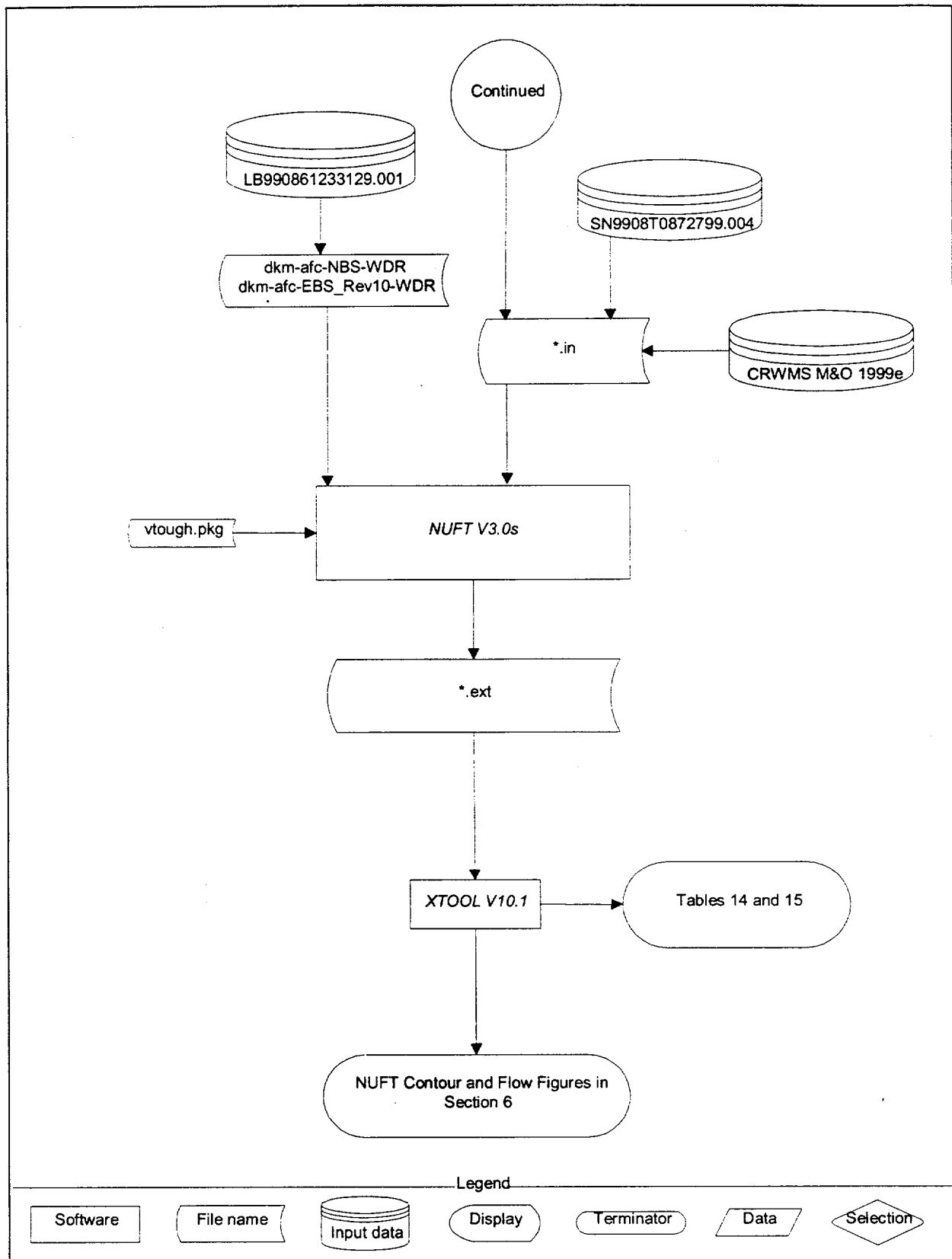
Figure 1. Input Data Manipulation Flowchart (Continued)

this document are qualified in accordance with AP-SI.1Q Section 5.1.1 and documented as follows: Chim_Surf_TP V1.1 is qualified in Attachment III, ColumnInfiltration V1.1 is qualified in Attachment IV, Cover V1.1 is qualified in Attachment I, and RME6 V1.1 is qualified in Attachment V.

3.2.1 XTOOL V10.1

XTOOL is classified as a qualified software routine (STN: 10208-10.1-00) per AP-SI.1Q (Table 1). The output from XTOOL is graphical (no actual data is produced with XTOOL). XTOOL is qualified and tracked in accordance with AP-SI.1Q because it is not commercial off the shelf software. XTOOL is used to develop graphical representations (Figures 8 through 23) of the results in the NUFT output files (VIII-files: *.ext). XTOOL is appropriate for the application used in this task, and was used within the range of its validation. XTOOL was run on a Sun Ultra 10 workstation with SunOS 5.6 operating system.

3.2.2 CONVERTCOORDS V1.1

CONVERTCOORDS V1.1 is classified as a qualified software routine (STN: 10209-1.1-00) per AP-SI.1Q (Table 1). CONVERTCOORDS is used to convert from Universal Transverse Mercator coordinates to Nevada State Plane coordinates, as well as to reformat the data (see Attachment VIII, files: *.inf). The desired format is columns of data, with the input files in a matrix format. CONVERTCOORDS is appropriate for the application used in this task, and was used within the range of its validation. CONVERTCOORDS was run on a Sun Ultra 2 workstation with SunOS 5.5.1 operating system.

3.2.3 YMESH V1.53

YMESH V1.53 is classified as a qualified software routine (STN: 10172-1.53-00) per AP-SI.1Q (Table 1). YMESH is used in this model to interpolate the thickness of the stratigraphic units as described in the flow chart of Figure 1. YMESH is appropriate for the application used in this task, and was used within the range of its validation. YMESH was run on a Sun Ultra 2 workstation with SunOS 5.5.1 operating system.

3.2.4 Chim_Surf_TP V1.1

Chim_Surf_TP V1.1 is classified as a routine per AP-SI.1Q, and is qualified in Attachment III. The purpose of Chim_Surf_TP V1.1 is to interpolate the temperature and pressure at the ground surface and at the water table for a given X-Y location using the inverse distance method (Isaaks and Srivastava 1989, p. 258). This routine executes the expected mathematical operations accurately (see Attachment III), and is therefore appropriate for the application in this task. Chim_Surf_TP V1.1 was run on a Sun Ultra 2 workstation with SunOS 5.5.1 operating system.

3.2.5 ColumnInfiltration V1.1

ColumnInfiltration V1.1 is classified as a routine per AP-SI.1Q, and is qualified in Attachment IV. The purpose of ColumnInfiltration V1.1 is to interpolate the infiltration at a given X-Y location using a Gaussian weighting function (Isaaks and Srivastava 1989, p. 208 and Kitanidis

1997, p. 54). This routine executes the required mathematical operations accurately (see Attachment IV), and is therefore appropriate for the application in this task. ColumnInfiltration V1.1 was run on a Sun Ultra 2 workstation with SunOS 5.5.1 operating system.

3.2.6 Cover V1.1

Cover V1.1 is classified as a routine per AP-SI.1Q, and is qualified in Attachment I. The purpose of Cover V1.1 is to develop a block model based on the plan view of the repository that approximates the area and location of emplacement. The results of this routine meet these objectives (see Attachment IV). The routine is, therefore, appropriate for the application in this task. Cover V1.1 was run on a Sun Ultra 2 workstation with SunOS 5.5.1 operating system.

3.2.7 rme6 V1.1

The routine rme6 V1.1 is classified as such per AP-SI.1Q, and is qualified in Attachment V. The purpose of rme6 is to reformat and combine specific files (Attachment VIII files: tspa99_primary_mesh, UZ99_3.grd, l4c4.dat). The resulting file, LBL99-YMESH is used by a subsequent software program, YMESH V1 (see Section 3.2.2; Figure 1 and Table 1). The results of this routine meet the objectives (see Attachment V) and, therefore, the routine is appropriate. The routine rme6 V1.1 was run on a Sun Ultra 10 workstation with SunOS 5.6 operating system.

3.3 OTHER SOFTWARE

In addition to the above listed items, both *Microsoft Excel 97* and *Mathcad 7 Professional* were used. These software items were used to perform support calculational activities as described in Section 6.3.6 and Attachment II. To provide documentation of the analysis in sufficient detail to allow independent repetition of the software in accordance with AP-3.10Q Attachment I, and to ensure compliance with AP-SI.1Q, the minimum information required by AP-SI.1Q Section 5.1.1.2 has been provided:

- Identification of the *Excel* and *Mathcad* files, including the version of the file, are provided in Section 6.3.6, Attachment II, and Attachment VIII.

- The name and version of the commercial software are provided as described above.

- The inputs, spreadsheet cell contents and equations, and results are provided in Attachment VIII. This provides sufficient documentation that these standard mathematical calculations provide correct results for the specified range of input parameters.

4. INPUTS

4.1 DATA AND PARAMETERS

The following sources of data for model geometry, hydrologic and thermal properties of the NBS and EBS infiltration, fluid and thermodynamic properties, and waste package parameters are used as inputs to the water distribution and removal model.

4.1.1 Model Geometry for the NBS and EBS

The UZ (unsaturated zone) site scale model (LB99EBS1233129.001) is a three-dimensional model used to estimate the thickness of stratigraphic units. A lithostratigraphic column was developed for the L4C4 column with coordinates Easting 170500.3 and Northing 233807.3 in this analysis as discussed in Section 6.2.1.

The EBS model geometry is developed from the License Application Design Selection (LADS) EDA-II (Wilkins and Heath 1999). The EBS model geometry is summarized in Table 2. The source of the in drift data is from DTN SN9908T0872799.004 (TBV-3471). This data is used to construct the in drift configuration for the water distribution and removal model described in Section 6.2.1.

The source of data for the temperature and pressure boundary conditions at the ground surface and water table are DTN LB99EBS1233129.003 from the UZ site scale model. The derivation of temperature and pressure boundary conditions based on the source data is described in Section 6.2.2.

Table 2. EBS Geometry (DTN: SN9908T0872799.004, TBV-3471)

Model Input	Value
Drift diameter	5.5 m
Waste package outer diameter	1.67 m
Location of waste package center above bottom of drift	1.945 m
Location of waste package center below the springline	0.805 m
Drip shield thickness	0.02 m
Location of backfill spoil peak (this is the location where the top of the backfill intersects the vertical drawn from the drift centerline) above the drift springline	2.25 m
Backfill/drift wall intersection point	1.0 m above the springline at the drift wall intersection
Inside radius of drip shield	1.231 m
Top of invert as measured from bottom of drift	0.606 m
Waste package spacing	0.1 m
Emplacement drift spacing	81 m

4.1.2 Hydrologic and Thermal Properties of the NBS

Tables 3 to 6 list hydrologic and thermal properties for the hydro-stratigraphic units considered in this model. The data are from DTN LB990861233129.001. Fracture porosity, matrix porosity, tortuosity factor, fracture bulk permeability, matrix bulk permeability, maximum and residual saturation in fractures, maximum and residual saturation in matrix, van Genuchten parameters α and m (or λ) for fractures, van Genuchten parameters α and m (or λ) for matrix, fracture porosity, and matrix porosity are used in the analysis.

4.1.3 Hydrologic and Thermal Properties of the EBS

The hydrologic and thermal properties for the backfill, the invert, and the combined material are obtained from DTN SN9908T0872799.004 (TBV-3471). Tables 7 and 8 summarize the properties. The backfill consists of Overton sand and the invert consists of crushed tuff. Additional descriptions of both the backfill and invert materials are provided in the *Water Diversion Model* (CRWMS M&O 2000b, Sections 6.2.1 and 6.2.2).

4.1.4 Infiltration

The infiltration data source for the glacial climate estimated for the UZ site scale model is used in this analysis. These data are from MO9911MWDEBSWD.000 and support the computer files *.inf in Attachment VIII.

4.1.5 Fluid and Thermodynamic Properties of Water and Air

Properties such as molecular weight, density, viscosity, diffusivity, enthalpy versus temperature/pressure, and specific volume as a function of temperature/pressure, are accepted data incorporated into the NUFT code.

4.1.6 Universal Constants

The Ideal Gas Constant R (1.987 cal/(g.mol-K)) and Gravitational Constant g (9.807 m/s^2) are accepted data incorporated into the NUFT code.

4.1.7 Waste Package Parameters

The waste package parameters used to support the repository heating cases include the waste package length and diameter, the number and initial heat generation rates, and time-dependent heat generation rates. These data are discussed in the following subsections.

4.1.7.1 Waste Package Length and Diameter

The length and diameter for waste packages are listed in Table 9 (TBV-3685), based on Enhanced Design Alternative (EDA) II Repository Estimated Waste Package Types and Quantities (CRWMS M&O 1999e, Item 1, pp. 25 to 26, TBV-3685).

Table 3. Matrix Hydrologic Parameters for NBS (DTN LB990861233129.001)

Unit	Permeability (m^2)	Porosity (Fraction)	van Genuchten α (Pa^{-1})	van Genuchten m	Residual Saturation (Fraction)	Satiated Saturation (Fraction)
Tcw11	3.86E-15	0.253	4.00E-05	0.47	0.07	1
Tcw12	2.74E-19	0.082	1.81E-05	0.241	0.19	1
Tcw13	9.23E-17	0.203	3.44E-06	0.398	0.31	1
Ptn21	9.90E-13	0.387	1.01E-05	0.176	0.23	1
Ptn22	2.65E-12	0.439	1.60E-04	0.326	0.16	1
Ptn23	1.23E-13	0.254	5.58E-06	0.397	0.08	1
Ptn24	7.86E-14	0.411	1.53E-04	0.225	0.14	1
Ptn25	7.00E-14	0.499	5.27E-05	0.323	0.06	1
Ptn26	2.21E-13	0.492	2.49E-04	0.285	0.05	1
Tsw31	6.32E-17	0.053	3.61E-05	0.303	0.22	1
Tsw32	5.83E-16	0.157	3.61E-05	0.333	0.07	1
Tsw33	3.08E-17	0.154	2.13E-05	0.298	0.12	1
Tsw34	4.07E-18	0.11	3.86E-06	0.291	0.19	1
Tsw35	3.04E-17	0.131	6.44E-06	0.236	0.12	1
Tsw36	5.71E-18	0.112	3.55E-06	0.38	0.18	1
Tsw37	4.49E-18	0.094	5.33E-06	0.425	0.25	1
Tsw38	4.53E-18	0.037	6.94E-06	0.324	0.44	1
Tsw39	5.46E-17	0.173	2.29E-05	0.38	0.29	1
Ch1z	1.96E-19	0.288	2.68E-07	0.316	0.33	1
Ch1v	9.90E-13	0.273	1.43E-05	0.35	0.03	1
Ch2v	9.27E-14	0.345	5.13E-05	0.299	0.07	1
Ch3v	9.27E-14	0.345	5.13E-05	0.299	0.07	1
Ch4v	9.27E-14	0.345	5.13E-05	0.299	0.07	1
Ch5v	9.27E-14	0.345	5.13E-05	0.299	0.07	1
Ch2z	6.07E-18	0.331	3.47E-06	0.244	0.28	1
Ch3z	6.07E-18	0.331	3.47E-06	0.244	0.28	1
Ch4z	6.07E-18	0.331	3.47E-06	0.244	0.28	1
Ch5z	6.07E-18	0.331	3.47E-06	0.244	0.28	1
ch6	4.23E-19	0.266	3.38E-07	0.51	0.37	1
pp4	4.28E-18	0.325	1.51E-07	0.676	0.28	1
pp3	2.56E-14	0.303	2.60E-05	0.363	0.1	1
pp2	1.57E-16	0.263	2.67E-06	0.369	0.18	1
pp1	6.40E-17	0.28	1.14E-06	0.409	0.3	1
bf3	2.34E-14	0.115	4.48E-06	0.481	0.11	1
bf2	2.51E-17	0.259	1.54E-07	0.569	0.18	1

Table 4. Fracture Hydrologic Parameters for NBS (DTN LB990861233129.001)

Unit	Permeability (m^2)	Porosity (Fraction)	van Genuchten α (Pa^{-1})	van Genuchten m	Residual Saturation (Fraction)	Satiated Saturation (Fraction)
tcw11	2.41E-12	0.028	3.15E-03	0.627	0.01	1
tcw12	1.00E-10	0.02	2.13E-03	0.613	0.01	1
tcw13	5.42E-12	0.015	1.26E-03	0.607	0.01	1
ptn21	1.86E-12	0.011	1.68E-03	0.58	0.01	1
ptn22	2.00E-11	0.012	7.68E-04	0.58	0.01	1
ptn23	2.60E-13	0.0025	9.23E-04	0.61	0.01	1
ptn24	4.67E-13	0.012	3.37E-03	0.623	0.01	1
ptn25	7.03E-13	0.0062	6.33E-04	0.644	0.01	1
ptn26	4.44E-13	0.0036	2.79E-04	0.552	0.01	1
tsw31	3.21E-11	0.0055	2.49E-04	0.566	0.01	1
tsw32	1.26E-12	0.0095	1.27E-03	0.608	0.01	1
tsw33	5.50E-13	0.0066	1.46E-03	0.608	0.01	1
tsw34	2.76E-13	0.01	5.16E-04	0.608	0.01	1
tsw35	1.29E-12	0.011	7.39E-04	0.611	0.01	1
tsw36	9.91E-13	0.015	7.84E-04	0.61	0.01	1
tsw37	9.91E-13	0.015	7.84E-04	0.61	0.01	1
tsw38	5.92E-13	0.012	4.87E-04	0.612	0.01	1
tsw39	4.57E-13	0.0046	9.63E-04	0.634	0.01	1
ch1z	3.40E-13	0.0002	1.43E-03	0.631	0.01	1
ch1v	1.84E-12	0.0007	1.09E-03	0.624	0.01	1
ch2v	2.89E-13	0.0009	5.18E-04	0.628	0.01	1
ch3v	2.89E-13	0.0009	5.18E-04	0.628	0.01	1
ch4v	2.89E-13	0.0009	5.18E-04	0.628	0.01	1
ch5v	2.89E-13	0.0009	5.18E-04	0.628	0.01	1
ch2z	3.12E-14	0.0004	4.88E-04	0.598	0.01	1
ch3z	3.12E-14	0.0004	4.88E-04	0.598	0.01	1
ch4z	3.12E-14	0.0004	4.88E-04	0.598	0.01	1
ch5z	3.12E-14	0.0004	4.88E-04	0.598	0.01	1
ch6	1.67E-14	0.0002	7.49E-04	0.604	0.01	1
pp4	3.84E-14	0.0004	5.72E-04	0.627	0.01	1
pp3	7.60E-12	0.0011	8.73E-04	0.655	0.01	1
pp2	1.38E-13	0.0011	1.21E-03	0.606	0.01	1
pp1	1.12E-13	0.0004	5.33E-04	0.622	0.01	1
bf3	4.08E-13	0.0011	9.95E-04	0.624	0.01	1
bf2	1.30E-14	0.0004	5.42E-04	0.608	0.01	1

Table 5. Hydrologic Parameters for Fracture-Matrix Interaction for NBS (DTN LB990861233129.001)

Unit	Active Fracture Parameter	Frequency (1/m)	Fracture to matrix connection area (m²/m³)
tcw11	0.30	0.92	1.56
tcw12	0.30	1.91	13.39
tcw13	0.30	2.79	3.77
ptn21	0.09	0.67	1.00
ptn22	0.09	0.46	1.41
ptn23	0.09	0.57	1.75
ptn24	0.09	0.46	0.34
ptn25	0.09	0.52	1.09
ptn26	0.09	0.97	3.56
tsw31	0.06	2.17	3.86
tsw32	0.41	1.12	3.21
tsw33	0.41	0.81	4.44
tsw34	0.41	4.32	13.54
tsw35	0.41	3.16	9.68
tsw36	0.41	4.02	12.31
tsw37	0.41	4.02	12.31
tsw38	0.41	4.36	13.34
tsw39	0.41	0.96	2.95
ch1z	0.10	0.04	0.11
ch1v	0.13	0.10	0.30
ch2v	0.13	0.14	0.43
ch3v	0.13	0.14	0.43
ch4v	0.13	0.14	0.43
ch5v	0.13	0.14	0.43
ch2z	0.10	0.14	0.43
ch3z	0.10	0.14	0.43
ch4z	0.10	0.14	0.43
ch5z	0.10	0.14	0.43
ch6	0.10	0.04	0.11
pp4	0.10	0.14	0.43
pp3	0.46	0.20	0.61
pp2	0.46	0.20	0.61
pp1	0.10	0.14	0.43
bf3	0.46	0.20	0.61
Bf2	0.10	0.14	0.43

Table 6. Thermal Parameters and Tortuosity Factor for NBS (DTN LB990861233129.001)

Unit	Rock Grain Density (Kg/m^3)	Rock Grain Specific Heat (J/Kg K)	Dry Conductivity (W/m K)	Wet Conductivity (W/m K)	Tortuosity
tcw11	2550	823	1.60	2.00	0.7
tcw12	2510	851	1.24	1.81	0.7
tcw13	2470	857	0.54	0.98	0.7
ptn21	2380	1040	0.50	1.07	0.7
ptn22	2340	1080	0.35	0.50	0.7
ptn23	2400	849	0.44	0.97	0.7
ptn24	2370	1020	0.46	1.02	0.7
ptn25	2260	1330	0.35	0.82	0.7
ptn26	2370	1220	0.23	0.67	0.7
tsw31	2510	834	0.37	1.00	0.7
tsw32	2550	866	1.06	1.62	0.7
tsw33	2510	882	0.79	1.68	0.7
tsw34	2530	948	1.56	2.33	0.7
tsw35	2540	900	1.20	2.02	0.7
tsw36	2560	865	1.42	1.84	0.7
tsw37	2560	865	1.42	1.84	0.7
tsw38	2360	984	1.69	2.08	0.7
tsw39	2360	984	1.69	2.08	0.7
ch1z	2310	1060	0.70	1.31	0.7
ch1v	2310	1060	0.70	1.31	0.7
ch2v	2240	1200	0.58	1.17	0.7
ch3v	2240	1200	0.58	1.17	0.7
ch4v	2240	1200	0.58	1.17	0.7
ch5v	2240	1200	0.58	1.17	0.7
ch2z	2350	1150	0.61	1.20	0.7
ch3z	2350	1150	0.61	1.20	0.7
ch4z	2350	1150	0.61	1.20	0.7
ch5z	2350	1150	0.61	1.20	0.7
ch6	2440	1170	0.73	1.35	0.7
pp4	2410	577	0.62	1.21	0.7
pp3	2580	841	0.66	1.26	0.7
pp2	2580	841	0.66	1.26	0.7
pp1	2470	635	0.72	1.33	0.7
bf3	2570	763	1.41	1.83	0.7
bf2	2410	633	0.74	1.36	0.7

Table 7. Hydrologic Properties for EBS (DTN SN9908T0872799.004, TBV-3471)

Material	Permeability (m^2)	Porosity	van Genuchten (1/Pa)	van Genuchten m	Residual Saturation	Satiated Saturation
Backfill	1.43x10^{-11}	0.41	2.7523x10^{-4}	0.5	0.024	1
Invert	6.152x10^{-10}	0.545	1.2232x10^{-3}	0.63	0.092	1

Table 8. Thermal Properties for EBS (DTN SN9908T0872799.004, TBV-3471)

Material	Rock Grain Density (Kg/m^3)	Rock Grain Specific Heat (J/Kg K)	Dry Conductivity (W/m K)	Wet Conductivity[a] (W/m K)	Tortuosity
Backfill	2700	795.432	0.33	0.33	0.7
Invert	2530	948	0.66	0.66	0.7

Note: [a] Wet conductivity value assumed to be the same as the dry conductivity value.

Table 9. Number and Initial Heat Generation Rates for Average CSNF and DHLW Waste Packages (CRWMS M&O 1999e, TBV-3685)

Waste Package Type		Length of Waste Packages (m)	Diameter of Waste Packages (m)	Number of Waste Packages	Initial Heat Generation Rate (kW/package)
21-PWR	Absorber Plates	5.305	1.564	4,279	11.3337
	Control Rods	5.305	1.564	87	2.3709
12-PWR	Long	5.791	1.250	158	9.5402
44-BWR	Absorber Plates	5.275	1.594	2,889	7.1346
24-BWR	Thick Plates	5.245	1.238	6	0.4910
5-DHLW	Short	3.73	2.030	1,249	4.0580
5-DHLW	Long	5.357	2.030	414	5.8280[a]
Navy	Combined	5.888	1.869	285	7.1350[b]
DOE/Other		5.57	No Data	598	0.7930

Note: [a] Assumed value by assuming that the initial heat generation rates for 5-DHLWs, short and long, are linearly proportional to their lengths (4.058kW×5.357m/3.73m=5.828kW).

[b] Averaged value equal to that of 44-BWR (CRWMS M&O, 1998b, p. 14, TBV-0389).

4.1.7.2 Number and Initial Heat Generation Rates of Waste Packages

Table 9 lists the number of the commercial spent nuclear fuel (CSNF) and defense high-level waste (DHLW) packages and their initial heat generation rates. The data are from Enhanced Design Alternative (EDA) II Repository Estimated Waste Package Types and Quantities (CRWMS M&O 1999e, Item 2, p.7 (TBV 3695), and Item 2, p.15 (TBV 3686)).

4.1.7.3 Average Waste Package Heat Generation Rates

The decay characteristics of the CSNF waste packages, as listed in Table 10, are used in this analysis. These values are provided in CRWMS M&O 1999e, Item 2, Table 3, pp. 7 to 9 (TBV 3695). The values of heat flux of the waste packages used in thermal models are calculated in Attachment VII.

4.1.8 Drip Shield Geometry for the Bounding Calculation

The drip shield length is 5.485 meters. This is used in the bounding calculation for flow through the drip shield. This value is taken from the Drip Shield Design transmittal (CRWMS M&O 1999d, TBV-3796).

4.2 CRITERIA

4.2.1 Drip Shield Material

The "Direction to Transition to Enhanced Design Alternative II" letter, Enclosure 2 – Guidelines for Implementation of EDA II (Wilkins and Heath 1999, Enclosure 2, Requirements 9.0, p.2), specifies that the drip shield will be titanium grade 7, at least 2 centimeters thick. From this statement it is inferred that a drip shield will be part of the Ex-Container design.

4.2.2 Ex-Container System

The Ex-Container System Description Document (CRWMS M&O 1998a, p. 4 of 19) states that "the Ex-Container System consists of the waste package support hardware (pedestal and pier) and any performance enhancing barriers (i.e., sorptive inverts, backfill, and drip shields) installed or placed in the emplacement drift". It is implicit that the drip shield is considered a part of the Ex-Container System. Further, Section 1.1.1, states "the system contributes to the isolation of waste from the Natural Barrier." and Section 1.1.3 states "the system minimizes the amount of water contacting the waste package...". From these sections it is inferred that a drip shield is part of the Ex-Container System and it is necessary to be included in modeling.

4.2.3 Backfill

The "Direction to Transition to Enhanced Design Alternative II" letter, Enclosure 2 – Guidelines for Implementation of EDA II (Wilkins and Heath 1999, Enclosure 2, Requirements 7.0, p.2), specifies that the design will include backfill.

Table 10. Time-dependent Heat Generation Rates for Average CSNF Waste Packages (CRWMS M&O 1999e, TBV-3695)

Time (years)	21-PWR Absorber Plates (kW/package)	21-PWR Control Rods (kW/package)	12-PWR Long (kW/package)	44-BWR Absorber Plates (kW/package)	24-BWR Thick Absorber Plates (kW/package)
0.01	11.3337	2.3709	9.5402	7.1346	0.4910
1	10.9954	2.3285	9.2722	6.9146	0.4829
5	9.9653	2.1785	8.4286	6.2682	0.4445
10	8.9956	2.0095	7.5901	5.6536	0.4030
15	8.1887	1.8547	6.8815	5.1467	0.3689
20	7.5138	1.7241	6.3149	4.7102	0.3341
25	6.9115	1.6038	5.8009	4.3098	0.3065
30	6.3792	1.4942	5.3407	3.9701	0.2806
40	5.4984	1.3106	4.5868	3.3915	0.2369
50	4.7912	1.1649	3.9792	2.9326	0.2033
60	4.2229	1.0443	3.5026	2.5621	0.1754
70	3.7685	0.9479	3.1031	2.2625	0.1536
80	3.3915	0.8698	2.7908	2.0227	0.1361
90	3.0866	0.8070	2.5304	1.8264	0.1222
100	2.8314	0.7545	2.3024	1.6685	0.1111
150	2.0790	0.5983	1.6766	1.1977	0.0799
200	1.7291	0.5244	1.3818	0.9878	0.0684
250	1.5128	0.4796	1.2029	0.8725	0.0622
300	1.3654	0.4452	1.0804	0.7889	0.0583
400	1.1571	0.395	0.9118	0.6679	0.0528
500	1.0046	0.3492	0.7901	0.5821	0.0485
600	0.8839	0.3167	0.6928	0.5188	0.0449
700	0.7888	0.2873	0.618	0.4629	0.0415
800	0.7071	0.2629	0.5533	0.4202	0.0386
900	0.6367	0.2415	0.4962	0.3832	0.0367
1000	0.5804	0.2245	0.4538	0.3538	0.0346
1500	0.3969	0.1653	0.3077	0.2477	0.0283
2000	0.3093	0.1363	0.2395	0.1984	0.0247
3000	0.2402	0.1134	0.182	0.1593	0.0221
4000	0.2167	0.1042	0.1664	0.1421	0.0206
5000	0.1995	0.0977	0.1529	0.1307	0.0194
6000	0.1867	0.0916	0.1428	0.1214	0.0185
7000	0.1728	0.0869	0.1315	0.1131	0.018
8000	0.1619	0.0823	0.1236	0.106	0.017
9000	0.1523	0.0781	0.1162	0.099	0.0158
10000	0.1432	0.0739	0.1088	0.0924	0.0154
15000	0.1075	0.0582	0.0816	0.0686	0.0125
20000	0.084	0.0468	0.0635	0.0532	0.0103
25000	0.0674	0.0393	0.0506	0.0431	0.0089
30000	0.0554	0.0323	0.0416	0.0343	0.0077
35000	0.0466	0.0279	0.0352	0.0286	0.0067
40000	0.0399	0.0239	0.0299	0.0246	0.0058
45000	0.0349	0.0208	0.0263	0.0211	0.005

Table 10. Time-dependent Heat Generation Rates for Average CSNF Waste Packages (Continued) (CRWMS M&O 1999e, TBV-3695)

Time (years)	21-PWR Absorber Plates (kW/package)	21-PWR Control Rods (kW/package)	12-PWR Long (kW/package)	44-BWR Absorber Plates (kW/package)	24-BWR Thick Absorber Plates (kW/package)
50000	0.0307	0.0183	0.023	0.0185	0.0046
55000	0.0267	0.0162	0.0202	0.0163	0.0041
60000	0.0242	0.0141	0.0185	0.0145	0.0036
65000	0.0212	0.0126	0.016	0.0128	0.0031
70000	0.0191	0.0111	0.0146	0.0119	0.0029
75000	0.0174	0.0101	0.0133	0.0106	0.0026
80000	0.0158	0.009	0.0121	0.0097	0.0024
85000	0.0145	0.0082	0.0112	0.0088	0.0022
90000	0.0134	0.0076	0.0103	0.0084	0.0019
95000	0.0126	0.0067	0.0096	0.0075	0.0019
100000	0.0118	0.0063	0.009	0.007	0.0019

4.3 CODES AND STANDARDS

There are no codes and standards applicable to the water distribution and removal model.

5. ASSUMPTIONS

The following assumptions have been used in this water distribution and removal model.

5.1 DRIP SHIELD AND OTHER EBS COMPONENTS

For ease of modeling, the top of the drip shield is assumed to be stair-stepped in shape rather than curved. The technical basis of this assumption is that a flatter shape will result in a conservative estimate of the saturation level above the drip shield. The modeled thickness of the drip shield is 2 cm and the dimensions of the drift, invert material, and drip shield are shown on the simulation grid, corresponding to the EDA II design (Wilkins and Heath 1999).

Crushed tuff is selected for the invert to provide geochemical compatibility with the surrounding host rock. The basis for the selection of the crushed tuff is that the material provides diffusion-barrier performance when transport from the waste package to the rock wall is diffusion dominated. This could occur if a waste package is breached but the protecting drip shield is intact, so that the invert ballast material immediately below the drip shield is unsaturated and protected from advective flow from other engineered barrier components.

Overton sand is selected for the backfill material. This material will work in conjunction with the nonporous drip shield comprised of titanium to divert water around the waste packages when a bounding assumption (Section 5.11) is made regarding the flow through apertures in the drip shield. The combination of a drip shield and backfill diverts flow by providing a contrast in unsaturated hydraulic conductivity.

5.2 HYDROLOGIC PROPERTIES OF DRIP SHIELD

The drip shield, which is made of titanium, is assumed to be impermeable with properties the same as the waste package. The technical basis for this assumption is that the drip shield by design would limit water. This assumption is discussed further in Section 6.3.5.

5.3 BACKFILL MATERIAL AND INVERT PLACEMENT

The Overton sand backfill is assumed to completely fill the outer annulus between the drip shield and the drift wall rather than leaving a relatively small air gap on top of the backfill. This assumption is conservative because it allows any influx into the crown of the drift to be in direct contact with the backfill and, thus, would facilitate flow to the invert of the drift.

5.4 TORTUOSITY FACTORS

A factor of 0.0 is assigned to simulated waste packages and drip shields since they are assumed to be air and water tight and to be impermeable. A factor of 0.7 is assigned to the invert material since it is a granular material similar to the lithostratigraphic units at the repository horizon. This coefficient was estimated for a range of liquid saturation in soils by Fetter (1993, p. 44) and was found to be 0.66 (~ 0.7) as an average value.

5.5 THERMAL-HYDROLOGICAL-CHEMICAL AND THERMAL-HYDROLOGICAL-MECHANICAL EFFECTS

The thermal-hydrological-chemical (THC) and thermal-hydrological-mechanical (THM) effects are accounted for by reducing the intrinsic permeability of the fractured welded tuff directly below the invert to the intrinsic permeability of the matrix for welded tuff. The technical basis for this assumption is that the THC effects would more likely affect the unsaturated flow properties of the existing fractures, and that THM effects would not likely induce additional fracturing (CRWMS M&O 2000c). This assumption is used in Section 6.3.3.

5.6 LOCATION OF MODEL

Inputs that vary with location are found by using an assumed location of the L4C4 block element, with coordinates Easting 170500.3 and Northing 233807.3 (Attachment II). This assumption is used in Attachment II and in all YMESH and NUFT input files. The technical basis for this assumption is that this point is near the center of the proposed repository. Since edge effects are not considered in this model, the center of the repository is used as the representative location. This model is not sensitive to this input.

5.7 FLOW FOCUSING — THE INFILTRATION INTO THE DRIFT IS VARIED OVER SEVERAL EXPECTED CLIMATES

The infiltration rate is concentrated spatially such that the flux into the model is focused into the drift. A "focused glacial" infiltration rate is defined as follows: assume a glacial infiltration rate (42 mm/yr) is concentrated spatially such that this flux is focused over the drift centerline, and then apply 90% of the infiltration across the top of the drift (5.5 m). The remaining 10% of infiltration is applied to the rest of the area. The technical basis for this assumption is that it is conservative to assume the focusing of flow. This assumption is used in Section 6.3.1.

5.8 STEADY STATE TWO DIMENSIONAL MODEL AT ISOTHERMAL TEMPERATURE OR REDUCED HEAT LOADING

The NUFT analysis is performed using a steady state two dimensional model at isothermal temperatures or with heat loading in which 100 percent of the heat is removed during the first 100 years. The technical basis for this assumption is that temperatures in the EBS will be less and water flux rates will be higher than those predicted with repository heating. The heat given off by waste packages can be neglected for purposes of assessing water flow diversion drainage. It is conservative to assume isothermal temperature conditions for the purposes of water drainage.

5.9 THERMAL CONDUCTIVITY OF STATIONARY COMPONENTS

The conductivity of the welded tuff as measured in laboratory experiments (Brodsky et al. 1997, pp. 27-34) is assumed to apply to the stationary components. The technical basis for this assumption is that measured values are in general agreement with values in the literature (Bear 1988, p. 650). This assumption is used in Section 6.2.4.

5.10 MODEL FOR THE CENTER OF THE REPOSITORY WITH REFLECTIVE SIDE BOUNDARIES

The analysis assumes that the side boundaries are reflective with no flow of water, air or heat occurring across the side boundaries. The technical basis for this assumption is that flow in the vadose zone is dominantly in the vertical direction for the vertical system of fractures. This assumption is used in Section 6.2.1.

5.11 THEORETICAL APERTURE DIMENSION CREATED BY OVERLAPPING DRIP SHIELDS

The flow through the interface of the drip shield overlap at a specific moisture potential is a function of the moisture retention and flow characteristics of the aperture. For the purposes of a bounding calculation, the thickness of the aperture, at the specified moisture potential, is assumed to be equal to the maximum aperture thickness that could retain water in the aperture. The basis for this assumption is that it is conservative to assume that water flow is governed by the maximum aperture thickness, since the presence of narrower apertures would result in lower flow rates through the aperture under the same moisture gradient. This assumption is used in Section 6.3.5.

5.12 THEORETICAL TREATMENT OF THE OVERLAP

The overlap of the drip shield is described as a parallel plate in the model. Hence the capillary rise law for parallel plates (Kwicklis and Healy 1993, p. 4094) can be applied. The basis for this assumption is the flow of water, through capillary tubes or plates, is opposed by viscous forces according to Newton's law of viscosity (Jury et al. 1991, p. 42). This bounding assumption is used in Section 6.3.5.

5.13 MODELING OF THE ROCK MASS AS A DUAL PERMEABILITY MEDIUM

The nonhomogeneous rock mass is modeled as two interacting materials representing the matrix, and a system of fractures. The interaction between the fractures and the matrix is explicitly calculated from the local temperature and pressure differences under transient flow conditions. The technical basis for this assumption is that rock mass is characterized by a matrix and system of fractures. Under low flux and high absolute moisture potential, flux occurs through matrix. Under high flux and low absolute moisture potential, flux occurs through the fractures.

5.14 POTENTIAL FIELD THEORY FOR CLOSED FORM ANALYTICAL SOLUTION

The solution is based upon potential field theory (Phillip 1991, p. 67) that assumes a small perturbation in one part of the field will effect the entire field, not just a local area. The basis for this assumption is that the flow is irrotational with vorticity equal to zero (Phillip, p. 67). This assumption is used in Attachment IX.

5.15 WATER FLUX RATE UNDER STEADY-STATE CONDITIONS FOR A DEEP WATER TABLE

The water flux rate under a specified percolation rate for a deep water table occurs under steady-state conditions in which the flux rate equals the unsaturated hydraulic conductivity (Jury et al. 1991, p. 127). The basis for this assumption is that over the long term, an equilibrium in hydraulic potential will develop along the boundary of the inclusion with the surrounding host rock. This assumption is used in Attachment IX.

6. ANALYSIS/MODEL

The purpose of the water distribution and removal analysis is to quantify and evaluate the distribution of liquid water within the emplacement drift and its removal by drainage, to support the EBS post-closure performance assessment. The water distribution and removal analysis is supported by several submodels and analyses that provide inputs. These include the *Drift Degradation Analysis* (CRWMS M&O 2000a), the *Water Diversion Model* (CRWMS M&O 2000b), the *Water Drainage Model* (CRWMS M&O 2000c), the *In-drift Thermal-Hydrological-Chemical Model* (CRWMS M&O 2000d), and the *Ventilation Model* (CRWMS M&O 2000e). The inputs to these models are discussed subsequently.

The *Drift Degradation Analysis* (CRWMS M&O 2000a) provides information on the potential changes in drift geometry during the post-closure period. The change in drift profile resulting from progressive deterioration of the emplacement drifts was assessed both with and without backfill. Drift profiles were determined for four time increments, including static (i.e., at excavation, year 200, year 2,000, and year 10,000. The effect of seismic events on rock fall was analyzed. Block size distributions and drift profiles were determined for three seismic events, including a 1,000-year event, a 5,000-year event, and a 10,000-year event. It was found that the seismic effect on rock fall was relatively minor. Time-dependent and thermal effects have a minor impact on rockfall.

The worst-case drift degradation profiles show that the highest percentage of drift affected by rock fall was 16% in the Tptpmn unit. Lower percentages occur in the Tptpll unit (approximately 1%) which is the predominant unit at the repository horizon. The expected case for drift configuration is a 5.5 m circular emplacement drift.

The *Water Diversion Model* (CRWMS M&O 2000b) developed the hydrologic and thermal properties of the backfill, the invert, and a combined material immediately outside the drip shield. This submodel also developed flow properties for the drip shield for flow through the connector assemblies between the drip shield. The hydrologic and thermal properties of these EBS components are direct inputs to the water distribution and removal model.

The *Water Drainage Model* (CRWMS M&O 2000c) was based on unsaturated flow through porous media, using an implicit dual permeability model (DKM) with an active fracture concept (AFC) (Liu et al. 1998). This model is a 2D, steady-state model representative of the center of the repository with waste package heat neglected and seepage forced into the backfill from the top of the drift (i.e., infiltration equals seepage).

Under these conditions, the EBS successfully drained water entering the EBS for even extreme infiltration rates. However, if fractures below the EBS become clogged as a result of THC/THM processes or repository construction activities, the performance may be impaired. The water distribution and removal model considers the properties for reduced fracture permeability developed in the *Water Drainage Model* (CRWMS M&O 2000c) for a "focused glacial" infiltration rate (Assumption 5.7).

The *In-drift Thermal-Hydrological-Chemical Model* (CRWMS M&O 2000d) predicted the temperatures at the surface of the waste package, the drip shield, and the drift wall during the

post-closure period. Additionally, the flow of vapor and liquid components of water into the drift was analyzed and the condensation potential in the drift, particularly underneath the drip shield. The analysis found that condensation is not expected to form underneath the drip shield during a period of 10,000 years, and beyond. However, the analysis showed a potential buildup of relative humidity underneath the drip shield. The analysis showed a tendency for saturation levels to increase above the drip shield which is consistent with an analysis of drip shield water exclusion performed in the *Water Diversion Model* (CRWMS M&O 2000b). The results suggested evaluation of the influence of heating on the invert and backfill materials as addressed in this water distribution and removal model.

The *Ventilation Model* (CRWMS M&O 2000e) analyzed the effects of preclosure continuous ventilation in the Engineered Barrier System (EBS) emplacement drifts and provided heat removal data to support the EBS design. The submodel provided a general description of the heat transfer effects of preclosure ventilation. The submodel estimated temperatures, and the degree of heat removal. The submodel treats the emplacement drift as a series of drift segments. Thermal analysis is performed for each drift-section sequentially from the air-inlet to the air-exhaust of the drift. Then heat transfer processes for the entire drift can be evaluated through assembly and comparison of the results from individual segments. The rate of heat removal was developed for emplacement drift ventilation rates of 10 cms, and 15 cms. Heat removed by ventilation at the rate of 10 cms was calculated to be 68% of the heat generated after 50 years, 73% of the heat generated after 100 years, and 77% after 200 years. Heat removed by ventilation at the rate of 15 cms was calculated to be 74% of the heat generated after 50 years, 78% after 100 years, and 82% after 200 years. The results suggest that a high percentage of the heat can be removed during the preclosure period. In the water distribution and removal model, the analysis assumes 100% heat removal after 100 years. This assumption tends to underestimates the temperature rise, and the return of water after peak temperatures develop within the repository is sooner. It is conservative to assume isothermal temperature conditions for the purposes of water drainage (Assumption 5.8).

Inputs to this water distribution and removal model also include the unsaturated hydrologic and thermal properties of the EBS component materials (Section 4.1.2) and of the geologic formation around the drift (Section 4.1.1). The inputs also include the waste package (WP) geometry and thermal output data (Section 4.1.7). The inputs include the EBS geometry and hydrologic properties of the invert and backfill materials (Sections 4.1.1 and 4.1.2). As discussed below, the analysis includes an evaluation of the chemical alteration of individual components, and how such alteration could change the thermal-hydrologic performance.

The output of the analysis will be a documented method for evaluating the EBS performance under the THC environments that are expected to prevail in the selected License Application Design Selection (LADS) design for the potential repository. The analysis provides input to the *Physical and Chemical Environment Process Model*.

6.1 CONCEPTUAL MODEL

The EBS water distribution and removal model consists of the backfill within the drift, the drip shield below the backfill, the invert (Sections 5.1 to 5.3) and the surrounding fractured media at

the repository horizon. The EBS is designed to divert water flow to the invert (Figure 2). A conceptual model is developed for how water is partitioned in the drift. As water enters the drift and flows through the backfill, the water flow will be partitioned into (1) water flow through the drip shield that contacts the waste packages; (2) water flow that flows through the backfill directly to the invert; and (3) water flow that contacts the drip shield but does not flow through the drip shield.

As water is diverted from the drip shield, it flows to the invert. Because the welded tuff at the repository horizon consists principally of a freely draining system of vertical fractures in its natural state, the surrounding welded tuff has significant capacity to drain water in its natural state.
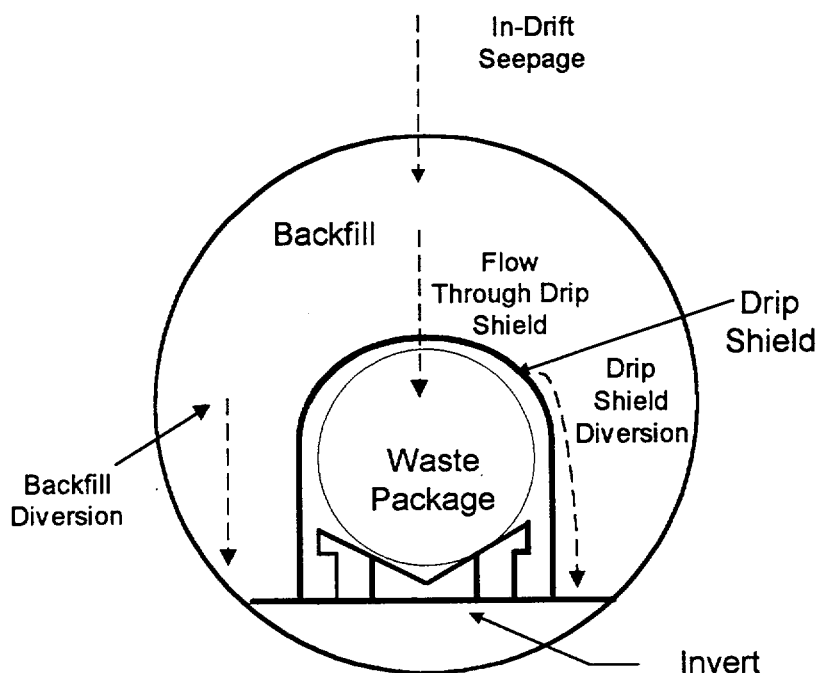
Figure 2. Conceptual Model for Diversion of Water Flow

6.1.1 Flow Focusing

An additional issue regarding flow under unsaturated flow conditions is the continuity of fractures. Because of variability encountered at the repository horizon, some fractures will exhibit vertical continuity while other fractures might not. The potential exists for local areas to exhibit reduced flow and increased saturation that would migrate laterally to other areas where increased flow would take place. In-drift seepage might increase locally due to an increased percolation rate.

6.1.2 Increased Backfill Saturation Levels Above the Drip Shield

Philip et al. (1989, pp. 16 to 28) present a model for unsaturated seepage in subterranean holes. It consists of analyzing the exclusion problem for cylindrical cavities. Philip et al. (1989, p. 16) present a general theory of water exclusion from or entry into cylindrical cavities from a steady vertical seepage under unsaturated conditions. It is known that the drip shield acts to exclude water. If the hydraulic potential is calculated based on the general theory of water exclusion, then the calculated water flow represents an upper bound to the hydraulic potential under ambient temperature conditions. This is because under static conditions of no flow, a maximum gradient would be maintained, while flow through the drip shield would tend to "draw down" the hydraulic potential, resulting in a reduced gradient.

The *Water Diversion Model* (CRWMS M&O 2000b, p. 36) provided an analysis of the drip shield for the Overton Sand backfill. The analysis showed that around the drip shield, the Kirschoff Potential is increased with a drip lobe forming to the side of the drip shield, and a dry shadow forming below the drip shield. The presence of the drip shield increases the moisture content everywhere outside the dry shadow above and to the side of the drip shield. Saturation levels are expected to increase above the drip shield with an increased potential for flow through the drip shield. The *In-drift Thermal-Hydrological-Chemical Model* (CRWMS M&O 2000d, p. 32) also concluded that there is a tendency for liquid saturation in the backfill to increase above the drip shield.

6.1.3 Floor Drainage and Performance of the Invert

During repository excavation, the in situ state of stress is relieved, and the potential exists for movement to occur due to elastic or elastoplastic deformation (Case and Kelsall, 1987, p. 1). The stress redistribution and TBM excavation combine to form a modified permeability zone that depends upon the in situ state of stress, rock deformational and strength properties. The drainage of the fractures might also be affected by rock fines resulting during TBM excavation. Further, during repository heating and cooling during the post-closure period, the potential exists for additional stress redistribution that would affect the retention and flow characteristics of the surrounding media. These combined effects result in alteration of the properties due to thermal and mechanical effects.

The effect of stress relief and dilatation on fractures would tend to result in an increase in the saturated hydraulic conductivity with an attendant reduction in retention characteristics. These combined effects may result in a lowering of unsaturated hydraulic conductivity. Rock fines resulting from TBM excavation will reduce the saturated hydraulic conductivity while increasing the retention characteristics of the fractures.

Other coupled processes (Hardin 1998 pp. 2-3) during the thermal period may significantly alter hydrologic properties that influence reflux activity and seepage. Because of mineral dissolution and precipitation reactions, and precipitation in response to the elevated temperature environment or evaporation, THC effects will cause alteration of flowpaths above and below the repository emplacement drifts.

The *In-drift Thermal-Hydrological-Chemical Model* (CRWMS M&O 2000d) modeled the open air void space inside the drip shield to evaluate the potential for convective and latent heat transfer from the invert to the drip shield. The model evaluated the tendency for liquid water to evaporate from the invert and to increase the relative humidity inside the drip shield. Latent heat transfer due to condensation on the inner surface might lower the temperature of the annulus to nearly that of the drip shield. If small temperature differences are maintained between the annulus and the drip shield, the rate of latent heat transfer rises rapidly.

The model results can be summarized as follows. Moisture conditions in the invert during the thermal period determine the potential for condensation under the drip shield. When the volumetric moisture content in the invert increases, the rate of evaporation increases (thermal output held constant). In the models developed for this report, the volumetric moisture content of the invert is directly related to the magnitude of the infiltration flux boundary condition. The increased evaporation increases the potential for mass transfer from the surface of the invert to the drip shield. As a limiting condition, condensation on the underside of the drip shield is unlikely unless the absolute humidity anywhere on the surface of the invert is equal to or greater than the absolute humidity corresponding to saturated humidity conditions at the drip shield temperature. This limiting condition relaxes the need for precise prediction of gas-phase water vapor transport under the drip shield, in order to predict conditions that could lead to condensation under the drip shield.

These studies suggest the importance of keeping the invert dry with a high moisture potential. If the natural variability of the rock mass results in the potential for a moist invert and potential evaporation, then engineering measures such as the construction of drains packed with sand may be necessary.

Moisture retention relationships based upon Unsaturated Flow Apparatus measurements have been developed (CRWMS M&O 1996) for moisture potentials greater than 100 cm. The results show that if the moisture potential exceeds 100 cm (Figure 3), the volumetric moisture content would be low, and the maximum potential evaporative flux from the invert directly below the drip shield would be dominated by capillary effects (Jury et al. 1991, p. 154). The curve in Figure 3 was constructed using a curve-fitting approach with the saturated volumetric water content set equal to the porosity (CRWMS M&O 2000b, Section 6.2.2.3 and Attachment IV).

6.2 DETAILED MODEL DESCRIPTION

In the following discussion, a water distribution and removal model based upon a NUFT analysis, which is based upon isothermal and elevated temperature conditions, is developed. For the isothermal runs, the current model conservatively assumes that peak temperatures due to the waste package heat loading have occurred in the repository, and that water flow under unsaturated conditions occurs to the drift under isothermal conditions (Assumption 5.8). To cover a broad range of conditions that might be encountered in the surrounding fractured media, the fractured tuff media is assumed to be undisturbed, which would provide optimal performance. Two scenarios are developed for plugging below the invert, and the EBS as discussed subsequently to cover the range of conditions for plugging (Assumption 5.5).

The following sections describe the detailed numerical modeling approach using NUFT, the model domain, and hydrologic properties of the fractures. Further, the model boundary conditions, and infiltration are described. Also, the following discusses the inputs from the several submodels and analyses used to support this water distribution and removal model.
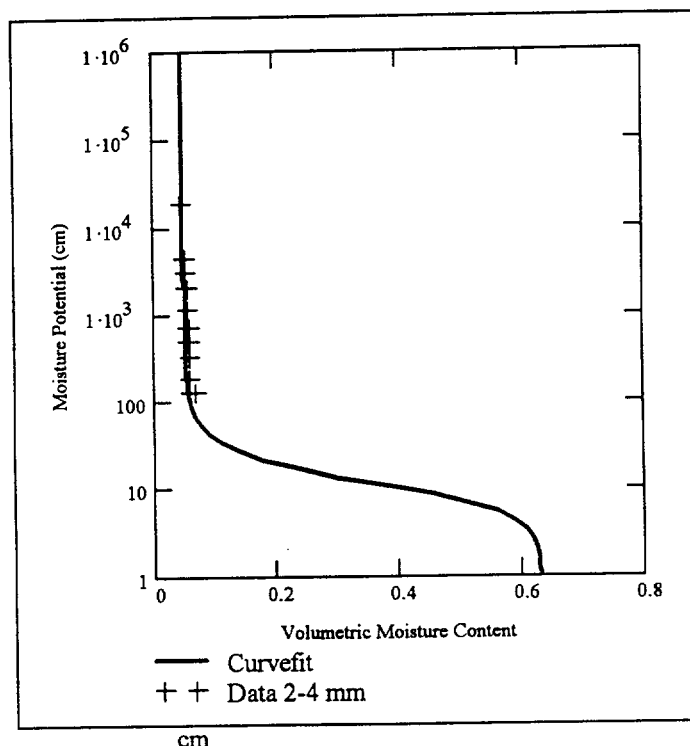
Figure 3. Moisture Retention Relationship for the Invert

6.2.1 Model Geometry for the NBS and EBS

The repository block model (Attachment I) is represented by a rectilinear array of 31 "chimney" locations, or columns of rock. Each location has a unique identifier, e.g. L4C4, which signifies the 4th row and the 4th column in the array. The locations of these columns are described in Attachment II. The L4C4 location is near the center of the repository layout, where the infiltration flux and rock properties are typical of much of the repository area. A lithostratigraphic column was developed for the L4C4 column with coordinates Easting 170500.3 and Northing 233807.3 (Attachment II) by the preprocessing software YMESH V.1, which develops the lithostratigraphic cross section (Table 11) from the computer file LBL99-YMESH (Attachment VIII) based upon the source data from UZ (unsaturated zone) site scale model (Section 4.1.1). The repository is located at a depth of 343.131 m in the TSw35 unit that corresponds to the Tptpll unit.

The EBS model geometry is developed from the License Application Design Selection (LADS) EDA-II (Wilkins and Heath 1999). The EBS model geometry and other in drift data is from Section 4.1.1.

Because of symmetry, a two-dimensional model of NUFT is constructed to include only half of the waste package and the drift spacing (40.5 m) according to the Enhanced Design Alternative (EDA) II design (Wilkins and Heath 1999) and the two vertical edges are treated as no-flow boundaries (Section 5.10). The model extends from the ground surface to the water table about 340 m below the repository invert level (CRWMS M&O 1997). A simulation grid for the entire section is presented in Figure 4, with the spacing varying from 0.02 to 45.0 m. Figure 5 is a section of the emplacement drift with the drip shield and waste package in place. A corresponding model grid (derived from the main grid) that represents the drift with various EBS components is also shown in Figure 5.

Table 11. Hydrostatigraphy for L4C4

Model Unit	Thickness (m)
tcw11	33
tcw12	89
tcw13	5
ptn21	6
ptn22	3
ptn23	2
ptn24	7
ptn25	14
ptn26	16
tsw31	2
tsw32	42
tsw33	89
tsw34	30
tsw35	112
tsw36	27
tsw37	14
tsw38	23
tsw39	4
ch1VI	10
ch2VI	0
ch3VI	0
ch4VI	0
ch5VI	0
ch1Ze	0
ch2Ze	14
ch3Ze	14
ch4Ze	14
ch5Ze	14
ch6	20
pp4	8
pp3	34
pp2	15
pp1	61
bf3	17
bf2	0
Total	739

Source: Attachment VIII file: l4c4.col.units
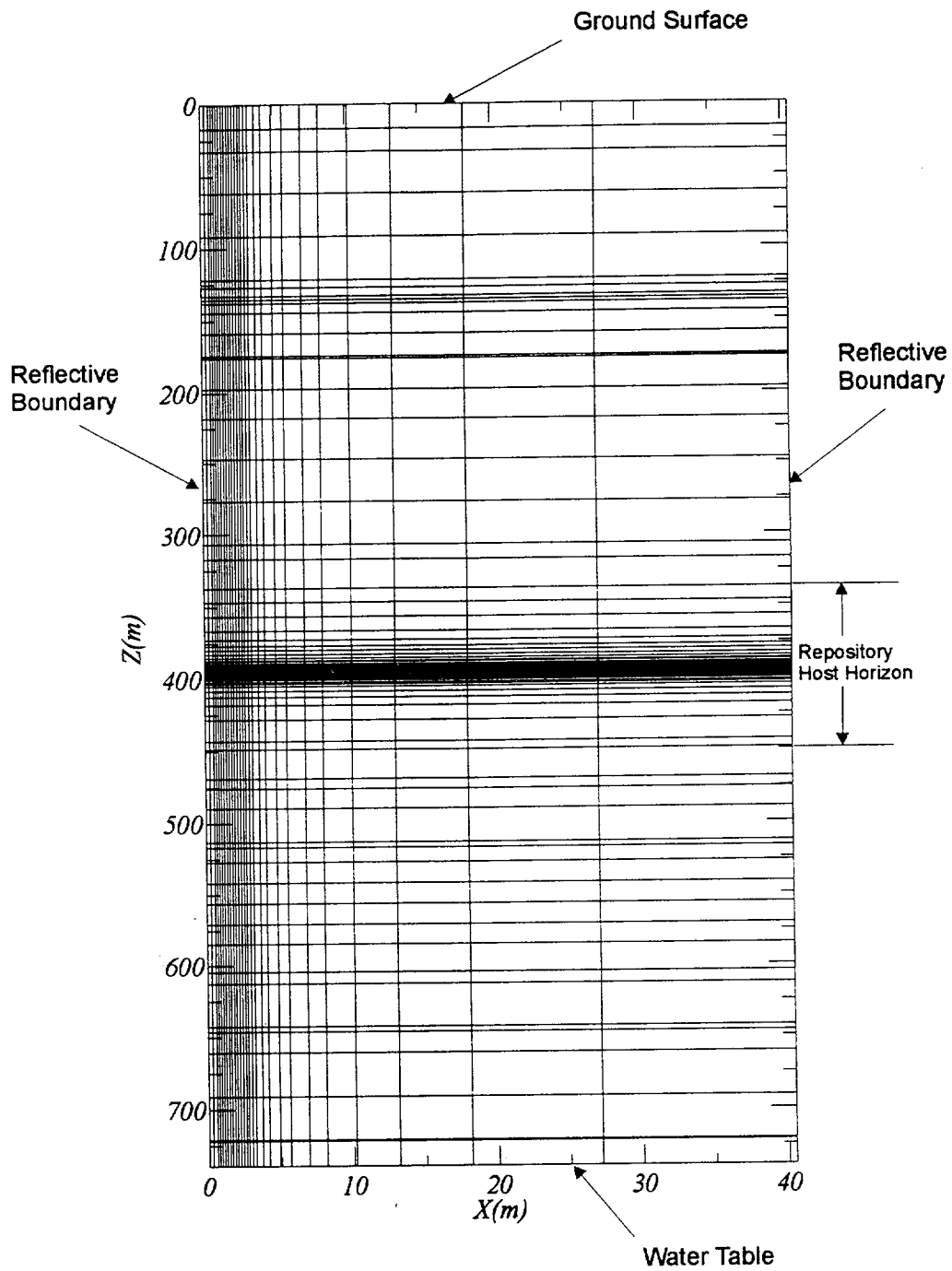
Figure 4. Model Domain and Boundary Conditions
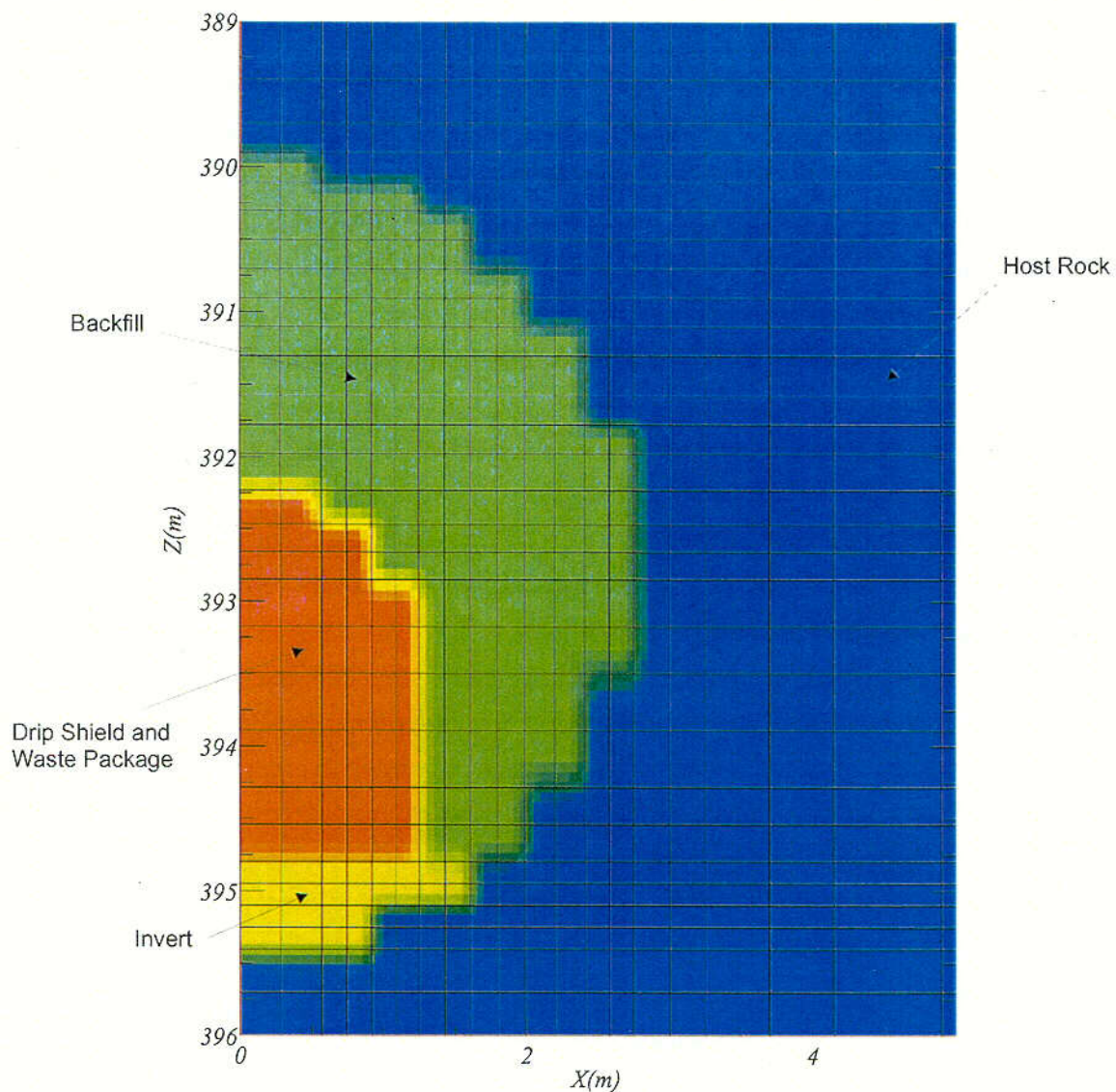
Figure 5. Engineered Barrier Segment Block Model

6.2.2 Temperature and Pressure Boundary Conditions

The temperature and pressure boundary conditions for the L4C4 chimney were obtained from the output of Chem_Surf_TP V1.1 as detailed in Attachment III. The source data for inputs to the Chem_Surf_TP V1.1 is from Section 4.1.1 (DTN LB99EBS1233129.003). Table 12 presents the ground surface and water table conditions used in the model.

CO1

Table 12. Ground Surface and Water Table Conditions

Temperature at ground surface	15.91 °C
Pressure at ground surface	0.845e5 Pa
Temperature at water table	32.54 °C
Pressure at water table	0.92e5 Pa

Source: Attachment VIII file: outpt and outpt_wt

6.2.3 Active Fracture Model and Inverse Modeling of NBS Properties

The unsaturated zone at Yucca Mountain is a complex hydrologic system in which a variety of important flow processes is involved. Liu et al. (1998, pp. 2633-2646) developed an active fracture model for unsaturated flow. The active fracture model assumes that only a fraction of the connected fractures is active in conducting water. In previous analyses, Liu et al. (1998, p. 2633) estimated that only 18% to 27% of the fractures actively flow water.

Section 4.1.2 presents hydrologic and thermal properties for the model units listed in Table 11. These data were developed from an inverse modeling technique. Fracture porosity, matrix porosity, tortuosity factor (Section 5.4), fracture bulk permeability, matrix bulk permeability, maximum and residual saturation in fractures, maximum and residual saturation in matrix, van Genuchten parameters α and m for fractures, van Genuchten α and m for matrix, fracture porosity, and matrix porosity are used in the analysis. The following provides a discussion of the active fracture model.

The fraction of active fractures, f_a is determined by flow and transport conditions, and the fractured rock properties. The value for f_a should satisfy several conditions: (1) all connected fractures are active if the system is fully saturated; (2) all fractures are inactive ($f_a = 0$) if the system is at residual saturation; and (3) f_a should be related to the water flux in fractures (i. e. the greater the water flux, the greater the active fracture participation). Liu et al. (1998, p. 2636) suggested the expression:

$$f_a = S_e^{\gamma}$$
(Eq. 1)

where γ is a positive constant depending on properties of the corresponding fracture network, and the effective water saturation in connected fractures (S_e) is given by:

$$S_e = \frac{S_f - S_r}{1 - S_r}$$
(Eq. 2)

where S_f is the water saturation of all connected fractures and S_r is the residual fracture saturation.

Liu et al. (1998, p. 2636) suggest an approach for modeling constitutive properties in connected fractures with a homogeneous continuum. Under the assumption that the active and inactive

fractures have the same residual saturation, the effective saturation of active fractures S_{ae} is related to the effective water saturation in connected fractures S_e by:

$$S_{ae} = \frac{S_e}{f_a}$$

(Eq. 3)

Substituting Equation 1 into Equation 3 yields:

$$S_{ae} = S_e^{1-\gamma}$$

(Eq. 4)

Liu et al (1998) develops the capillary pressure for fractures in a continuum by:

$$P_c(S_e) = \frac{1}{\alpha} \cdot \left[S_e^{\frac{(\gamma-1)}{m}} - 1 \right]^{\frac{1}{n}}$$

(Eq. 5)

where alpha (α), n and m = 1-1/n are the van Genuchten parameters. Figure 6 presents a plot of Equation 5 for various values of the active fracture parameter gamma (γ). For a given effective saturation in the connected fractures, a larger value of γ corresponds to a larger effective water saturation in the active fractures, and therefore a capillary pressure curve that shows less retention.

The liquid-phase relative permeability for the active fracture continuum k_{ar} is directly determined by the effective water saturation of active fractures. To account for the proportion of fractures that are active, the relative permeability of the active fractures is multiplied by f_a (Liu et al. 1998, p. 2636). Liu developed the following van Genuchten permeability relation based on the Mualem model:

$$k_r = S_e^{\frac{(1+\gamma)}{2}} \cdot \left[1 - \left[1 - S_e^{\frac{(1-\gamma)}{m}} \right]^m \right]^2$$

(Eq. 6)

where k_r is the relative permeability of the entire fracture continuum, and the value should be the relative permeability of active fractures (k_{ar}) multiplied by f_a.

In developing hydrologic properties for the NUFT water distribution and removal model, the drift scale properties set was adopted from inverse modeling (Section 4.1.2). The drift scale properties set included a modification to the properties of the welded tuff units at the repository horizon as discussed below.

The *Calibrated Properties Model* (CRWMS M&O 2000f, p. 31) describes the process for selecting the fracture and matrix properties presented in Section 4.1.2. The properties sets determined in the *Calibrated Properties Model* are used by several thermal-hydrological models such as the *Unsaturated Zone Flow and Transport Model* (CRWMS M&O 2000g) and the
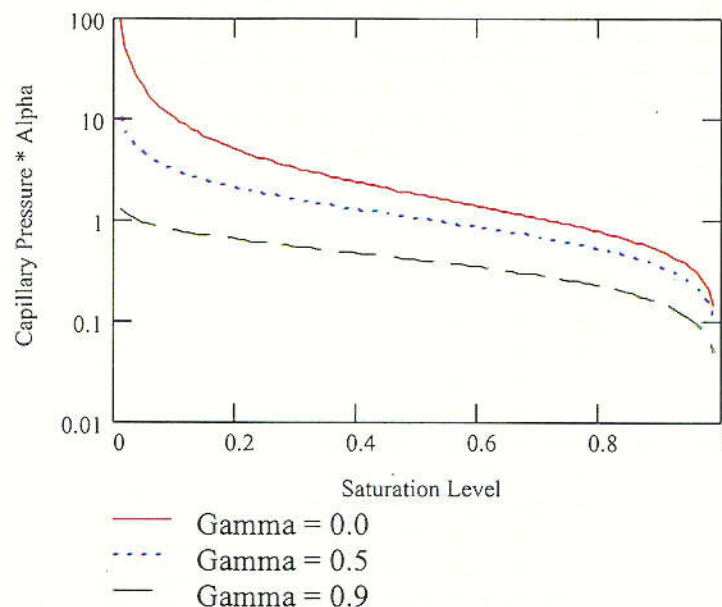
Figure 6. Influence of the Parameter Gamma on Retention

Multiscale Thermohydrologic Model (CRWMS 2000h) on the Yucca Mountain Project. These hydrological properties set are applied to the water distribution and removal model.

The calibration of the properties sets are carried out in a series of steps. One dimensional vertical-column submodels are used for the calibration of the rock mass (nonfault) parameters for the drift-scale conceptual models. The one-dimensional submodels correspond to 11 surfaced-based boreholes from which saturation, water potential, and pneumatic pressure have been measured (CRWMS M&O 2000f, p. 32).

The software ITOUGH2 V3.2 is used in the *Calibrated Properties Model* (CRWMS M&O 2000f) to carry out the automatic portion of the inversion process. This analysis method not only allows the consideration of both data and prior information, but also allows them to be weighted. The data and prior information are weighted according to the uncertainty of the estimated values. The analysis method attempts to minimize the sum of the squared, weighted residuals for the objective function. When the objective function reaches a minimum, the resulting parameter set is judged to be the best estimate of hydrological parameters.

For certain cases supporting this water distribution and removal model, the fracture permeability was set equal to the matrix permeability (as discussed in Section 6.3.3) to investigate the effects of plugging on flow distribution. It should be noted that the temperature and pressure boundary conditions, and the stratigraphic contact elevations used in the NUFT calculations for this model differ from the values used in the TOUGH2 V1.4 calculations in the *Unsaturated Zone Flow and Transport Model* (CRWMS M&O 2000g). The locations used for the NUFT calculations do not coincide exactly with the locations used for the TOUGH2 calculations. Importantly, the boundary conditions and stratigraphic contacts are based on the *Unsaturated Zone Flow and Transport Model* by direct interpolation from TOUGH2 output files for the three-dimensional

C02

unsaturated zone model. This process is documented in the *Multiscale Thermohydrologic Model* (CRWMS 2000h, p. 62).

As a result of inverse modeling, the site-scale fracture permeabilities in most of the TSw model layers were increased by almost two orders of magnitude, compared with the prior information determined from the air injection tests. This was mainly because pneumatic data result from the mountain-scale gas flow processes, while air injection tests correspond to scales on an order of several meters or less.

It is well documented in the literature that large-scale effective permeabilities are generally larger than smaller scale ones (Neuman, 1994). An intuitive explanation for this scale-dependent behavior is that at a large observation scale, in an average sense, corresponds to a larger opportunity to encounter more permeable zones or paths when observations are made, which considerably increases values of the observed permeability. Because of this scale difference, site-scale fracture permeabilities, determined from the pneumatic inversion, cannot be directly applied to the drift-scale. Therefore, development of drift-scale properties was needed.

Unlike the connected fracture networks and soils, studies on the scale-dependent behavior of matrix properties in unsaturated fractured rocks are very limited. However, it is reasonable to consider that the scale-dependent behavior of the matrix is different from fracture networks. For example, relatively large fractures can act as capillary barriers for flow between matrix blocks separated by these fractures, even when the matrix is essentially saturated (capillary pressure is close to the air entry value). This might limit the matrix scale-dependent behavior to a relatively small scale associated with the spacing between relatively large fractures.

The evidence suggests that the matrix properties are the same for both the site and drift scales. The inversion results for the site-scale matrix permeabilities are comparable to prior information developed on the project.

Based upon the preceding discussion, the drift scale property set used in the NUFT water distribution and removal model, included modification of the fracture permeabilities near the repository horizon (layers TSw32-37) while other properties were unchanged.

The thermal conductivity parameters for the NBS system shown in Table 6 were based upon laboratory measurements for welded and nonwelded tuff (Brodsky et al. 1997, pp. 27-34) that was a direct application of Fourier's Law of Heat Transfer (Brodsky et al. 1997, p. 11). The measurements included variations in thermal conductivity due to variations in temperature, and moisture saturation levels for welded and nonwelded tuff sampled from the major thermal mechanical units. The saturation levels included oven dry and saturated conditions.

Since measurements were made for selected units, and other information was available on porosity, and saturation levels for various thermal mechanical units, a multiple linear regression analysis was applied to these data, and a general multiple linear predictive equation was developed. This equation was then used to predict thermal conductivity for the various hydrologic units listed in Table 6. Figure 7 presents a figure showing the relationship of thermal

conductivity under saturated conditions for the major stratigraphic units as a function of porosity for comparison to other measurements reported (Bear 1988, p. 650).

The experimental technique for oven dry conditions was validated by measurement of the thermal conductivity of glass of known thermal conductivity (Brodsky et al. 1997, p. 11). It should be noted that while the experimental technique was applied to the porous tuff that constitutes a wetting material, the glass is considered a nonwetting material. In the measurements made, a higher degree of confidence exists in the oven dry measurements.

Heat energy may be transported through a porous media by a number of different mechanisms (Jury et al. 1991, p. 173). In addition to conduction through stationary components, heat may be transferred by radiation, convection of heat by flowing water, convection of heat by moving air, and convection of latent heat. The two most important processes of heat transport in porous media include conduction, and convection of latent heat. Latent heat if present would tend to increase the apparent thermal conductivity from a direct application of Fourier's Law.

In the NUFT calculations presented in this AMR, the thermal conductivity of the NBS is based upon the multiple linear regression analysis that in turn is based upon the measurement of thermal conductivity through a direct application of Fourier's Law. The thermal properties are assumed to apply to the stationary components for tuff, and water (Assumption 5.9). The technical basis for this assumption is that the measured data as presented in Figure 7 are in general agreement with values reported in the literature (Bear 1988, p. 650). The wet thermal conductivity of the more porous nonwelded PTn tuff are higher than the less porous welded TSw2 tuff.

In the thermal-hydrological analysis presented in this AMR, the assumption presented above does not need confirmation because as discussed subsequently in Section 6.3.2, the effects of repository heating are to reduce the water flow rates through and around the EBS. The NUFT analysis based upon these properties for the cases of repository heating will conservatively overestimate water flow rates or the refluxing of water to the repository horizon after the thermal pulse has occurred. This is because if the functional dependence of thermal conductivity on saturation is weaker, then the thermal conductivity, and in turn the thermal diffusivity are lower. This in turn would result in a higher temperature environment which would tend to result in lower saturation levels, and a reduced water flux rate.

6.2.4   Hydrologic and Thermal Properties of the EBS

This water distribution and removal model presents a discussion of the geotechnical and hydrologic properties for the backfill, the invert, and the combined material (Section 6.1.1). The source data for the properties is presented in Section 4.1.3. The drip shield was modeled as an impermeable material (Section 5.2). The hydrologic and thermal properties for the NUFT water distribution and removal model include the dry bulk density and porosity, the moisture retention, the intrinsic permeability, the relative permeability and the material thermal properties.
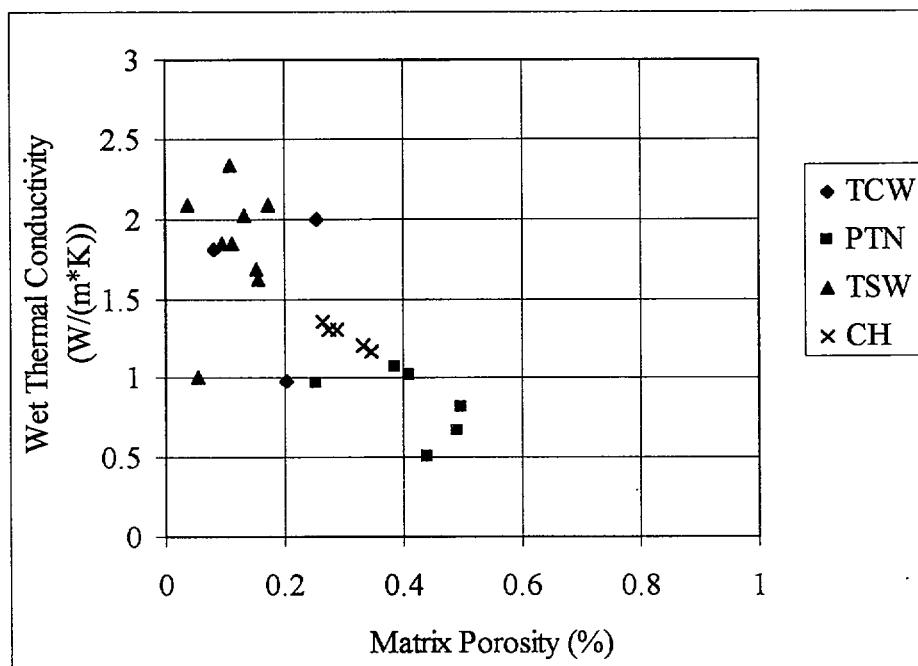
DTN: LB990861233129.001

Figure 7. Relationship of Wet Thermal Conductivity for Tuff to Matrix Porosity

6.2.5   Infiltration

The infiltration data for the UZ site scale model (MO9911MWDEBSWD.000), presented in Section 4.1.4, was used to derive the infiltration input for the analyses. Calculations of the infiltration rate input from the source data are presented in Figure 1 and Attachment VI.

The present day, monsoon, and glacial infiltration rates are calculated in Attachment VI. As presented in Table VI-1 for the chimney location L4C4, the mean glacial infiltration rate is 42 mm/yr.

Given the glacial infiltration rate of 42 mm/yr, drift diameter of 5.5 m (Section 4.1.3) and a drift spacing of 81 m (Section 4.1.4), the focused glacial infiltration rate is calculated as follows (Assumption 5.7):

$$42 \text{ mm/yr} * 81\text{m} * 90\% / 5.5\text{m} = 557 \text{ mm/yr}$$

The infiltration rate assumed for the area from the drift is then:

$$42 \text{ mm/yr} * 81\text{m} * 10\% / (81\text{m} - 5.5\text{m}) = 4.5 \text{ mm/yr}$$

6.2.6 Waste Package Heat Loading

The main purpose of this report is to predict flow into various EBS components of the drift during the cooling phase of the repository, the first 100 years of thermal loading was ignored in the analyses (Assumption 5.8). This is done to decrease the turnaround time of the production runs. The impact of this assumption is to under estimate temperature, but over estimate the refluxing of water to the repository during the post closure period.

The initial linear heat load for various types of spent fuel are presented in Attachment VII based upon the source data for, waste package length and diameter (Section 4.1.7.1), number of waste packages (Section 4.1.7.2), and the initial heat generation rate of waste packages (Section 4.1.7.3). An average initial linear heat load of 1.547 kW/m was calculated based upon the total heat output, total drift length, and thermal decay data (Section 4.1.7.3). The linear heat load estimated for various times up to 100,000 years were calculated based upon the initial heat load (1.547 kW/m) and the thermal decay percentage (Attachment VII, Table VII-2).

6.2.7 NUFT Model Input Preparation

The NUFT model input included a grid, initial conditions and materials properties files based upon the model geometry, initial boundary conditions, and hydrologic and thermal properties presented previously. In the dual permeability model, the entire model domain is represented by both fracture and matrix continua. For the backfill and invert, permeability and total porosity are allocated equally to these continua (i.e., the same values are used for both backfill and invert, and the sum of the values for each property equals the bulk value), and the parameters that control the interaction between continua are set to values that ensure moisture potential equilibrium. In addition, the NUFT computer code uses accepted data (Sections 4.1.5 to 4.1.6) for fluid and thermodynamic properties of water and air.

6.3 SUMMARY OF PARAMETRIC STUDIES PERFORMED

Table 13 summarizes the following parametric studies performed using the active fracture model option in NUFT 3.0S for the water distribution and removal model. The glacial infiltration rate was adopted, as this rate provides a bound to infiltration. Analyses were performed using the glacial climate for uniform and focused flow at ambient temperature and under heated conditions without fracture plugging (Cases 1 to 4). After completion of the 4 runs listed above, analyses were then performed for the glacial climate for uniform and focused flow (Assumption 5.6) under ambient temperature for the fracture plugging scenario (Cases 5 and 6). The plugging scenario included plugging of fractures below the drift out to 3 meters into the rock (Assumption 5.6). To assess the influence of a sand drain, a run was made under the assumption that a drain extends approximately 6 meters below the invert, and is backfilled with same material used over the drip shield (Case 9).

After the initial assessment, an additional run (Case 10) was made with a vertical sand drain to demonstrate how sand drains would enhance the performance of the EBS system under an unplugged condition.

The total water flow through the invert was determined by an integration of the water flux over (1) the invert directly below the drip shield, and (2) the invert zone adjacent to the drip shield as discussed subsequently in Section 6.3.6.

6.3.1 Base Case and Flow Focusing

The results of the NUFT analysis for the water distribution and removal model for the base case of focused flow at isothermal temperature are presented in Figures 8 to 11 for the absolute value of the matrix capillary pressure (Pa), fracture mass flux rates (kg/(s-m^2)), and fracture and matrix saturation levels. Note that to convert an absolute capillary pressure in Pa to a moisture potential in cm, divide the capillary pressure by 98.14. This conversion factor is derived as follows. From Jury et al. (1991, p. 49), the moisture potential equals:

$$\psi = \frac{Pw}{\rho_w * g}$$

(Eq. 7)

Table 13. Summary of Parametric Cases for the Water Distribution Model

| Case Number | Infiltration Rate | | | Focusing | | Heating | | Plugging | | Design | |
	Glacial	Monsoon	Current	Uniform	Focused	Ambient	Elevated	None	Plugged	No Sand Drains	Sand Drains
1	X				X	X		X		X	
2	X			X		X		X		X	
3	X				X		X	X		X	
4	X			X			X	X		X	
5	X				X	X			X	X	
6	X			X		X			X	X	
7	X				X		X		X	X	
8	X			X			X		X	X	
9	X				X	X			X		X
10	X				X	X		X			X
11			X		X	X		X		X	
12			X	X		X		X		X	
13			X		X	X			X		X
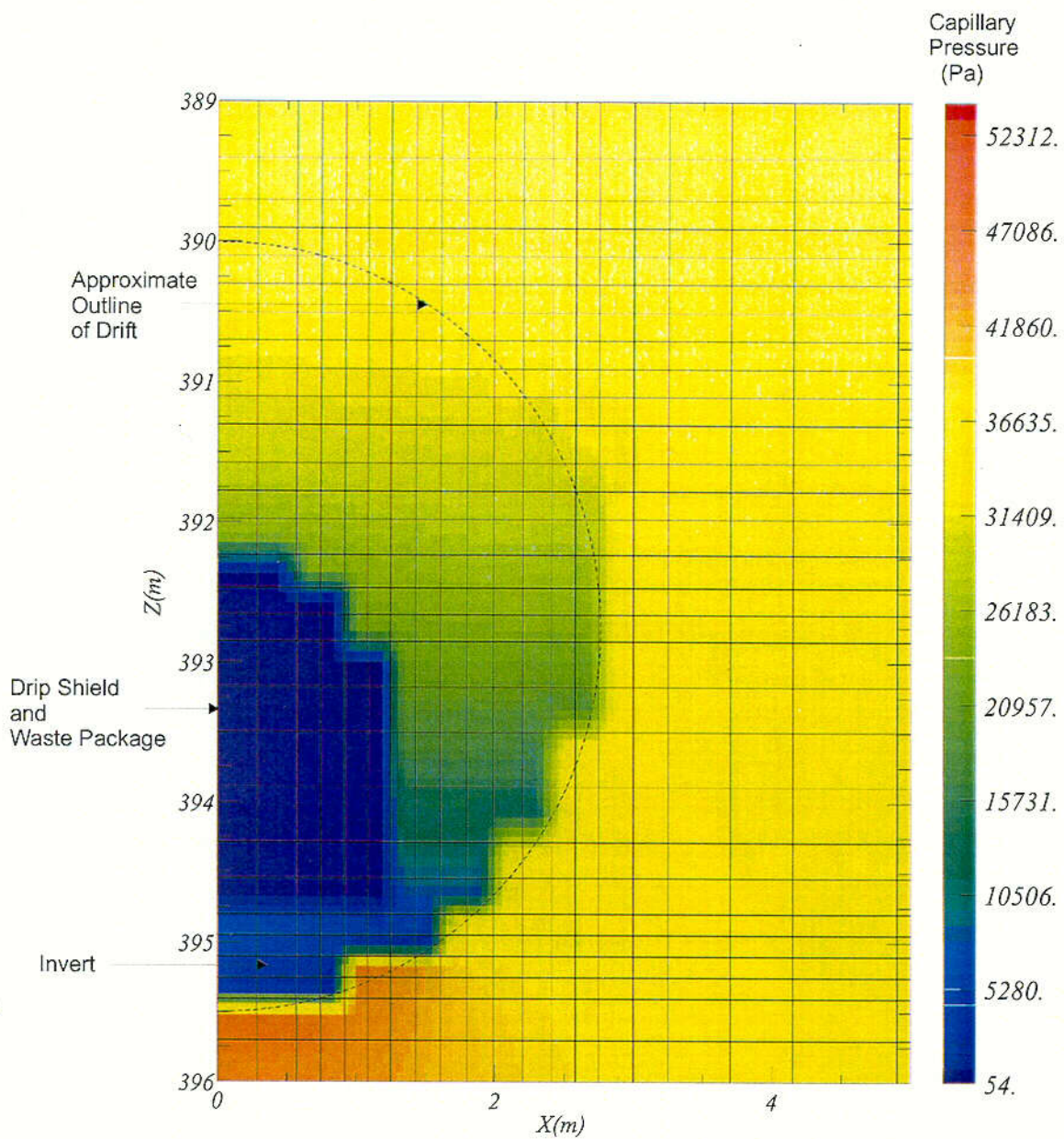
Figure 8. Absolute Matrix Capillary Pressure for Focused Flow at Steady State at Isothermal Temperature Near the Repository Horizon (Case 1)

C03

C 04
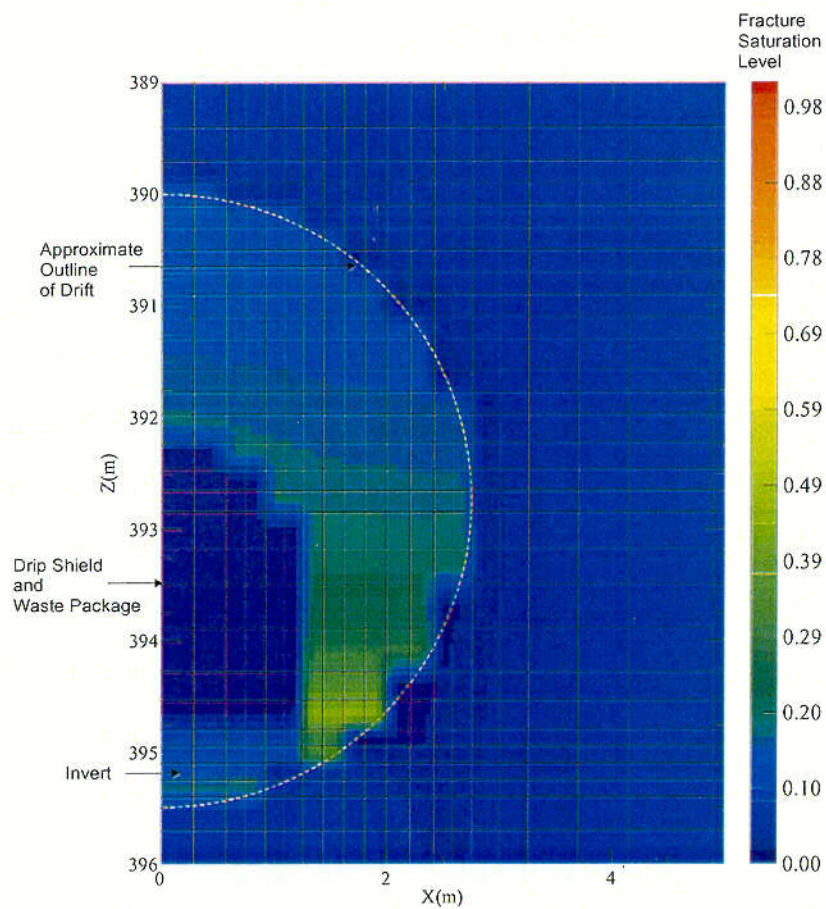
Figure 9. Fracture Saturation Levels for Focused Flow at Steady State at Isothermal Temperature Near the Repository Horizon (Case 1)
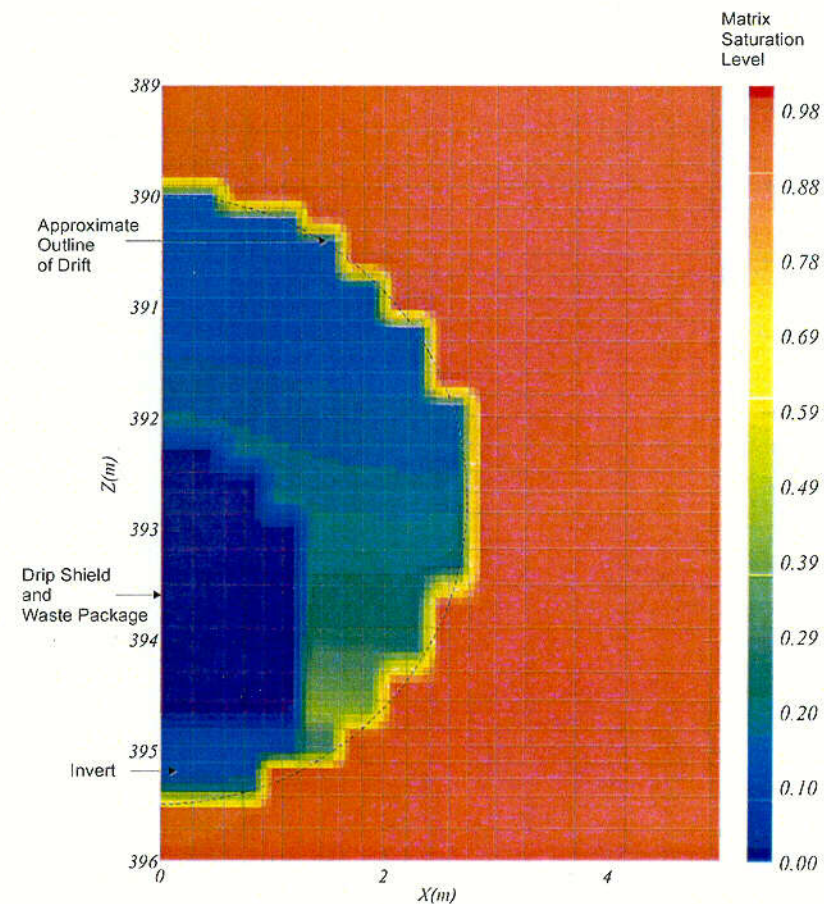
Figure 10. Matrix Saturation Levels for Focused Flow at Steady State at Isothermal Temperature Near the Repository Horizon (Case 1)
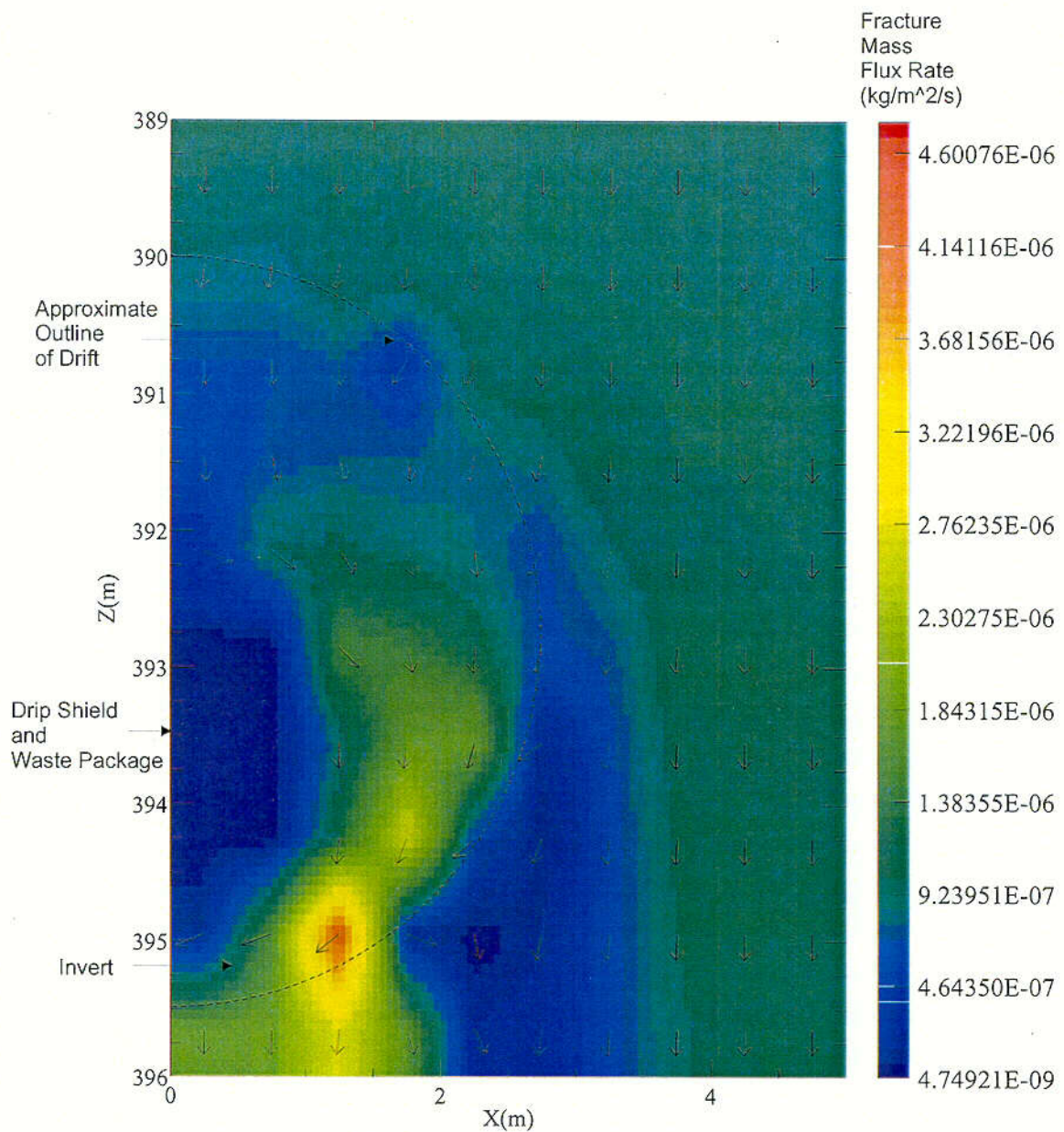
Figure 11. Fracture Mass Flux Rates (kg/m²-s) and Direction of Flow for Focused Flow at Steady State at Isothermal Temperature Near the Repository Horizon (Case 1)

C05

$$\psi = 1 * \left(\frac{N}{m^2}\right) \frac{1}{1.0 * \frac{gm}{cm^3} * 98.14 * \frac{cm}{s^2}} = \frac{10000 * \frac{gm*cm}{s}}{10000 * \frac{cm^2}{m^2} * \frac{gm}{cm^3} * 98.14 * \frac{cm}{s}} = \frac{cm}{98.14}$$

To convert the mass flux rate expressed in (kg/(s-m^2)) at ambient temperature to a volumetric flux rate, divide by the mass density of water:

$$J_w = 1 * \frac{kg}{s*m^2} * \frac{1}{\frac{1000*kg}{m^3}} * 1000 * \frac{mm}{m} * 3.1557 * 10^7 * \frac{s}{yr}$$

To convert from a mass flux rate in kg/(s-m^2)) to a volumetric flux rate in mm/yr, multiply by $3.1557*10^7$.

The capillary pressure distribution from the first case or base case shows that within the drift, the absolute value of the backfill capillary pressure (moisture potential) above the drip shield ranges from approximately 36,000 Pa (370 cm) in the rock matrix above and adjacent to the drift to 22,000 Pa (220 cm) within the drift above the drip shield. Saturation levels are elevated immediately the above drip shield relative to the rock matrix. These changes are similar to the change in moisture potential predicted above the drip shield in the backfill in the *Water Diversion Model* (CRWMS M&O 2000b, p. 36) based upon a closed form solution for the Kirchhoff potential around a cylindrical cavity. In that analysis, the exponential representation of the unsaturated hydraulic conductivity curve was used in conjunction with a percolation rate of 25 mm per year while this analysis is based upon a somewhat higher percolation rate, and the van Genuchten relations for moisture retention and unsaturated hydraulic conductivity of the backfill.

Below the drip shield, the absolute value of the capillary pressure is increased from approximately 36,000 Pa (370 cm) to approximately 50,000 Pa (510 cm). As predicted by the conspectus and exclusion analysis for cylindrical cavities (Philip et al. 1989, p. 21), a "dry shadow" forms below the drip shield in which the absolute value of the capillary pressure is increased and the saturation levels are reduced.

Further, Figure 11 illustrates that the fracture mass flux rates (volumetric flux rate) are increased adjacent and somewhat below the drip shield to an approximate maximum value of 4.6 * 10^{-6} kg/m^2-s (145 mm per year). These values are in qualitative agreement with the prediction of a "roof drip lobe" as illustrated in the *Water Diversion Model* (CRWMS M&O 2000b, Figure 16). As discussed by Philip et al. (1989, p. 25), a roof drip shield lobe is defined more precisely in terms of the downward mass flux rate that expresses the deflection sideways from the drip shield produced by the runoff of water unable to penetrate the drip shield.

The NUFT analysis results using the active fracture concept for the selected fracture and matrix constitutive properties show in Figure 10 that the matrix saturation levels are high (exceeding approximately 0.90), while fracture saturation levels (Figure 9) are near the residual saturation level. Unsaturated flow is dominated by fracture flow in the surrounding media as the matrix exhibits low unsaturated hydraulic conductivity for the glacial climate percolation rate.

The analysis in the base case assumed that 90 percent of the infiltration flux of 42 mm per year was concentrated over the centerline of the drift at the ground surface with the remaining 10 percent applied uniformly at the ground surface (Section 6.2.5). The fracture and matrix mass flux rates for Cases 1 and 2 at three horizons above the repository, and at three locations within each horizon, are presented in Tables 14 and 15. In Case 2, the infiltration flux was applied uniformly at the ground surface. A comparison of the capillary pressures, saturation levels, and mass flux rates between the two cases (Tables 14 and 15) shows that the flow regime is nearly identical, and flow focussing is not significant at the repository horizon.

Table 14. Fracture Mass Flux Rate

| Direction of Mass Flux | Depth (m) | Horizontal Distance from Center Line (m) | | | | | |
| | | 5.27 | | 15.65 | | 33.82 | |
		Case 1	Case 2	Case 1	Case 2	Case 1	Case 2
Fracture Mass Flux Rate (Kg/m^2/sec) in the Horizontal Direction	100	9.70E-08	4.60E-21	2.80E-10	0.00E+00	9.10E-12	1.20E-21
	200	2.30E-10	7.40E-20	3.50E-10	1.80E-19	1.20E-10	9.00E-20
	350	1.80E-10	2.40E-15	2.90E-10	5.00E-15	9.90E-11	2.00E-15
Fracture Mass Flux Rate (Kg/m^2/sec) in the Vertcal Direction	100	2.00E-06	1.30E-06	6.30E-08	1.30E-06	1.40E-08	1.30E-06
	200	1.20E-06	1.30E-06	1.20E-06	1.30E-06	1.10E-06	1.30E-06
	350	1.20E-06	1.30E-06	1.20E-06	1.30E-06	1.10E-06	1.30E-06

Table 15. Matrix Mass Flux Rate

| Direction of Mass Flux | Depth (m) | Horizontal Distance from Center Line (m) | | | | | |
| | | 5.27 | | 15.65 | | 33.82 | |
		Case 1	Case 2	Case 1	Case 2	Case 1	Case 2
Matrix Mass Flux Rate (Kg/m^2/sec) in the Horizontal Direction	100	2.50E-12	3.70E-23	1.20E-12	6.70E-23	1.90E-13	1.40E-24
	200	3.90E-10	1.60E-18	8.20E-10	3.90E-18	3.50E-10	1.90E-18
	350	6.00E-11	1.10E-14	1.20E-10	1.60E-14	4.90E-11	2.80E-15
Matrix Mass Flux Rate (Kg/m^2/sec) in the Vertcal Direction	100	1.00E-09	1.00E-09	9.90E-10	1.00E-09	9.90E-10	1.00E-09
	200	3.50E-08	1.00E-09	3.40E-08	1.00E-09	3.30E-08	1.00E-09
	350	3.50E-08	1.00E-09	3.50E-08	1.00E-09	3.40E-08	1.00E-09

6.3.2 Repository Heating

The results of the NUFT analysis (Case 3) for the water distribution and removal model for the case of focused flow with repository heating after 1,000 years are presented in Figures 12 to 15 for the absolute value of the matrix capillary pressure (Pa), fracture mass flux rates (kg/(s-m^2)), and fracture and matrix saturation levels. These figures can be compared to the base case. The effects of repository heating for the waste package initial heat loading (Section 4.1.7.2) for the waste package heat decay rates (Section 4.1.7.3) after 100 years results in a reduction in the liquid mass flux rate into the drift.

The effects of heating results in a reduction in saturation levels with an increase in the absolute value of capillary pressure for liquid water during this period that results in a reduction in permeability of the backfill, and a reduction in the liquid mass flux rate through the backfill. During the period of from 100 to 1,000 years, peak temperatures are reached within the backfill.

The liquid saturations in the fractures and matrix within the WP are preset, initial conditions rather than results of analyses. The saturation in matrix is set different from that in the fractures to facilitate numerical convergence. As the permeability of the WP (lumped with the drip shield as a monolithic form) is assigned as zero, there is no flow into and out of the WP and, therefore, the saturation within the WP will remain the same as the initial conditions.

After a period of 1,000 years, there is refluxing of water to the EBS. The results show that the absolute values of the capillary pressures and saturation levels within the EBS are of comparable magnitude. The absolute value of the capillary pressures in the backfill is increased due to repository heating and reflects a reduction in saturation levels. Table 16 presents a summary of capillary pressures at various locations at different times. A comparison of the mass flux rates within the drift shows some reduction in backfill percolation rates immediately above the drip shield (7*10^{-7} kg/(m^2-sec) versus 13*10^{-7} kg/(m^2-sec)).

The results of the analysis for the case of uniform flow with repository heating (Case 4) is very similar to the case of focused flow with repository heating (Case 3). As discussed previously in comparing the cases of focused and uniform flow at ambient temperature, the flow fields between these cases are very similar near the repository horizon. Since the flow fields are quite similar, the latent heat transfer due to advection is similar for the two cases.

6.3.3 Fracture Plugging

The water distribution and removal model considers the properties for reduced fracture permeability developed in the *Water Drainage Model* (CRWMS M&O 2000c) for a "focused glacial" infiltration rate (Assumption 5.6). In this analysis for Cases 5 to 6, the fracture permeability was set equal to the matrix permeability in a 3 meter zone extending down from the drift. The results of the NUFT analysis for the water distribution and removal model for the case of fracture plugging of focused flow at isothermal temperature are presented in Figures 16 to 19 for the absolute value of the matrix capillary pressure (Pa), fracture mass flux rates (kg/(s-m^2), and fracture and matrix saturation levels. These figures can be compared directly to the results from the base case. Note that the results of the analysis for the case of uniform flow with repository heating are again very similar to the cases of focused flow.
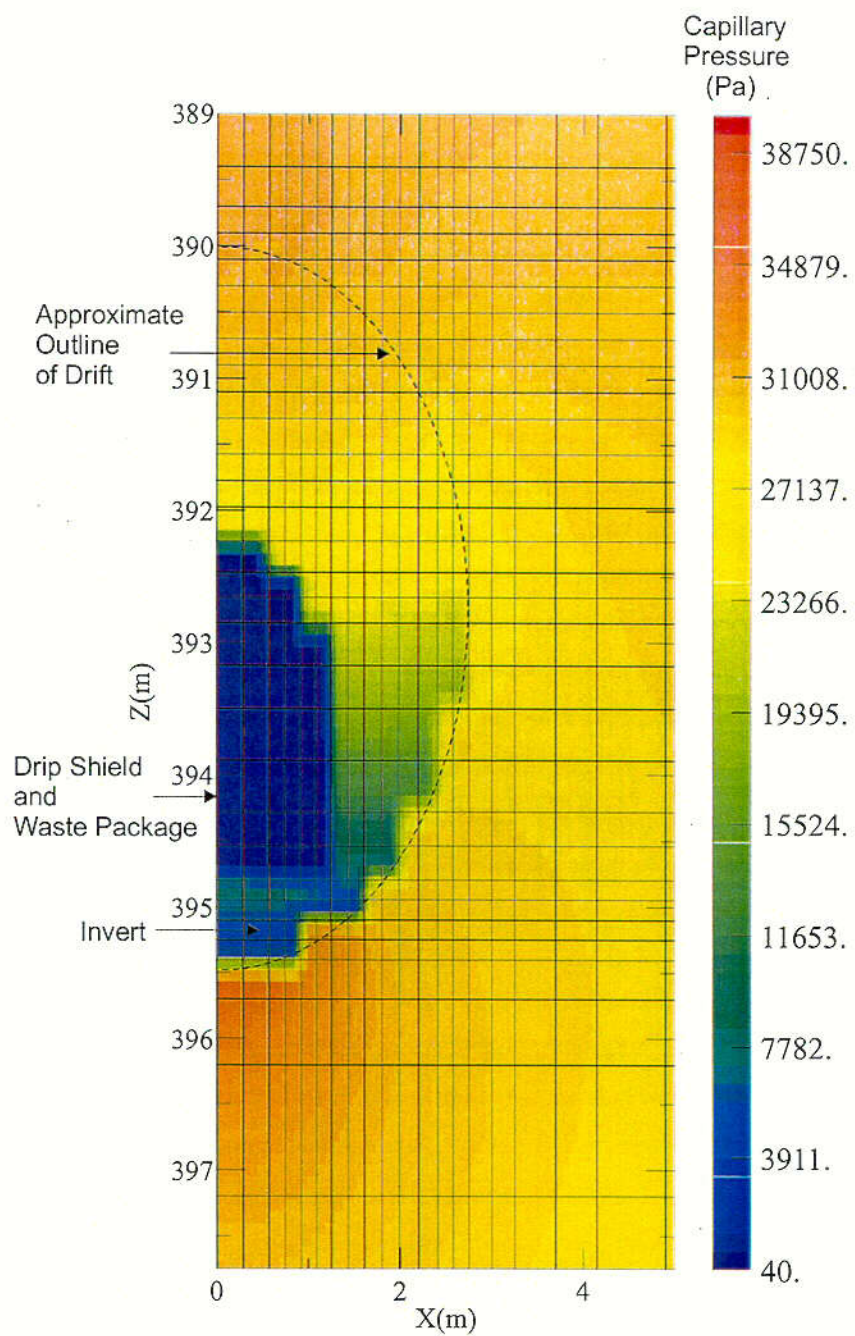
Figure 12. Absolute Matrix Capillary Pressure for Focused Flow for Repository Heating Near the Repository Horizon After 1,000 Years (Case 3)

C06
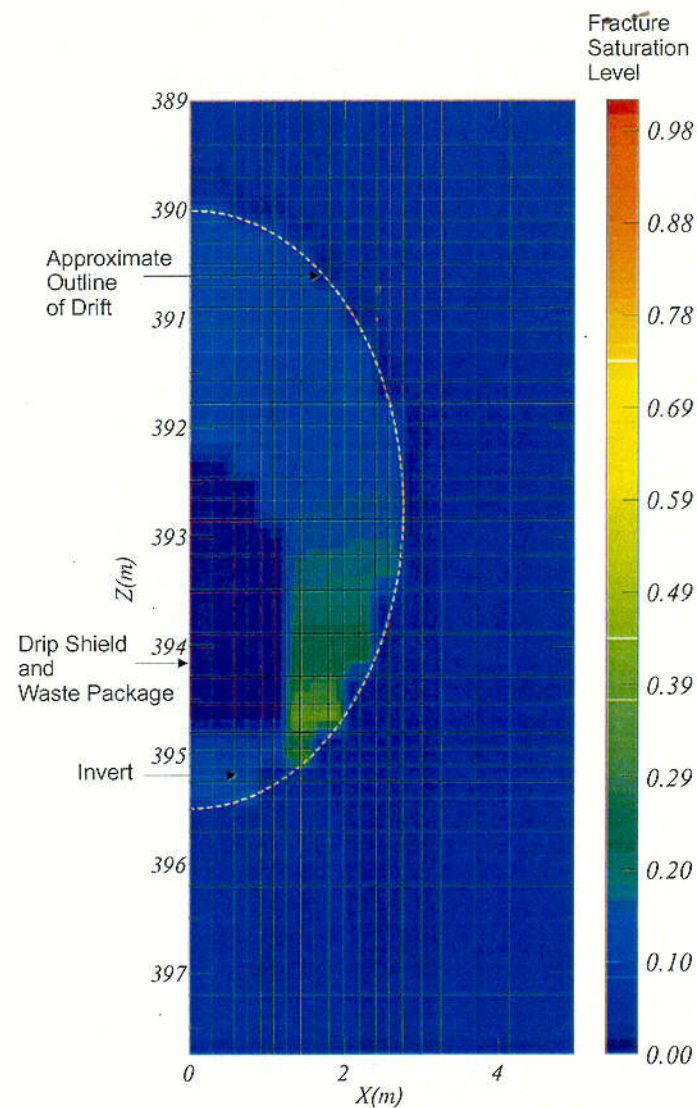
Figure 13. Fracture Saturation Levels for Focused Flow
for Repository Heating Near the Repository Horizon
After 1,000 Years (Case 3)
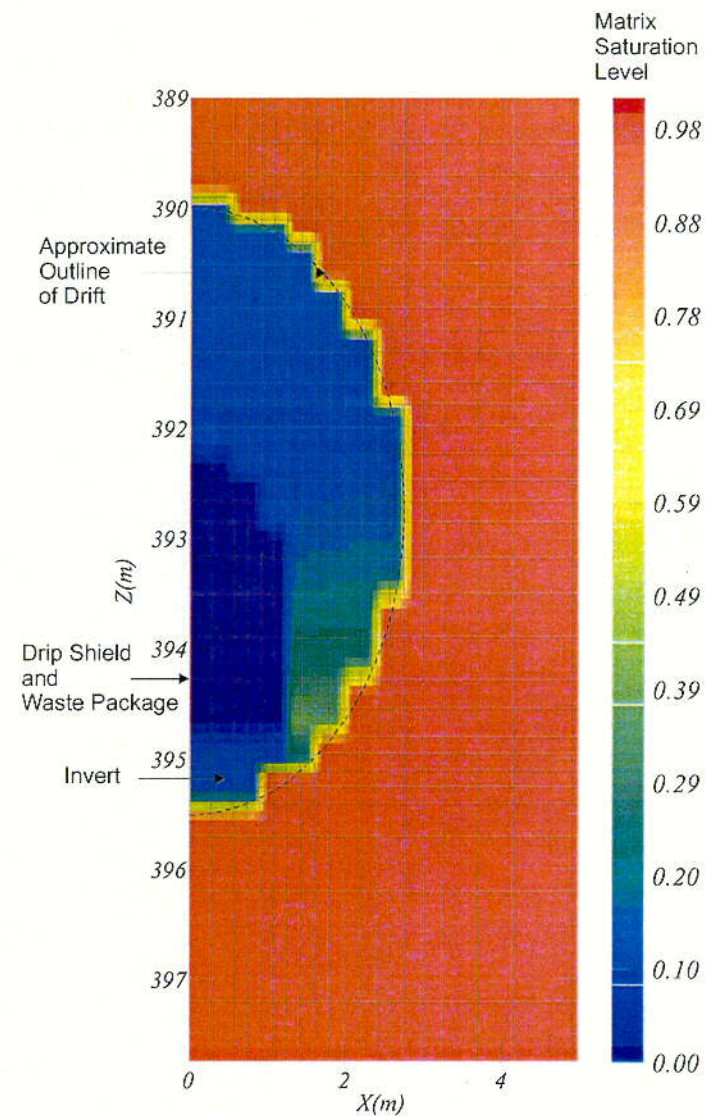
Figure 14. Matrix Saturation Levels for Focused Flow
for Repository Heating Near the Repository Horizon
After 1,000 Years (Case 3)
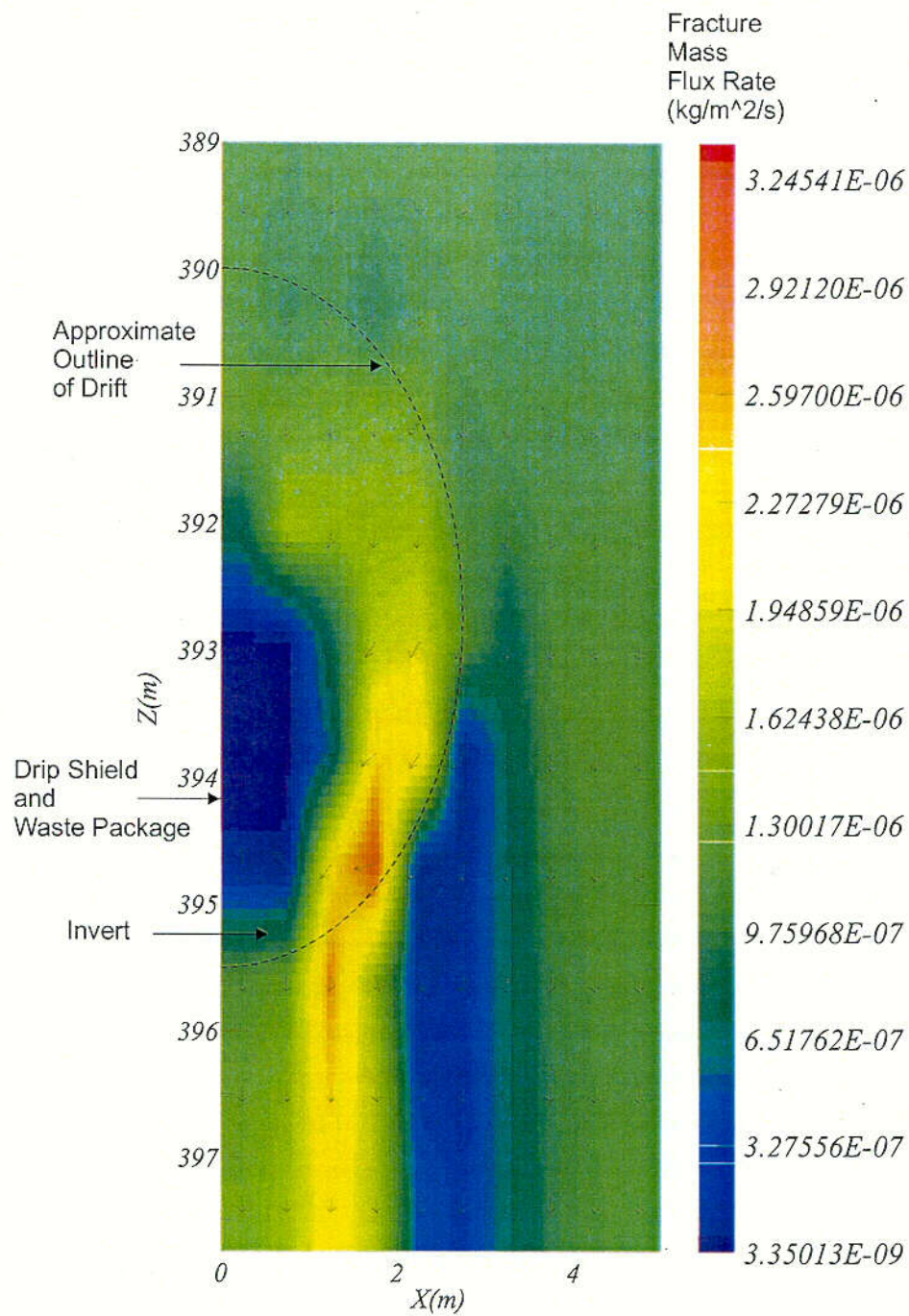
Figure 15. Fracture Mass Flux Rates (kg/m²-s) and Direction of Flow for Focused Flow for Repository Heating Near the Repository Horizon After 1,000 Years (Case 3)

C08
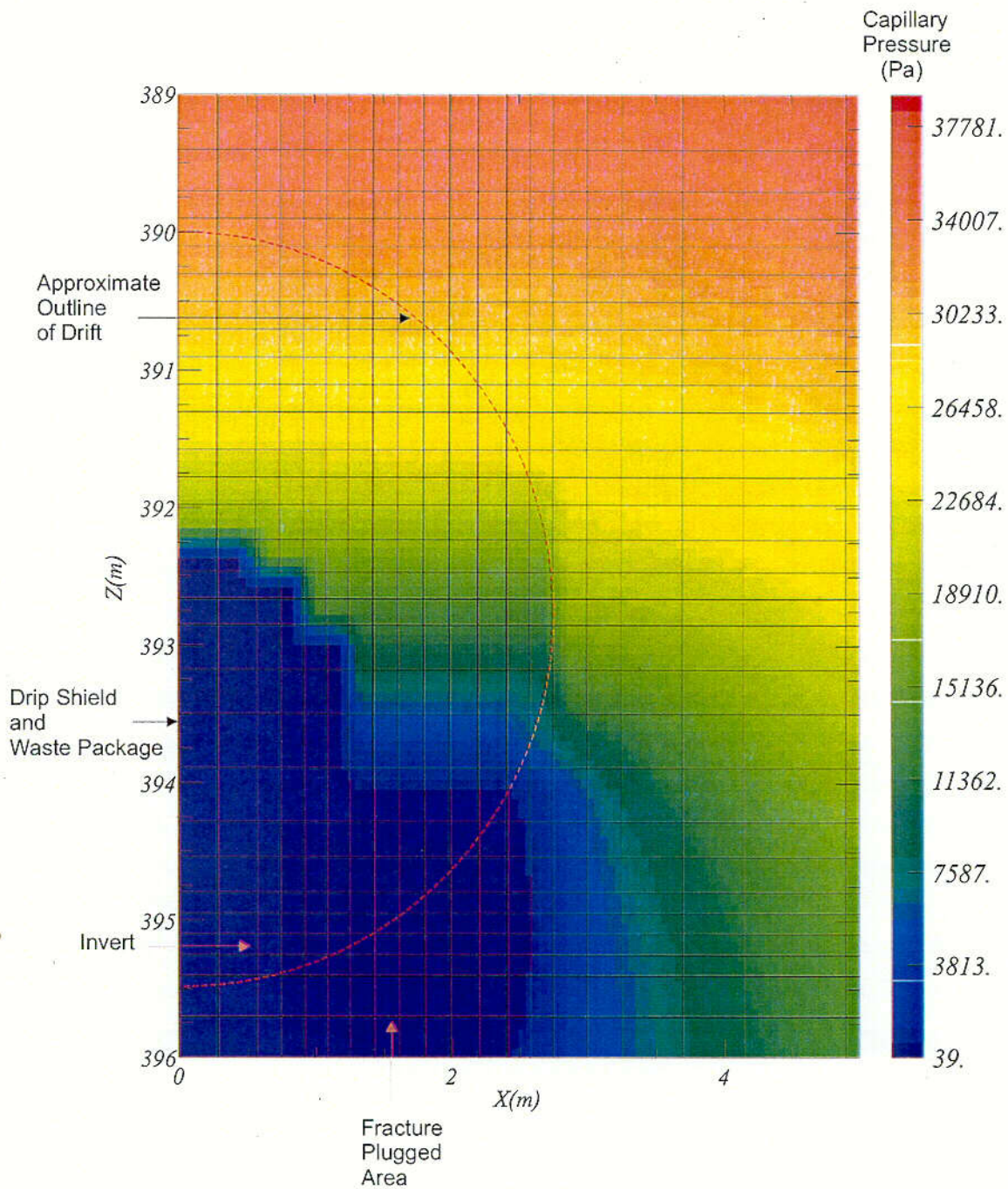
Figure 16. Absolute Matrix Capillary Pressure for Focused Flow at Steady State at Isothermal
Temperature Near the Repository Horizon for Plugged Fractures (Case 5)

C09
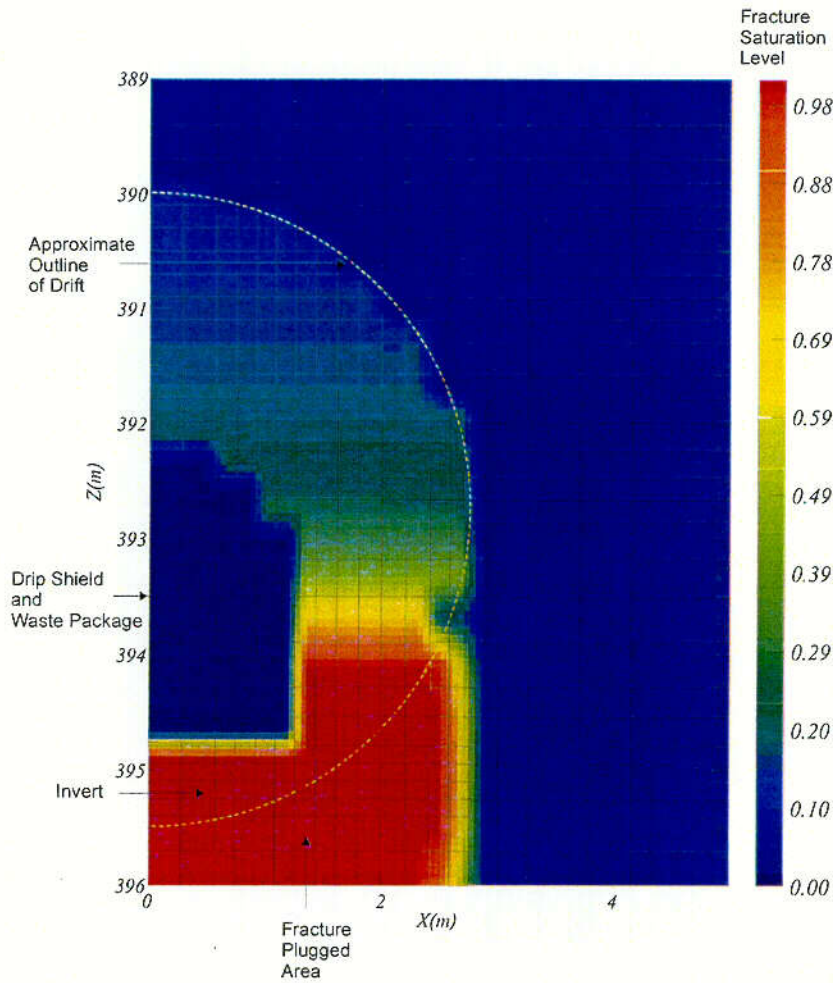
Figure 17. Fracture Saturation Levels for Focused Flow at Steady State at Isothermal Temperature Near the Repository Horizon for Plugged Fractures (Case 5)
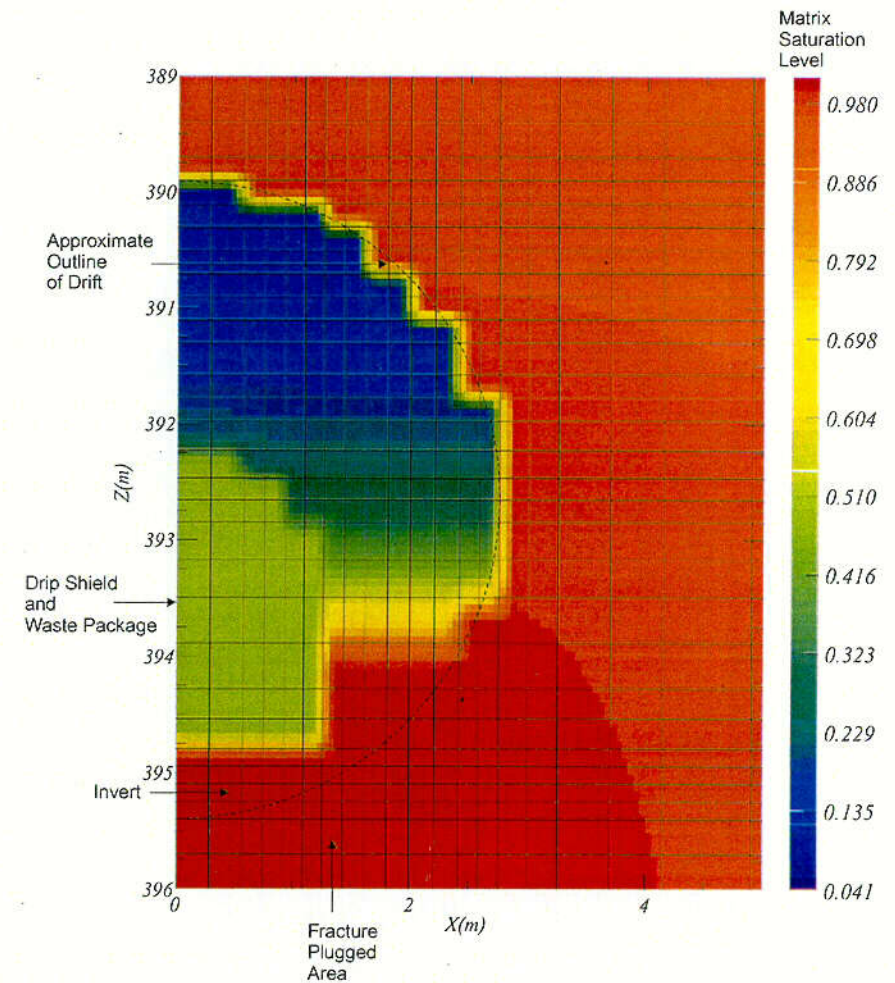
Figure 18. Matrix Saturation Levels for Focused Flow at Steady State at Isothermal Temperature Near the Repository Horizon for Plugged Fractures (Case 5)

C 10
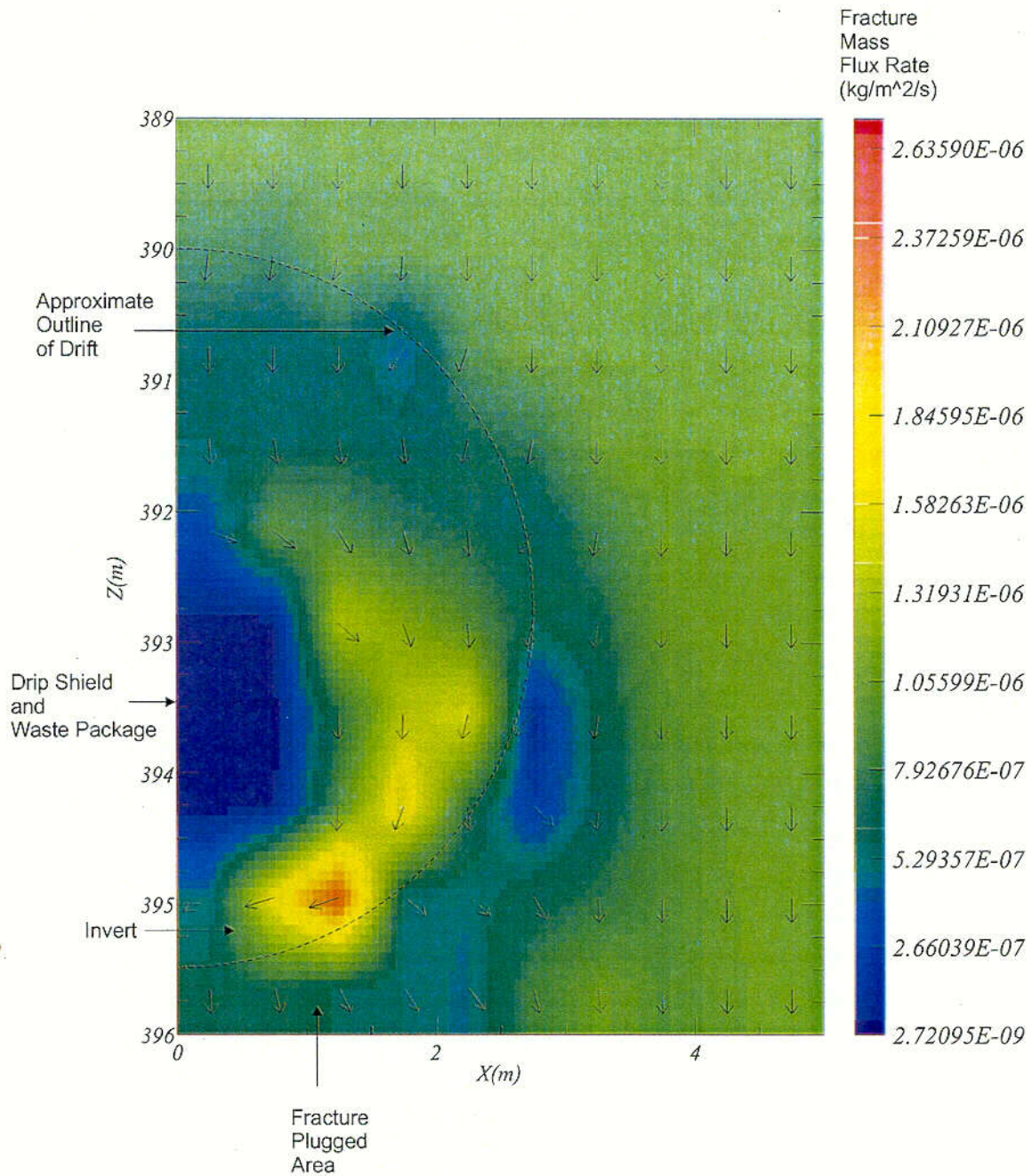
Figure 19. Fracture Mass Flux Rates (kg/m²-s) and Direction of Flow for Focused Flow at Steady State at Isothermal Temperature Near the Repository Horizon for Plugged Fractures (Case 5)

CII

Table 16. Summary of Absolute Capillary Pressures (Pa)

Time	Matrix Around the Drift	Backfill, Top	Backfill Spring Line	Backfill Corner of Invert	Invert Outside Drip Shield
100 Years	4,900	480,000	480,000	4,700,000	480,000
1,000 Years	30,000	30,000	22,000	8,000	5,000
10,000 Years	34,000	34,000	20,000	11,000	5,000

The results show that mass flux rates into the drift through the backfill to the side of the drip shield are reduced from approximately $1.5 * 10^{-6}$ kg/(sec-m^2) to $1.2 * 10^{-6}$ kg/(sec-m^2) (44 mm per year to 35 mm per year). This reflects the reduced permeability in the floor rock. The absolute values of the capillary pressures within the backfill are reduced from 36000 Pa (370 cm) to 26000 Pa (260 cm), resulting in higher saturation levels (0.14 versus 0.18).

The most significant effect due to plugging of the floor rock is to increase saturation levels in the surrounding floor rock and adjacent invert to near saturation (Figure 18 and 19). Saturation levels in the invert directly above the plugged floor rock are increased to near saturation with the absolute value of matrix capillary pressure near zero. Saturation levels through the rock matrix in the floor rock are increased from 0.88 to 0.98 or near saturation. Saturation levels in the invert increase from 0.15 to 0.98 or near saturation.

The plugging of fractures does not significantly divert the mass flux rate of water through the EBS to the NBS. In comparing Figure 11 to Figure 19, the diversion of flow in terms of both direction and magnitude around the drip shield appears to be the dominant flow mechanism. In these analyses, the impermeable flow properties of the drip shield result in the exclusion of water, and flow patterns that reflect this exclusion of water.

Below the drip shield in the invert, the effects of plugging result in a circulation within the invert, and a flow divide at the boundary between the crushed tuff invert, and the plugged fractured rock below. Because of the contrast in permeability between the crushed tuff, and the floor rock directly below, the vertical line of symmetry, and the upper surface of the drip shield-waste package, a circulation develops towards the centerline of the model at the lower surface of the invert, up the line of symmetry, and away from the centerline of the model at the upper surface of the invert. For the cases involving plugged fractures, there exists the potential for radionuclides released from the waste package to migrate laterally towards the flow zone outside the drip shield.

6.3.4 Sand Drains

The results of the NUFT analysis (Case 9) for the water distribution and removal model for the plugged flow at isothermal temperature with a sand drain are presented in Figures 20 to 23 for the absolute value of the matrix capillary pressure (Pa), fracture mass flux rates (kg/(s-m^2), and fracture and matrix saturation levels. These figures can be compared directly to the results from Case 5 for plugged fractures (Figures 16 to 19).
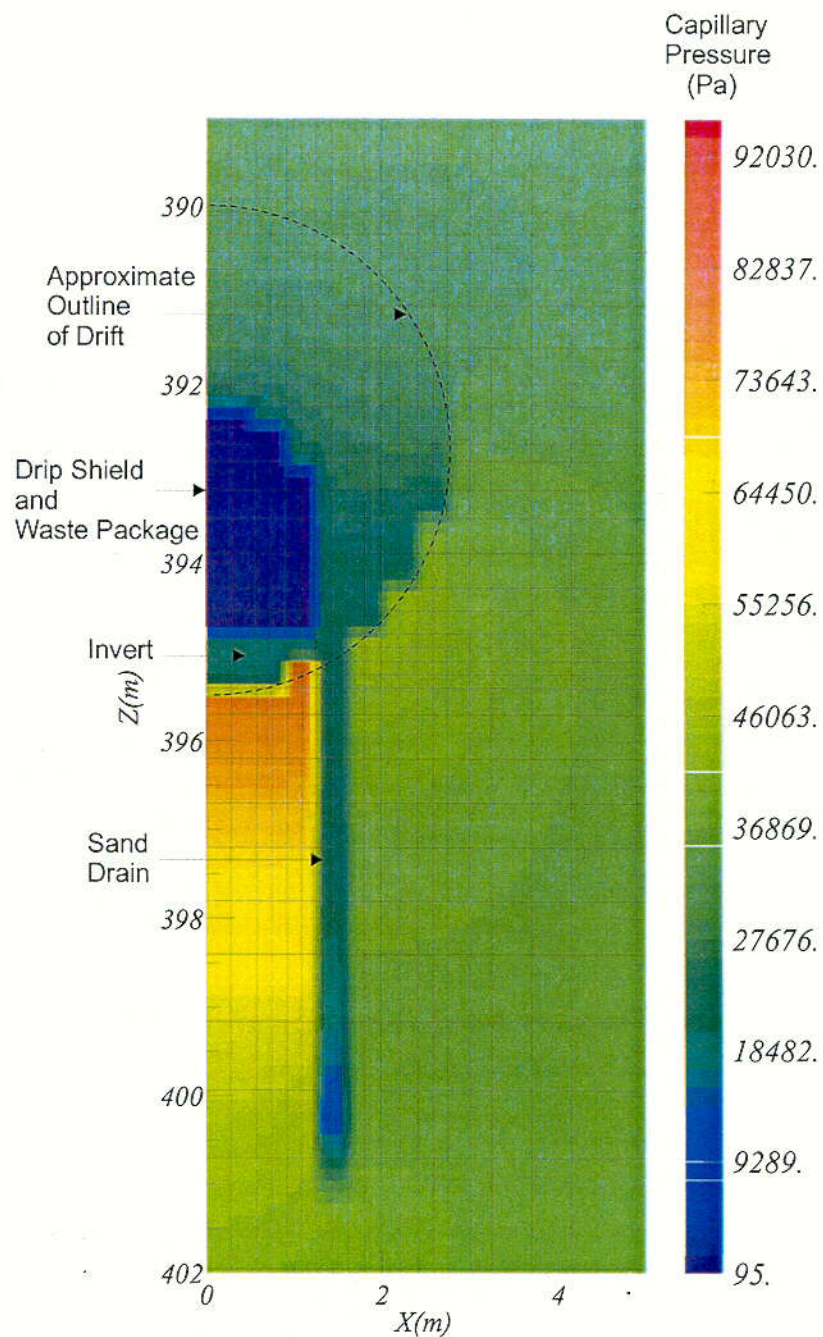
Figure 20. Absolute Matrix Capillary Pressure for Focused Flow at Steady State at Isothermal Temperature Near the Repository Horizon for Plugged Fractures with a Sand Drain (Case 9)

C/2

C/3
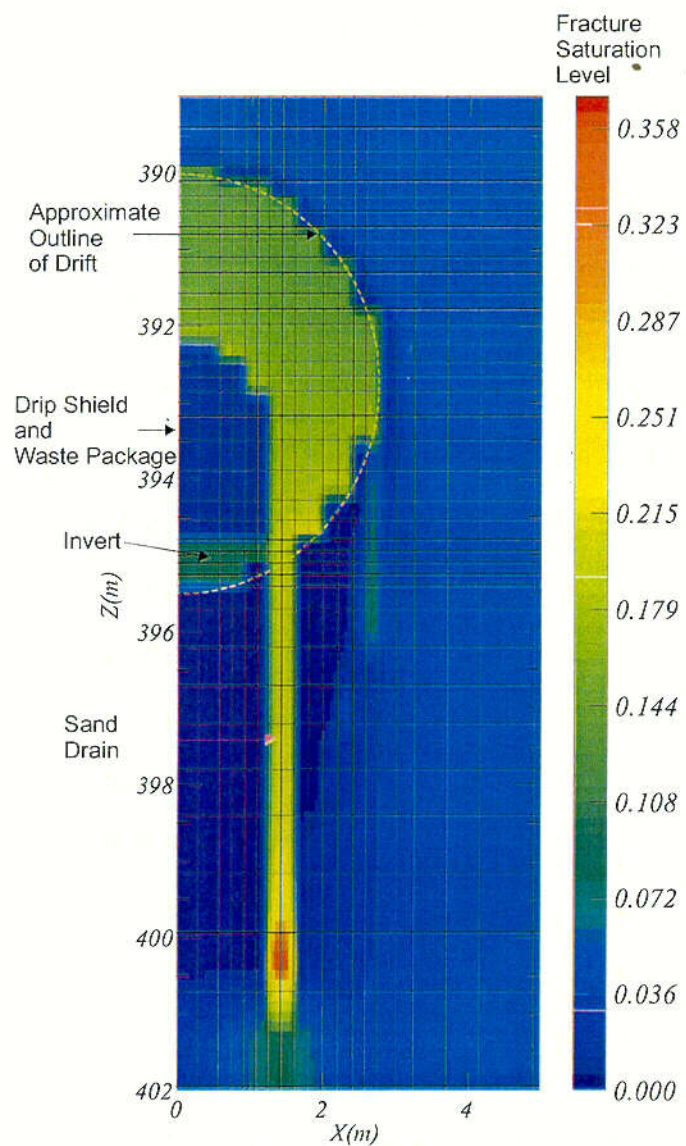
Figure 21. Fracture Saturation Levels for Focused Flow at Steady State at Isothermal Temperature Near the Repository Horizon for Plugged Fractures with a Sand Drain (Case 9)
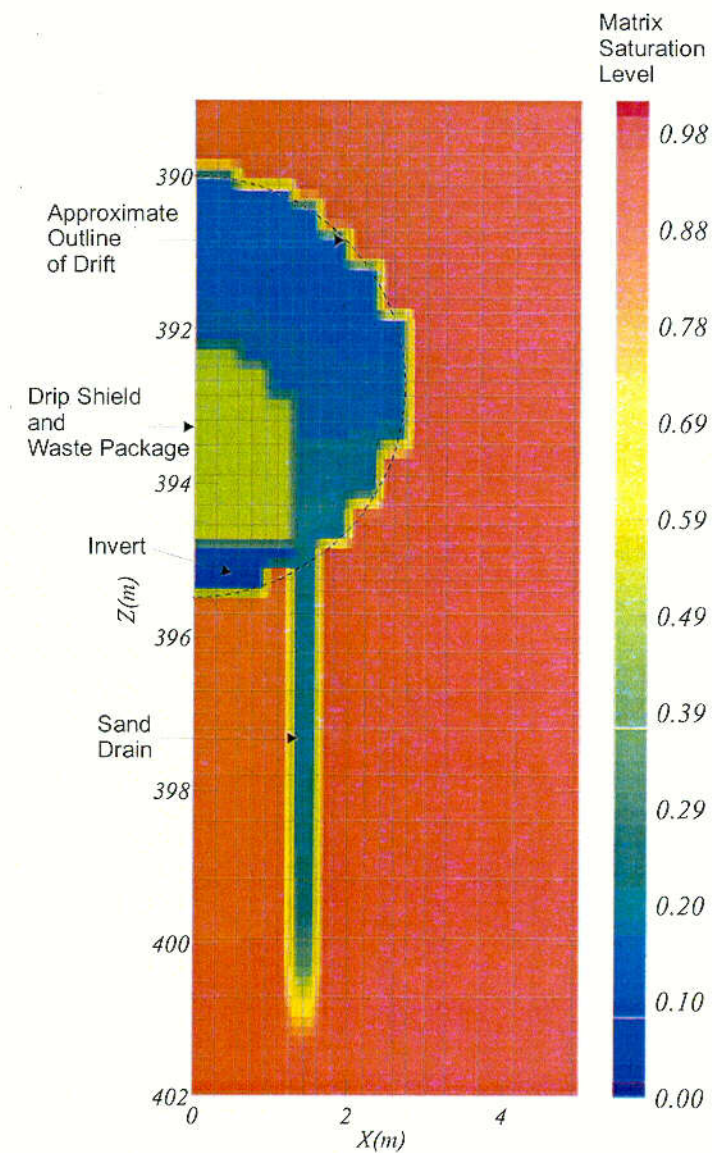
Figure 22. Matrix Saturation Levels for Focused Flow at Steady State at Isothermal Temperature Near the Repository Horizon for Plugged Fractures with a Sand Drain (Case 9)
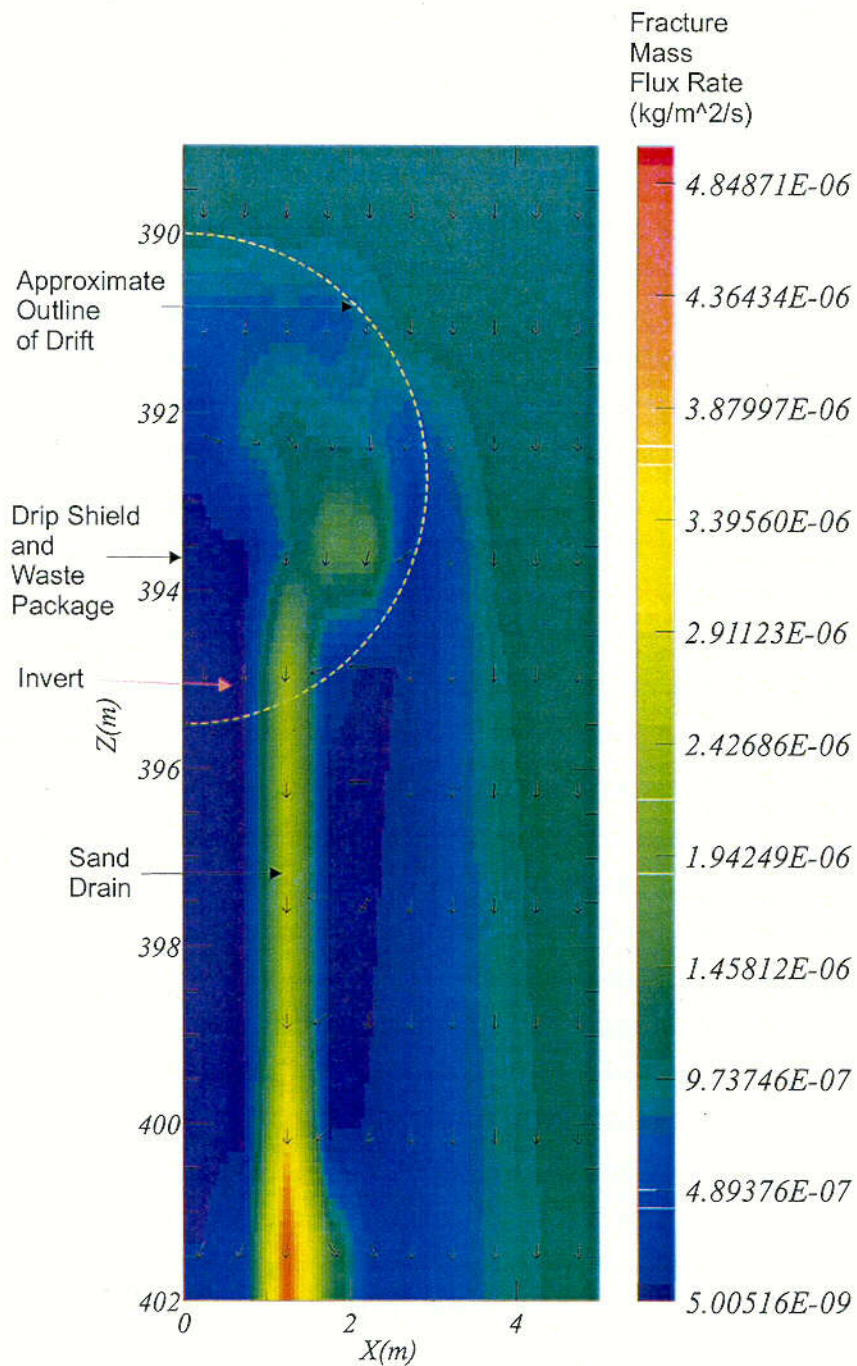
Figure 23. Fracture Mass Flux Rates (kg/m²-s) and Direction of Flow for Focused Flow at Steady State at Isothermal Temperature Near the Repository Horizon for Plugged Fractures with a Sand Drain (Case 9)

C/4

The results show that a sand drain comprised of the Overton Sand backfill strongly influences the flow regime in the invert and below the repository horizon. The distribution of the absolute value of capillary pressure (Figure 20) shows lower absolute values of capillary pressures than the surrounding tuff matrix, which is reduced near the base of the sand drain. The saturation levels within the sand drain are higher, and show nearly saturated conditions near the base of the sand drain.

The sand drain strongly influences the mass flux rate into the floor as shown in Figure 23. The results show that mass flux rates locally are high relative to the fractured media and flow through the backfill. The mass flux rate at the top of the hole is of the order of 3.5 * 10^{-6} kg/(m^2-sec) [100 mm/yr]. The mass flux rate at the base of the sand drain is 4.8 *10^{-6} kg/(m^2-sec) [140 mm/yr].

The high mass flux rate in the sand drain results in an increase in the absolute value of capillary pressure, and an attendant reduction of saturation level in the invert directly above the plugged fractures. The absolute value of the capillary pressure is of the order of 20,000 Pa (200 cm) for this case while for the case of plugged fractures the absolute value of the capillary pressure in the invert was near zero. A further discussion of the influence of the sand drains on invert mass flux rates is presented in Section 6.3.6.

6.3.5 Flow Through the Drip Shield to the Waste Packages

The analysis presented in previous sections assumed that the drip shield was impermeable relative to the other components of the EBS (Assumption 5.2). In this section, an estimate is made under a bounding assumption used in the *Water Diversion Model* (CRWMS M&O 2000b, p. 37). In this previous analysis, the drip shield design currently shows that the length of each individual drip shield is 5,485 mm long or 5.485 m long (Section 4.1.8). The placement of drip shields end to end would result in multiple interior joints between the drip shields. For the current design, the drip shields are placed with an overlap over each joint (Assumption 5.12). The geometry of the flow path can be identified (Assumption 5.11).

The NUFT analysis for the base case (Figure 8) presented in the previous section shows that for the isothermal case that capillary pressures immediately adjacent to and around the drip shield in the backfill are uniform from the top of the drip shield to the invert. The NUFT analysis is consistent with a steady state percolation rate equal to the unsaturated hydraulic conductivity, for the case of steady state flow in a deep water table (Jury et al. 1991, p. 127). The moisture potential in the backfill is uniform.

An aperture between the overlapping drip shields is characterized by a moisture potential ψ. The basic retention relation can be rewritten to express the relation of the largest aperture that could retain water to the absolute value of moisture potential ψ (CRWMS 2000b, p. 31):

$$B = \frac{2\sigma}{\rho_w g} \frac{1}{\psi}$$

(Eq. 8)

According to Section 5.11, the analysis assumes that the physical aperture equals the aperture that maximizes flow rate. In other words, the aperture between the overlapping joint and the drip

shield is assumed to be uniform, and equal the aperture from Equation 8. Thus, $B_1 = B_2 = \ldots B_N = B$, the uniform aperture is filled with water, and the width of the aperture (w_c) equals the wetted perimeter for the overlapping joint. Substituting Equation 8 into the Cubic Law (CRWMS M&O 2000b, p. 31) under unit gradient gives:

$$Q = \frac{\rho_w \cdot g}{12 \cdot \nu} \cdot \left(\frac{2 \cdot \sigma}{\rho_w \cdot g \cdot \psi} \right)^3 \cdot P \qquad \text{(Eq. 9)}$$

Figure 24 presents the relationship of backfill and drip shield flow rate that contacts the waste packages for a single drip shield to moisture potential. The backfill flow rate is determined as the unsaturated hydraulic conductivity for the backfill (CRWMS M&O 2000b, p. 22) multiplied by the plan area of the drip shield (length of the drip shield times the drift diameter). Equation 9 is used to determine the drip shield flow rate. The analysis shows that over the range of moisture potential within the backfill, the bounding flow rate through the drip shield, and that could contact the waste packages is a small percentage of the backfill flow rate. Figure 25 presents the same relationships for backfill and drip shield flow rates plotted against the backfill percolation rate that is determined from the unsaturated hydraulic conductivity for the backfill (CRWMS M&O 2000b, p. 22).
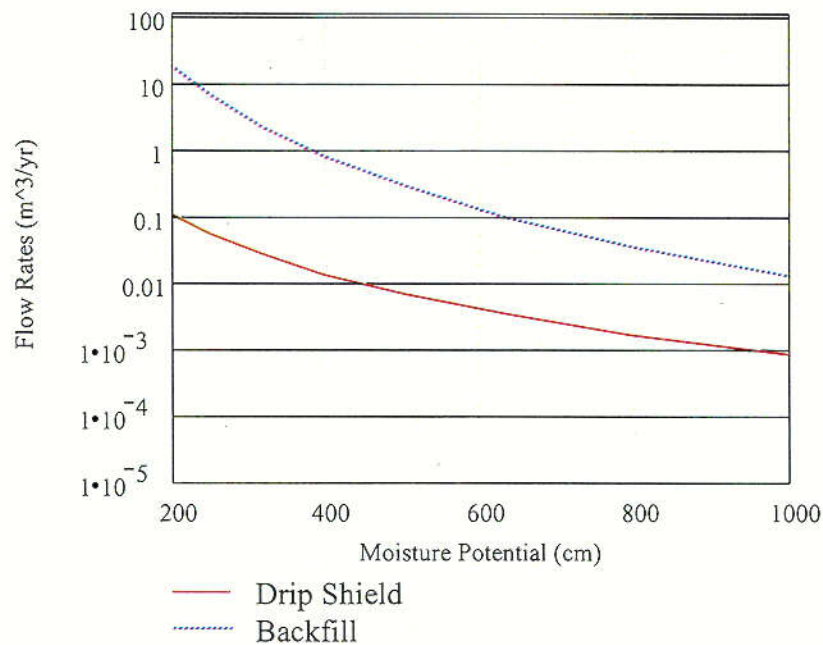
Figure 24. Drip Shield and Backfill Flow Rates as a Function of Moisture Potential

c/5
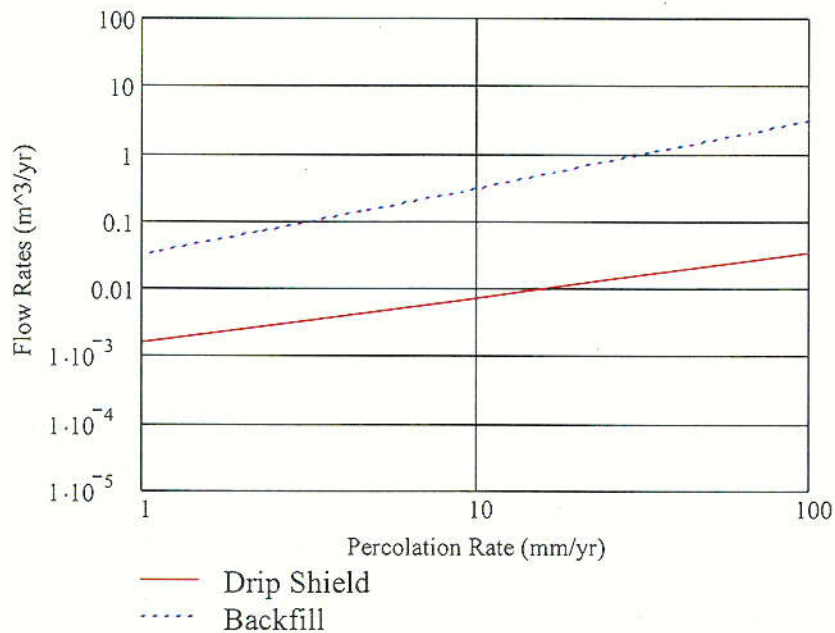
Figure 25. Drip Shield and Backfill Flow Rates as a Function of Percolation Rate

6.3.6 Flow Through the Invert

The groundwater travel time in the EBS is measured from the top of the invert to the base of the invert. The water flow rates from the base of the invert below the drip shield and outside the drip shield for several of the cases are presented in Table 17. Tables 18 and 19 present the results for groundwater travel time, and average seepage velocity at the centerline of other cases, and in an adjacent column for comparison to the base case for the water distribution and removal model. Table 20 presents the saturation levels. Two groundwater paths through the invert are presented in Tables 18, 19, and 20. The first path (first column) is through the grid blocks nearest the centerline of the model, while the other path (second column) is through the adjacent grid blocks. These two paths are used to evaluate the magnitude of the effect on flow, from the dry shadow under the drip shield. The volumetric flow rate results are calculated from NUFT analysis by integration of the vertical mass flux rate divided by the mass density of water. The results show that that the volumetric flow rates are comparable for the several cases with the exception of the plugged cases and the sand drain. The results reflect the development of the dry shadow below the drip shield as was discussed previously in Section 6.3.1. For Case 8, the flux from the floor in the invert is upward reflecting the plugging of fractures, and the capillary driven flow of water vertically and to the side where the drip shield lobe forms to conduct water vertically downwards.

The placement of a sand drain for Cases 9 and 10 for plugged and unplugged floor results in a significant reduction of flux rates in the invert (Table 17), and the extension of the dry shadow in

C/6

the rock below the invert. The sand drain provides a high degree of capillary driven flow in the same vicinity of the drip shield lobe.

Table 17. Summary of Flow Rates through the Invert for Various Cases (Attachment VIII)

Case Number	Flow Below the Drip Shield (m³/yr)	Flow Outside of the Drip Shield (m³/yr)	File Name
1	0.16	0.25	Case1_Flux V1.0.mcd
2	0.17	0.26	Case2_Flux V1.0.mcd
3	0.17	0.25	Case3_Flux V1.0.mcd
4	0.17	0.26	Case4_Flux V1.0.mcd
8	-0.83	0.005	Cases899.1_Flux V1.0.mcd
9	$1.6*10^{-5}$	0.36	Cases899.1_Flux V1.0.mcd
10	$1.6*10^{-5}$	0.36	Cases899.1_Flux V1.0.mcd
11	0.039	0.05	Invert Fluxes Case 19 V1.0.mcd
12	0.041	0.04	Invert Fluxes Case 20 V1.0.mcd
13	$7.5*10^{-6}$	0.008	Invert Fluxes Case 27 V1.0.mcd

Table 18. Travel Times for Various Cases (Attachment VIII)

Case Number	Travel Time along the Center Line (yr)	Travel Time along the Second Column (yr)	Infiltration	Sand Drain	File Name
1	19.4	8.2	Glacial	No	Case1 V1.0.mcd
2	18.6	7.9	Glacial	No	Case2 V1.0.mcd
3	18.6	7.9	Glacial	No	Case3 V1.0.mcd
4	18.8	8.1	Glacial	No	Case4 V1.0.mcd
9	13150.0	13150.0	Glacial	Yes	Case9 V1.0.mcd
10	13210.0	13180.0	Glacial	Yes	Case9.1 V1.0.mcd
11	62.0	30.0	Present Day	No	Case19 V1.0.mcd
12	60.4	27.9	Present Day	No	Case20 V1.0.mcd
13	47320.0	NC	Present Day	Yes	Case27 V1.0.mcd

Table 19. Average Pore Water Velocities for Various Cases (Attachment VIII, *summary of travel time calculation V1.0.xls*)

Case Number	Average Pore Water Velocity along the Center Line (mm/yr)	Average Pore Water Velocity along the Second Column (mm/yr)	Infiltration	Sand Drain
1	31	74	Glacial	No
2	33	77	Glacial	No
3	33	77	Glacial	No
4	32	75	Glacial	No
9	$4.6*10^{-2}$	$4.6*10^{-2}$	Glacial	Yes
10	$4.6*10^{-2}$	$4.6*10^{-2}$	Glacial	Yes
11	10	20	Present Day	No
12	10	22	Present Day	No
13	$1.3*10^{-2}$	NC	Present Day	Yes

Table 20. Saturation Levels for Various Cases (Attachment VIII, NUFT Output Files)

Case Number	Average Saturation Levels Along the Centerline	Average Saturation Levels in the Adjacent Column	Infiltration	Sand Drain
1	0.13	0.13	Glacial	No
2	0.13	0.13	Glacial	No
3	0.13	0.13	Glacial	No
4	0.13	0.13	Glacial	No
9	0.12	0.12	Glacial	Yes
10	0.12	0.12	Glacial	Yes
11	0.13	0.13	Present Day	No
12	0.13	0.13	Present Day	No
13	0.13	0.13	Present Day	Yes

The total travel time was determined as follows. The pore water velocity was determined for the column of four grid blocks directly below the invert, and in the adjacent column of grid blocks. The volumetric flux rate was calculated as the mass flux rate for each grid block divided by the mass density of water (1.0 gm/cm^3). The pore water velocity for each grid block is determined as the volumetric flux rate divided by the volumetric moisture content (Jury et al., 1991, p. 222). The volumetric moisture content is determined as the product of the porosity, and the saturation level from Table 20. The travel time is determined for each grid block was based upon the grid block length divided by the porewater velocity. The total travel time is calculated as the sum of the individual travel times through each grid block (Table 18). For Case 1, this travel time equals approximately 20 years at the model centerline, and about 8 years in the adjacent column of grid blocks. The average linear or pore velocity can be determined by the invert thickness divided by the travel time (Table 19).

Figures 26 and 27 present a plot of the matrix and fracture pore water velocities. Note that within the invert away from the drift boundary, the velocity vectors are identical while for grid blocks near the boundary, the flow is dominantly into the fractures. The pore water velocity in the adjacent column of grid blocks is increased by an approximate factor of 2.4.

The removal of water in the invert increases the total groundwater travel time for plug flow through the invert for Cases 9 and 10. Consider the case of a sand drain (Case 9). The breakthrough time for plug flow through a length of 0.6 m is estimated to be 13,000 years. The breakthrough times for the case of the sand drain for sand drains are two orders of magnitude higher than the base case. The presence of the sand drain for the case of glacial infiltration reduces advective transport through the invert, and increases the likelihood of the invert to act as a diffusion barrier.

The pore water velocity vectors for this case shown in Figures 28 and 29 for the fracture and matrix components respectively show that dominant drainage occurs vertically downward through the sand drain for this case. In contrast, the base case or Case 1 reflects a flow pattern in which flow exclusion takes place due to the drip shield. For the base case, there is a horizontal component of flow below the drip shield (Figures 26 and 27) while this component of flow is not apparent in the case of the sand drain.
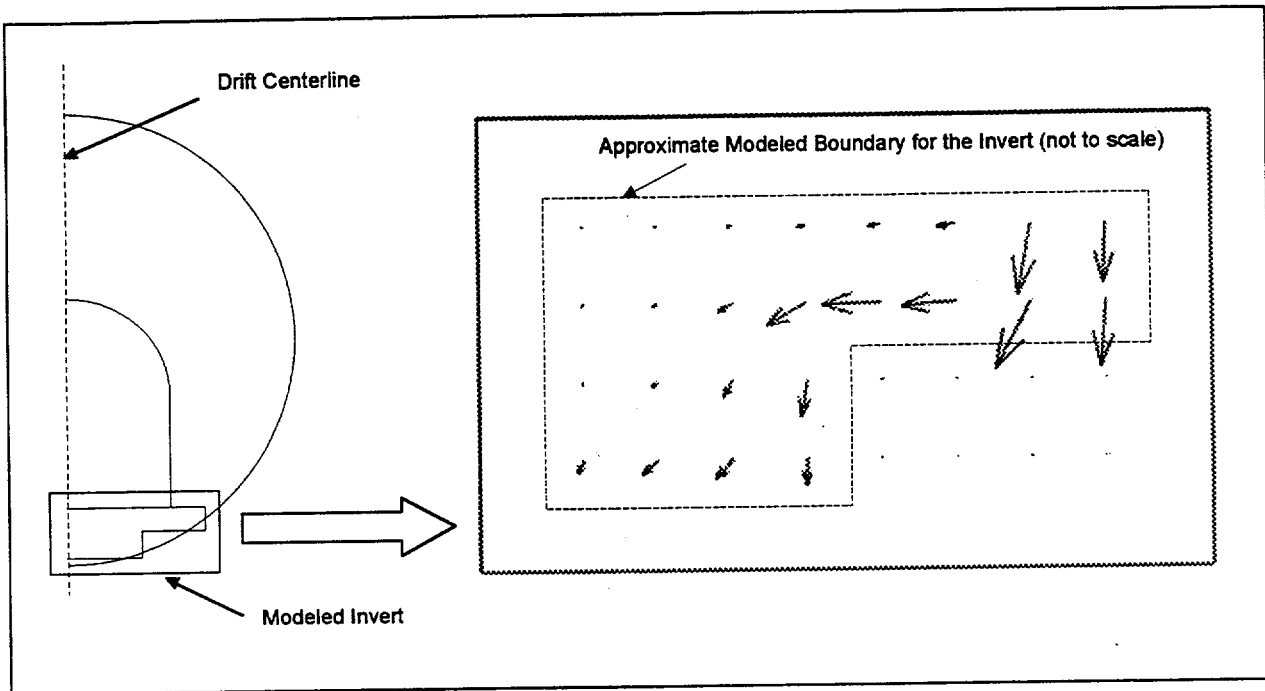
Figure 26. Fracture Pore Water Velocity Vectors in the Invert for the Base Case
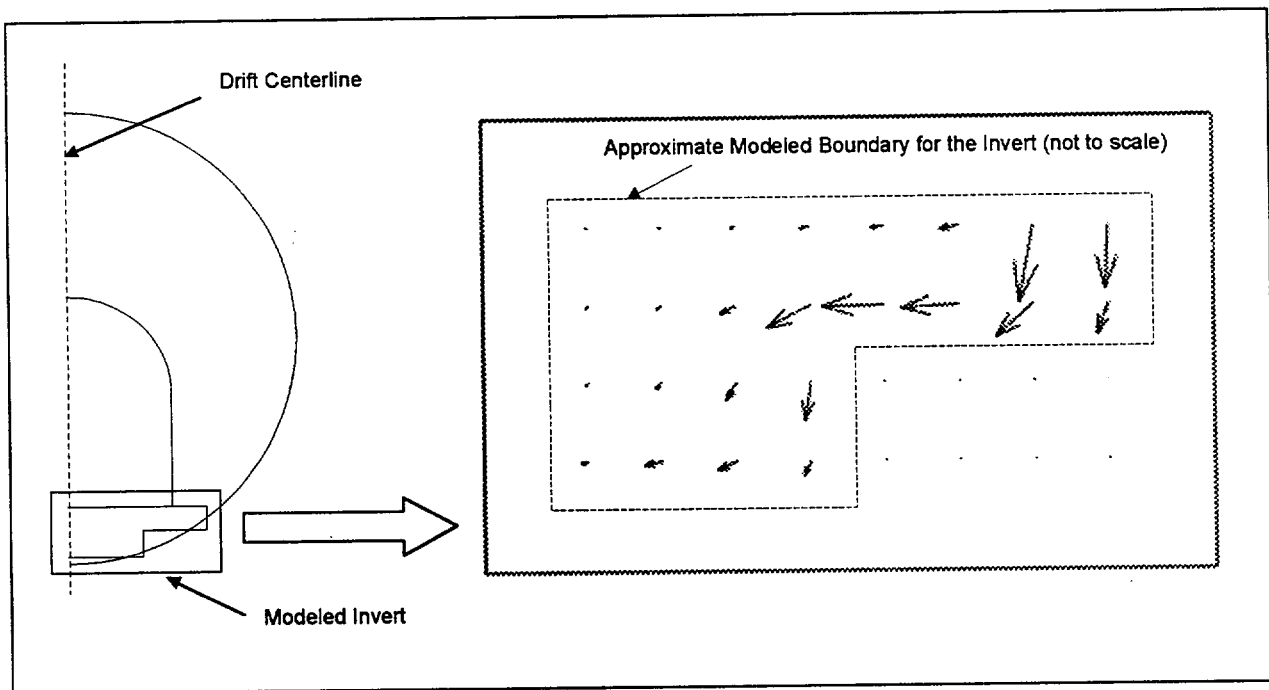
Figure 27. Matrix Pore Water Velocity Vectors in the Invert for the Base Case
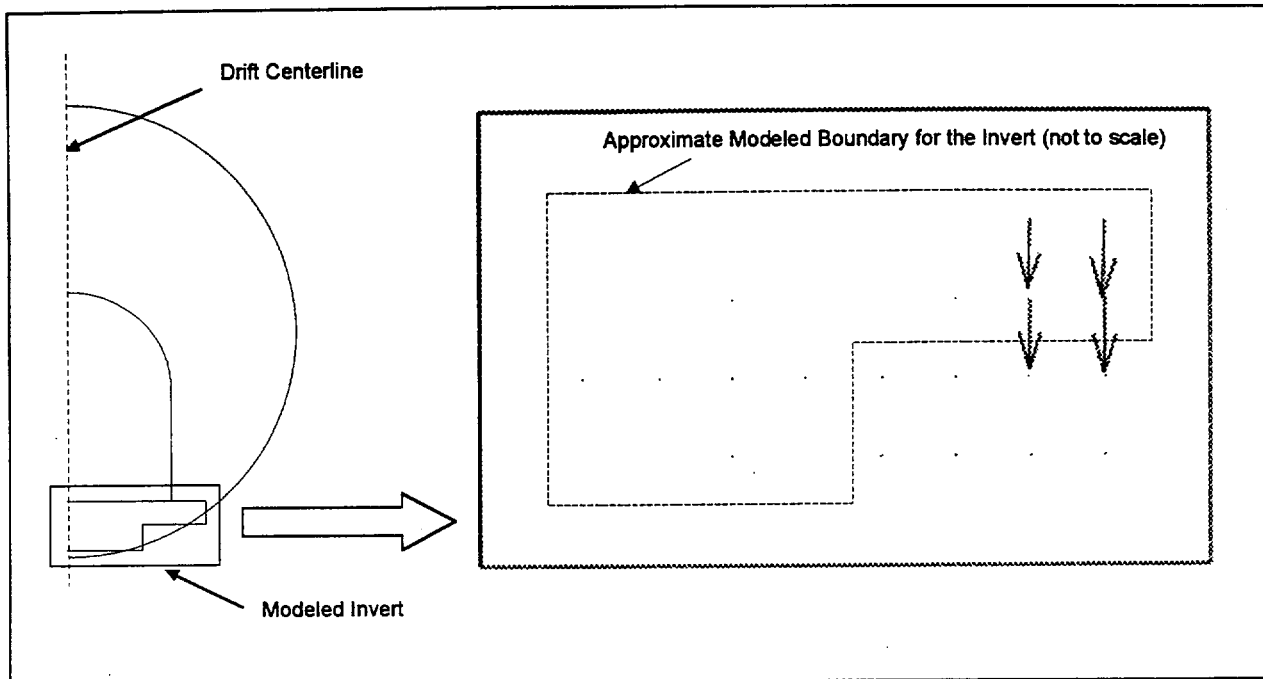
Figure 28. Fracture Pore Water Velocity Vectors in the Invert for the Case 9
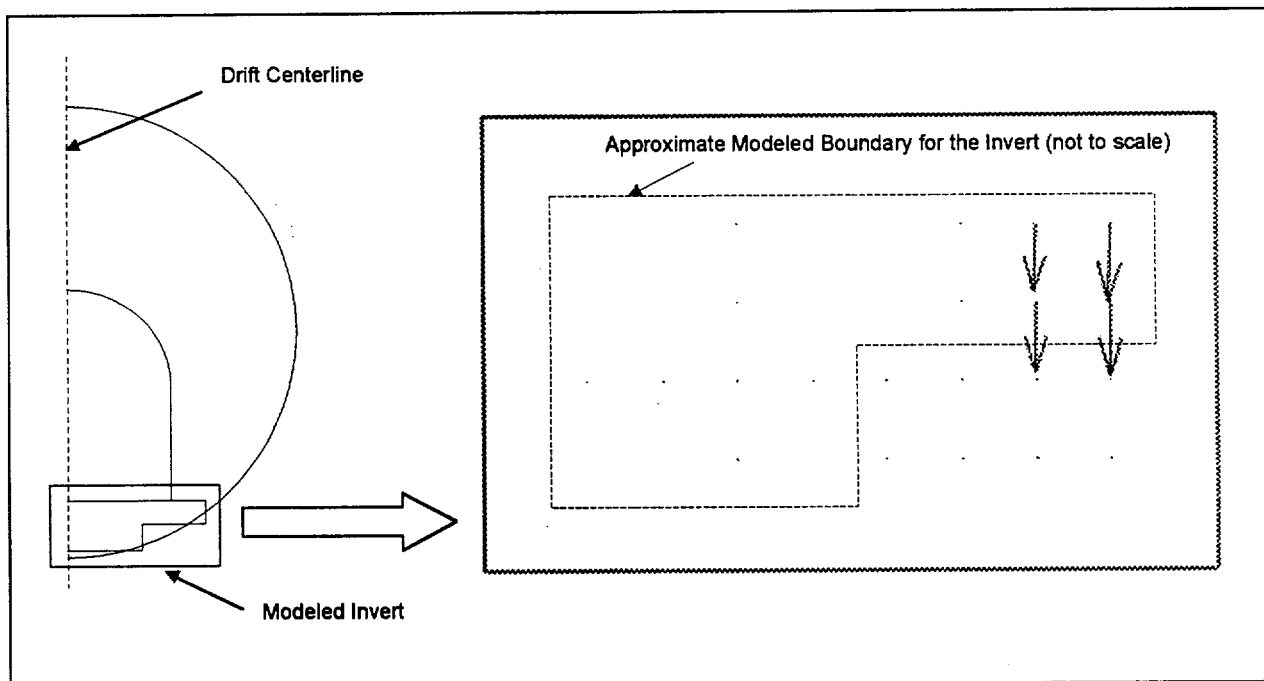
Figure 29. Matrix Pore Water Velocity Vectors in the Invert for the Case 9

6.4 MODEL VALIDATION

The water distribution and removal model was performed using a finite difference technique (i.e., the NUFT code) supplemented by other standard calculations. The approach used to validate the model includes a comparison of the base-case model output to a closed-form solution. The validation criteria used to evaluate the model are that the closed-form solution and the model results shall qualitatively agree. Data trends and magnitudes from both the closed-form solution and the model shall reasonably agree. These criteria are appropriate for demonstrating that the model results are reasonable and that the model is suitable for its intended use of evaluating the EBS water distribution and removal.

The development of a closed-form solution and the subsequent comparison of the model base-case results to the closed-form solution are provided in Attachment IX. The comparison shows that the two approaches are in general agreement. It is determined that the model is validated and appropriate for its intended use. Additionally, when EBS pilot-scale testing results become available, this test data can be compared to predicted results using NUFT to provide further validation of the model.

7. CONCLUSIONS

7.1 SUMMARY

This AMR quantifies and evaluates the distribution of liquid water within the emplacement drift to support the EBS post-closure performance assessment. This AMR uses information developed in previous AMRs that support the water distribution and removal model as discussed in Section 6.1. A conceptual model was presented in Section 6.2 that discusses flow focusing, increased backfill saturation levels above the drip shield, and floor drainage and performance of the invert. The NUFT water distribution and removal model in terms of model geometry for the NBS and the EBS, pressure and temperature boundary conditions, and hydrologic and thermal properties of the NBS and the EBS were presented in Section 6.2. Based upon the developed NUFT model, a series of parametric studies were performed to address flow focusing, repository heating, fracture plugging, and sand drains as presented in Section 6.3. Data developed in this modeling and analysis activity are provided by DTN: MO0003SEPRWDRM.001.

The major conclusions from this AMR are as follows:

- The fracture mass flux rates (volumetric flux rate) are increased adjacent and somewhat below the drip shield to an approximate maximum value of $4.6 * 10^6$ kg/m^2-s (145 mm per year). These values are in qualitative agreement with the prediction of a "roof drip lobe" as illustrated in the *Water Diversion Model* (CRWMS M&O 2000b, Figure 16).

- A drip shield lobe (zone of increased flux rate) is evident from an analysis of the base case (Section 6.3.1). The downward mass flux rate that expresses the deflection sideways from the drip shield produced by the runoff of water unable to penetrate the drip shield is in qualitative agreement with the exclusion analysis for a circular cavity (Philip et al. 1989, p. 25). The fluxes in the zone adjacent to the drip shield are increased by a factor of three to four with respect to farfield flow.

- The NUFT results for the water distribution and removal model using the active fracture concept for the selected fracture and matrix constitutive properties show that the matrix saturation levels are high (exceeding approximately 0.90), while fracture saturation levels (Figures 8-10) are near the residual saturation level. Unsaturated flow is dominated by fracture flow in the surrounding media as the matrix exhibits low unsaturated hydraulic conductivity resulting in low fluxes through the matrix.

- A comparison of the capillary pressures, saturation levels, and mass flux rates between the base case involving focused flow (Assumption 5.7) and the case of a uniform flux applied uniformly at the ground surface shows that the flow regime is nearly identical, and flow focussing is not significant.

- The analysis shows that after 1,000 years for the thermal case, there is some slight reduction of saturation levels immediately above the drip shield. The effect of heating 100 years after repository closure after the start of heating (Assumption 5.8) increases the absolute value of the capillary pressure, the saturation level, and reduces the mass flux rate into the drift (Section 6.3.2). However, for the case of repository heating, the

capillary pressures, saturation levels, and mass flux rates after 1,000 years are nearly comparable to the base case at isothermal temperature.

- The results show that for the case of fracture plugging, the mass flux rates into the drift through the backfill between the drip shield and the drift wall are reduced from approximately $1.5 * 10^{-6}$ kg/(sec-m^2) to $1.2 * 10^{-6}$ kg/(sec-m^2) (48 mm per year to 38 mm per year). This reflects the reduced permeability in the floor rock. The absolute values of the capillary pressures within the backfill are reduced from 36000 Pa (370 cm) to 26000 Pa (260cm), and saturation levels are increased (0.14 versus 0.18) for this case.

- The most significant effect due to plugging of the floor rock is to increase saturation levels in the surrounding floor rock and adjacent invert to near saturation (Section 6.3.3). Saturation levels in the invert extending 0.8 m into the backfill directly above the plugged floor rock are increased to saturation with the absolute value of matrix capillary pressure near zero. Saturation levels through the rock matrix in the floor rock are increased from 0.88 to 0.98 or near saturation. Saturation levels in the invert increase from 0.15 to 0.98 or near saturation.

- The results from the case of the sand drain strongly influence the mass flux rate into the floor (Section 6.3.4). The results show that for this case, the mass flux rates locally are high relative to the fractured media and flow through the backfill. The mass flux rate at the top of the hole is of the order of $3.5 * 10^{-6}$ kg/(m^2-sec) [110 mm/yr]. The mass flux rate at the base of the sand drain is $4.8 * 10^{-6}$ kg/(m^2-sec) [150 mm/yr].

- The results from the case of the sand drain show an increase in the mass flux rate in the sand drain. The results show an increase in the absolute value of capillary pressure, and an attendant reduction of saturation level in the invert directly above the plugged fractures. The absolute value of the capillary pressure in the invert is of the order of 20,000 Pa (200 cm) for this case while for the case of plugged fractures the absolute value of the capillary pressure in the invert was near zero.

- The placement of drip shields end to end would result in multiple interior joints between the drip shield, and a potential flow path for water. A bounding assumption used in the *Water Diversion Model* (CRWMS M&O 2000b, p. 37) is used to estimate the flow through the drip shield to the waste packages (Equation 9). This bounding assumption is used in conjunction with the observation that capillary pressures immediately adjacent to and around the drip shield in the backfill are uniform from the top of the drip shield to the invert. The analysis shows that over the range of moisture potential within the backfill, the bounding flow rate through the drip shield that could contact the waste packages is a small percentage of the backfill flow rate (Section 6.3.5).

- The placement of a sand drain for Cases 9 and 10 for plugged and unplugged floor results in a significant reduction of flux rates in the invert, and the extension of the dry shadow below the rock (Section 6.3.6). The sand drain provides a high degree of capillary driven flow in the same vicinity of the drip shield lobe.

- Section 6.3.6 developed mass flux rates through the invert for several of the NUFT cases run for the water distribution and removal model for the glacial climate. For the base case at ambient temperature (Case 1), the calculated average linear velocity is of the order of 0.55 cm/yr, and breakthrough to the base of an invert approximately 0.5 m thick invert is of the order of 75 years. With the sand drain in place, and plugged fractures below the invert, the flow is directed to the sand drain. The advection in the vertical direction is of the order of 0.03 mm/yr, and the breakthrough time increase is of the order of 15,000 years.

- The inputs presented in Section 4 are appropriate for their intended purpose of developing the water distribution and removal model. The analyses and model presented in this report are appropriate for their intended use of evaluating the EBS water distribution and removal.

7.2 ASSESSMENT

This analysis involved the use of the finite difference code, NUFT, supplemented by other standard calculations to address flow through the drip shield. These methods are based on project accepted approaches for performing hydrologic and thermal analysis. The results of the model are based on unqualified technical information and unqualified software. Therefore, the use of any unqualified technical information or results from this model as input in documents supporting construction, fabrication, or procurement, or as part of a verified design to be released to another organization, is required to be identified and controlled in accordance with appropriate procedures.

7.3 TBV IMPACT

TBV-3828, which is the result of using the unqualified code, NUFT V3.0s, is the primary TBV item impacting the conclusions of this study. Significant modifications to this code as a result of the qualification process are not anticipated, therefore, the resolution of this TBV is not expected to significantly impact the results presented in this report.

The results presented in this report are based partially on unqualified data as identified in Section 4 (TBV-0389, TBV-3471, TBV-3685, TBV-3686, TBV-3695, and TBV-3796). This document may be affected by technical product input information that requires confirmation. Any changes to the document that may occur as a result of completing the confirmation activities will be reflected in subsequent revisions. The status of the input information quality may be confirmed by review of the Document Input Reference System database.

8. INPUTS AND REFERENCES

8.1 DOCUMENTS CITED

Bear, J. 1988. *Dynamics of Fluids in Porous Media*. New York, New York: Dover Publications. TIC: 217568.

Beyer, W. H., ed 1987. *CRC Standard Mathematical Tables*. 28th Edition. 674. Boca Raton, Florida: CRC Press. TIC: 240507.

Birkholzer, J.T. and Tsang, Y.W. 1998. *Numerical Analysis of Thermal-Hydrological Conditions in the Single Heater Test at Yucca Mountain*. Technical Paper TPM# 826. Berkeley, California: Lawrence Berkeley National Laboratory. ACC: MOL.19980715.0257.

Brodsky, N.S.; Riggins M.; Connolly, J.; and Rici P. 1997. *Thermal Expansion, Thermal Conductivity, and Heat Capacity Measurements for Boreholes UE25 NRG-4, UE25 NRG-5, USW NRG-6, and USW NRG-7/7A*. SAND95-1955 Albuquerque, New Mexico.: Sandia National Laboratories. ACC: MOL.19980311.0316.

Case, J.B. and Kelsall, P.C. 1987. *Modification of Rock Mass Permeability in the Zone Surrounding a Shaft in Fractured, Welded Tuff*. SAND86-7001. Albuquerque, New Mexico: Sandia National Laboratories. ACC: HQS.19880517.2264.

CRWMS M&O (Civilian Radioactive Waste Management System Management and Operating Contractor) 1996. *Engineered Barrier System Performance Requirements Systems Study Report*. BB0000000-01717-5705-00001 REV 01. Las Vegas, Nevada: CRWMS M&O. ACC: MOL.19970407.0169.

CRWMS M&O 1997. *Determination of Available Volume for Repository Siting*. BCA000000-01717-0200-00007 REV 00. Las Vegas, Nevada: CRWMS M&O. ACC: MOL.19971009.0699.

CRWMS M&O 1998a. *Ex-Container System Description Document*. BCA000000-01717-1705-00019 REV 00. Two volumes. Las Vegas, Nevada: CRWMS M&O. ACC: MOL.19981211.0159.

CRWMS M&O 1998b. *Repository Subsurface Waste Emplacement and Thermal Management Strategy*. B00000000-01717-0200-00173 REV 00. Las Vegas, Nevada: CRWMS M&O. ACC: MOL.19980918.0084. (TBV-0389)

CRWMS M&O 1999a. *Development Plan for the Engineered Barrier System Water Distribution and Removal Model*. TDP-EBS-MD-000007 REV 01. Las Vegas, Nevada: CRWMS M&O. ACC: MOL.20000103.0348.

CRWMS M&O 1999b. *Engineered Barrier System Process Modeling for Process Model Report–Site Recommendation (WP#1201213EM1)*. Activity Evaluation, October 11, 1999. Las Vegas, Nevada: CRWMS M&O. ACC: MOL.19991012.0118.

CRWMS M&O 1999c. *Classification of the MGR Ex-Container System.* ANL-XCS-SE-000001 REV 00. Las Vegas, Nevada: CRWMS M&O. ACC: MOL.19990928.0221.

CRWMS M&O 1999d. *Drip Shield Design.* Input Transmittal EBS-WP-99292.T. Las Vegas, Nevada: CRWMS M&O. ACC: MOL.19991014.0107. (TBV-3796)

CRWMS M&O 1999e. *Enhanced Design Alternative (EDA) II Repository Estimated Waste Package Types and Quantities.* Input Transmittal EBS-SR-99325.T. Las Vegas, Nevada: CRWMS M&O. ACC: MOL.19991103.0236. (TBV-3685, TBV-3686, TBV-3695)

CRWMS M&O 2000a. *Drift Degradation Analysis.* ANL-EBS-MD-000027 REV 00. Las Vegas, Nevada: CRWMS M&O. ACC: MOL.20000107.0328.

CRWMS M&O 2000b. *Water Diversion Model.* ANL-EBS-MD-000028 REV 00. Las Vegas, Nevada: CRWMS M&O. ACC: MOL.20000107.0329.

CRWMS M&O 2000c. *Water Drainage Model.* ANL-EBS-MD-000029 REV 00. Las Vegas, Nevada: CRWMS M&O. ACC: MOL.20000117.0216.

CRWMS M&O 2000d. *In-Drift Thermal-Hydrological-Chemical Model.* ANL-EBS-MD-000026 REV 00. Las Vegas, Nevada: CRWMS M&O. ACC: MOL.20000113.0488.

CRWMS M&O 2000e. *Ventilation Model.* ANL-EBS-MD-000030 REV 00. Las Vegas, Nevada: CRWMS M&O. ACC: MOL.20000107.0330.

CRWMS M&O 2000f. *Calibrated Properties Model.* MDL-NBS-HS-000003 REV 00. Las Vegas, Nevada: CRWMS M&O. ACC: MOL.19990721.0520.

CRWMS M&O 2000g. *Unsaturated Zone Flow and Transport Model Process Model Report.* TDR-NBS-HS-000002 REV 00. Las Vegas, Nevada: CRWMS M&O. ACC: MOL.20000320.0400.

CRWMS M&O 2000h. *Multiscale Thermohydrologic Model.* ANL-EBS-MD-000049 REV 00. Las Vegas, Nevada: CRWMS M&O. ACC: MOL.20000609.0267.

DOE (U.S. Department of Energy) 2000. *Quality Assurance Requirements and Description.* DOE/RW-0333P, Rev. 10. Washington, D.C.: DOE, Office of Civilian Radioactive Waste Management. ACC: MOL.20000427.0422.

Fetter, C.W. 1993. *Contaminant Hydrogeology.* New York, New York: Macmillan Publishing. TIC: 240691.

Hardin, E.L. 1998. *Near-Field/Altered-Zone Models Report.* UCRL-ID-129179. Livermore, California: Lawrence Livermore National Laboratory. ACC: MOL.19980630.0560.

Isaaks, E.H. and Srivastava, R.M. 1989. *Applied Geostatistics.* New York, New York: Oxford University Press. TIC: 200301.

Jury, W.R.; Gardner, W.R.; and Gardner, W.H. 1991. *Soil Physics.* 5th Edition. New York, New York: John Wiley & Sons. TIC: 241000.

Kitanidis, P.K. 1997. *Introduction to Geostatistics: Applications in Hydrogeology.* New York, New York: Cambridge University Press. TIC: 236758.

Kwicklis, E.M. and Healy, R.W. 1993. "Numerical Investigation of Steady Liquid Water Flow in a Variably Saturated Fracture Network." *Water Resources Research, 29* (12), 4091-4102. Washington, D.C.: American Geophysical Union. TIC: 226993.

LLNL (Lawrence Livermore National Laboratory) 1999. *Software Code: NUFT V3.0s.* V3.0s. 10088-3.0s-00. (TBV-3828)

LLNL 1999. *Software Routine: CONVERTCOORDS V1.1.* V1.1. 10209-1.1-00.

LLNL 1999. *Software Routine: XTOOL V10.1.* V10.1. Sun SPARC, UNIX OS.

LLNL 1999. *Software Routine: YMESH V1.53.* V1.53. 10172-1.53-00.

Liu, H.H., Doughty, C. and Bodvarsson, G.S. 1998. "An Active Fracture Model for Unsaturated Flow and Transport in Fractured Rocks." *Water Resources Research, 34* (10), pp. 2633 – 2646. Washington, D. C.: American Geophyscial Union. TIC: 243012.

Neuman, S. P. 1994. "Generalized Scaling of Permeabilities: Validation and Effect of Support Scale." *Geophysical Research Letters, 21* (5), 349-352. Washington, D. C.: American Geophyscial Union. TIC: 240142.

Nitao, J.J. 1998. *Reference Manual for the NUFT Flow and Transport Code, Version 2.0.* UCRL-MA-130651. Livermore, California: Lawrence Livermore National Laboratory. TIC: 238072.

Philip, J.R.; Knight, J.H.; and Waechter, R. T. 1989. "Unsaturated Seepage and Subterranean Holes: Conspectus, and Exclusion Problem for Circular Cylindrical Cavities." *Water Resources Research, 25,* (1), pp. 16-28. Washington D.C.: American Geophysical Union. TIC: 239117.

Phillips, O. M. 1991. *Flow and Reactions in Permeable Rocks.* New York, New York: Cambridge University Press. TIC: 236237.

Sokolnikoff, I.S. and Redheffer, R.M. 1966. *Mathematics of Physics and Modern Engineering.* 2nd Edition. New York, New York: McGraw-Hill. TIC: 238682.

Wilkins, D.R. and Heath, C.A. 1999. "Direction to Transition to Enhanced Design Alternative II." Letter from D.R. Wilkins and C.A. Heath (CRWMS M&O) to Distribution, June 15, 1999, LV.NS.JLY.06/99-026, with enclosures, "Strategy for Baselining EDA II Requirements" and "Guidelines for Implementation of EDA II." ACC: MOL.19990622.0126; MOL.19990622.0127; MOL.19990622.0128.

YMP (Yucca Mountain Site Characterization Project) 2000. *Q-List.* YMP/90-55Q, Rev. 6. Las Vegas, Nevada: Yucca Mountain Site Characterization Office. ACC: MOL.20000510.0177.

8.2   CODES, STANDARDS, REGULATIONS, AND PROCEDURES

AP-2.13Q, Rev. 0, ICN 1. *Technical Product Development Planning.* Washington, D.C.: U.S. Department of Energy, Office of Civilian Waste Management. ACC: MOL.19991115.0230.

AP-3.10Q, Rev. 2, ICN 2. *Analyses and Models.* Washington, D.C.: U.S. Department of Energy, Office of Civilian Radioactive Waste Management. ACC: MOL.20000619.0576.

AP-3.15Q, Rev. 1, ICN 1. *Managing Technical Product Inputs.* Washington, D.C.: U.S. Department of Energy, Office of Civilian Radioactive Waste Management. ACC: MOL.20000218.0069.

AP-SI.1Q, Rev. 2, ICN 4. *Software Management.* Washington, D.C.: U.S. Department of Energy, Office of Civilian Radioactive Waste Management. ACC: MOL.20000223.0508.

AP-SIII.3Q, Revision 0, ICN 3. *Submittal and Incorporation of Data to the Technical Data Management System.* Washington, D.C.: U.S. Department of Energy, Office of Civilian Radioactive Waste Management. ACC: MOL.20000418.0808.

QAP-2-0, Revision 5, ICN 1. *Conduct of Activities.* Las Vegas, Nevada: CRWMS M&O. ACC: MOL.19991109.0221.

QAP-2-3, Revision 10. *Classification of Permanent Items.* Las Vegas, Nevada: CRWMS M&O. ACC: MOL.19990316.0006.

8.3   SOURCE DATA, LISTED BY DATA TRACKING NUMBER

LB990861233129.001. Drift Scale Calibrated 1-D Property Set, FY99. Submittal date: 08/06/1999.

LB99EBS1233129.001. Natural Environment Data for Engineered Barrier System (EBS) Basecase. Submittal date: 11/29/1999.

LB99EBS1233129.003. Natural Environment Data for Engineered Barrier System (EBS) Basecase. Submittal date: 11/29/1999.

MO9911MWDEBSWD.000. EBS Water Drainage Model. Submittal date: 11/29/1999.

SN9908T0872799.004. Tabulated In-Drift Geometric and Thermal Properties Used in Drift-Scale Models for TSPA-SR (Total System Performance Assessment – Site Recommendation). Submittal date: 08/30/99. (TBV-3471)

ATTACHMENT I

VERIFICATION OF SOFTWARE ROUTINE COVER V1.1

VERIFICATION OF SOFTWARE ROUTINE COVER V1.1

ROUTINE IDENTIFICATION

Cover Version 1.1. Initial issue of routine. This routine was developed using MatLAB. The source code for this routine is *cover.m* (Attachment VIII).

ROUTINE PURPOSE AND VALIDATION

The purpose of this routine is to develop a block model of the repository from information contained in *dft1.dat* (Attachment VIII), which is listed in Table I-2. The output of this routine contains the edges of the block model in the file *shape1.dat* (Attachment VIII) which is listed in Table I-1. The resulting repository block model is intended to have a similar area to the original layout. The block model is used to develop infiltration rates over the repository footprint.
Range of validation: this routine is limited to developing a block model from information in the file *shape1.dat* (Attachment VIII). Validation is achieved by verifying that the objective of the code (i.e., similar footprint area) was achieved. The area outlined in *dft1.dat* (Attachment VIII) is calculated and compared to the area contained in the block model (*shape1.dat*).

Table I-1. Area of Repository Block Model

Location ID	Easting	Northing	Equation I-1
A	171368.06	235822.06	4303909
B	170422.51	235872.29	-121804376
C	170343.91	234392.62	-125402076
D	170205.80	234399.95	-195258392
E	170083.53	232098.24	-196365687
F	170221.63	232090.90	-28610852
G	170204.16	231762.08	-32257943
H	171149.71	231711.85	347432200
A	171368.06	235822.06	352179357
		Total Area:	4216139

The exact area of a solid by coordinates is found by the following equation:

$$Area = \frac{1}{2} \cdot [x_1(y_2 - y_{(n)}) + x_2(y_3 - y_1) + \ldots + x_{(n)}(y_1 - y_{(n-1)})]$$

(Eq. I-1)

where:

Area -area enclosed by coordinates
x   -x coordinate
y   -y coordinate
n   -last point of figure
Source: (Hartman, H. L. 1992, p. A-37)

The routine is verified by finding the area of the repository using equation I-1 and visual inspection of the original and derived boundaries of the repository. The routine predicted an area of 4,216,139 ft^2 (see Table I-1), and the actual area is 4,310,041 ft^2 (see Table I-2). This is an error of less than three percent. This documents the accuracy of the output of this routine. The visual inspection result is presented in Figure I-1. As indicated in Figure I-1, the derived boundary closely follows the original boundary.
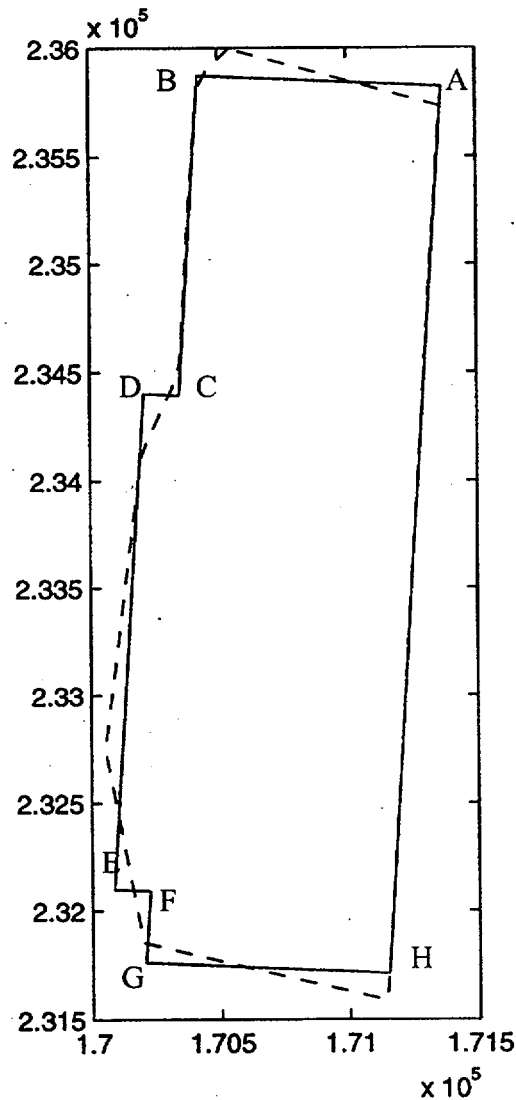
Note: The dotted line is from the drift endpoints in the file dft1.dat (Attachment VIII) and the solid line is from the file shape1.dat (Attachment VIII).

Figure I-1. Repository and Repository Block Model

Table I-2. Calculation of Actual Area of Repository (unit in ft^2)

East Boundary		West Boundary		Calculation Using Equation I-1	
Northing	Easting	Northing	Easting	East pts	West pts
235997.80	170544.61	235732.05	171362.51	19825811	26327279
235964.55	170515.90	235690.53	171359.24	-8505333	10680821
235898.04	170458.47	235607.39	171353.01	-12019879	14298552
235823.52	170425.70	235523.64	171348.62	-13295761	14349590
235742.01	170414.44	235439.90	171344.23	-14059191	14348366
235658.52	170409.28	235356.16	171339.84	-14227471	14347998
235575.03	170404.11	235272.42	171335.46	-14227039	14348488
235491.54	170398.95	235188.67	171331.07	-14226608	14348120
235408.05	170393.78	235104.93	171326.68	-14226177	14346896
235324.56	170388.62	235021.19	171322.29	-14225746	14346529
235241.07	170383.45	234937.45	171317.90	-14238945	14347018
235157.42	170378.77	234853.70	171313.51	-14259851	14346650
235073.68	170374.38	234769.96	171309.12	-14267151	14345426
234989.94	170369.99	234686.22	171304.73	-14267635	14345058
234906.19	170365.60	234602.48	171300.35	-14267267	14345548
234822.45	170361.21	234518.73	171295.96	-14266048	14345180
234738.71	170356.83	234434.99	171291.57	-14265681	14343956
234654.97	170352.44	234351.25	171287.18	-14266165	14343588
234571.22	170348.05	234267.51	171282.79	-14120150	14344077
234489.19	170338.41	234183.76	171278.40	-13495061	14343710
234412.77	170311.48	234100.02	171274.01	-12918977	14342486
234337.48	170281.06	234016.28	171269.62	-12819610	14342118
234262.20	170250.64	233932.54	171265.24	-12817319	14342608
234186.91	170220.23	233848.79	171260.85	-12985250	14342240
234109.63	170195.95	233765.05	171256.46	-13568021	14341016
234027.47	170186.69	233681.31	171252.07	-13998706	14340648
233945.12	170178.03	233597.57	171247.68	-14015012	14341137
233862.76	170169.37	233513.82	171243.29	-14014298	14340769
233780.41	170160.72	233430.08	171238.90	-14013586	14339545
233698.05	170152.06	233346.34	171234.51	-14013724	14339178
233615.69	170143.41	233262.60	171230.13	-14012161	14339667
233533.34	170134.75	233178.85	171225.74	-14011447	14339300
233450.98	170126.10	233095.11	171221.35	-14010735	14338076
233368.63	170117.44	233011.37	171216.96	-14010022	14337708
233286.27	170108.78	232927.63	171212.57	-14010159	14338197
233203.91	170100.13	232843.88	171208.18	-14008596	14337829
233121.56	170091.47	232760.14	171203.79	-14007883	14336605
233039.20	170082.82	232676.40	171199.40	-14007171	14336238
232956.85	170074.16	232592.66	171195.02	-14006457	14335871
232874.49	170065.50	232508.92	171190.63	-14006595	14336359
232792.13	170056.85	232425.17	171186.24	-14317086	14335992
232706.11	170059.48	232341.43	171181.85	-14949079	14334768
232616.32	170073.70	232257.69	171177.46	-15270918	14334401
232526.53	170087.93	232173.95	171173.07	-15272195	14334889
232436.74	170102.15	232090.20	171168.68	-15273472	14334521
232346.95	170116.37	232006.46	171164.29	-15274749	14333298
232257.16	170130.59	231922.72	171159.91	-15276026	14332931
232167.37	170144.81	231838.98	171155.52	-15277302	14333419
232077.58	170159.03	231755.23	171151.13	-15277729	14333051
231987.80	170173.25	231671.49	171146.74	-15279005	14331828
231898.01	170187.47	231587.75	171142.35	-11461275	10748595
231853.11	170194.58	231545.88	171140.16	-29965309	-22706876
			SUM:	-7.09E+08	713361262
				Total Area:	4310040.8

ATTACHMENT II

CALCULATION OF THE COORDINATES OF THE CHIMNEY LOCATIONS

CALCULATION OF THE COORDINATES OF THE CHIMNEY LOCATIONS

The repository block model developed in Attachment I, shape1.dat (see Figure I-1), is divided into 31 sections. The block model is composed of a rectangle with a smaller rectangle attached to the southern half of the west boundary of the repository. The 31 sections of the block model are derived by dividing the block model into 4 columns with seven rows, plus one additional column (3 rows) in the extension on the southwest side of the repository. The location for the center of each chimney is presented in Figure II-1. The process of calculating the coordinates for the 31 chimney locations is described in this Attachment.

The coordinates for the 31 chimney locations derived from the repository boundary corner points (shape1.dat) were calculated based on transformation of the coordinate system (See Figure II-1). The calculation was included in the *EXCEL 97* spreadsheet file *repository_shape V1.0.xls* (Attachment VIII). The five steps used in the calculation are described below.

Step1: calculate the coordinate of the origin (Point O in Figure II-1) for the transformed coordinate system (X'Y' in Figure II-1).

The coordinate of Point O (X_0, Y_0) was calculated as the intersection point of line GH and line DE. The coordinate of Point O was calculated as Easting of 170,066.1 and Northing of 231,769.4.

Step 2: calculate the angle α for the rotation of the coordinate system (see Figure II-1).

Angle α was calculated based on the coordinates of Point G (X_G, Y_G) and Point H (X_H, Y_H) using the equation:

$$\alpha = a\tan\left[\frac{(Y_H - Y_G)}{(X_H - X_G)}\right]$$

The angle was calculated as $-3.04°$.

Step 3: obtain the transformed coordinates for the repository boundary corner points based on the coordinate transformation equation.

The transformed coordinates for the repository boundary corner points were obtained based on the following equation:

$$\begin{bmatrix} x' \\ y' \end{bmatrix} = \begin{bmatrix} \cos\alpha & \sin\alpha \\ -\sin\alpha & \cos\alpha \end{bmatrix} \bullet \begin{bmatrix} x - x_0 \\ y - y_0 \end{bmatrix}$$

The transformed coordinates are tabulated in Table II-1.

Step 4: calculate the spacings between the chimney locations.

The spacings between the chimney location were calculated as follows:

$$S_{x'1} = L_{GH}/4$$

$$S_{x'2} = L_{OH}/5$$

$$S_{y'} = L_{HA}/7$$

where

$S_{x'1}$ is the spacing along X' axis for Rows 1, 2, 3 and 7 (L1, L2, L3, and L7, see Figure II-1).
$S_{x'2}$ is the spacing along X' axis for Rows 4, 5 and 6 (L4, L5, and L7, see Figure II-1).
$S_{y'}$ is the spacing along Y' axis for all Rows (L1 to L7, see Figure II-1).

Step 5: calculate the coordinates (in X'Y' coordinate system) for all the chimney locations.

The coordinates for all the chimney locations were calculated based on the spacings obtained in Step 4. The coordinates in X'Y' are presented in Table II-2.

Step 6: obtain the coordinates (in original coordinate system) for all the chimney locations based on the coordinate transformation equation.

The original coordinates for the chimney locations were transformed based on the following equation:

$$\begin{bmatrix} x \\ y \end{bmatrix} = \begin{bmatrix} \cos\alpha & -\sin\alpha \\ \sin\alpha & \cos\alpha \end{bmatrix} \bullet \begin{bmatrix} x' \\ y' \end{bmatrix} + \begin{bmatrix} x_0 \\ y_0 \end{bmatrix}$$

The calculated coordinates for all the chimney locations tabulated in Table II-3. The coordinates are included in an ASCII text file *column.data* (Attachment VIII).

Table II-1. Repository Boundary Corner Points Coordinates in X'Y' Coordinate System

Location ID	x'	y'
A	1085.2	4116.0
B	138.3	4116.0
C	138.3	2634.2
D	0.0	2634.2
E	0.0	329.3
F	138.3	329.3
G	138.3	0.0
H	1085.2	0.0

Table II-2. Coordinates of Chimney Locations in X'Y' Coordinate System

Chimney Location ID	x'	y'
I7c4	256.7	294.0
I7c3	493.4	294.0
I7c2	730.1	294.0
I7c1	966.8	294.0
I6c5	108.5	882.0
I6c4	325.6	882.0
I6c3	542.6	882.0
I6c2	759.6	882.0
I6c1	976.7	882.0
I5c5	108.5	1470.0
I5c4	325.6	1470.0
I5c3	542.6	1470.0
I5c2	759.6	1470.0
I5c1	976.7	1470.0
I4c5	108.5	2058.0
I4c4	325.6	2058.0
I4c3	542.6	2058.0
I4c2	759.6	2058.0
I4c1	976.7	2058.0
I3c4	256.7	2646.0
I3c3	493.4	2646.0
I3c2	730.1	2646.0
I3c1	966.8	2646.0
I2c4	256.7	3234.0
I2c3	493.4	3234.0
I2c2	730.1	3234.0
I2c1	966.8	3234.0
I1c4	256.7	3822.0
I1c3	493.4	3822.0
I1c2	730.1	3822.0
I1c1	966.8	3822.0

Table II-3. Coordinates of the Chimney Locations

Chimney Location ID	Easting	Northing
I7c4	170338.0	232049.4
I7c3	170574.3	232036.8
I7c2	170810.7	232024.3
I7c1	171047.1	232011.7
I6c5	170221.2	232644.4
I6c4	170437.9	232632.9
I6c3	170654.7	232621.4
I6c2	170871.4	232609.9
I6c1	171088.1	232598.4
I5c5	170252.4	233231.6
I5c4	170469.1	233220.1
I5c3	170685.9	233208.6
I5c2	170902.6	233197.1
I5c1	171119.3	233185.5
I4c5	170283.6	233818.8
I4c4	170500.3	233807.3
I4c3	170717.1	233795.7
I4c2	170933.8	233784.2
I4c1	171150.5	233772.7
I3c4	170462.7	234398.1
I3c3	170699.1	234385.5
I3c2	170935.5	234373.0
I3c1	171171.9	234360.4
I2c4	170493.9	234985.3
I2c3	170730.3	234972.7
I2c2	170966.7	234960.1
I2c1	171203.1	234947.6
I1c4	170525.1	235572.4
I1c3	170761.5	235559.9
I1c2	170997.9	235547.3
I1c1	171234.3	235534.8
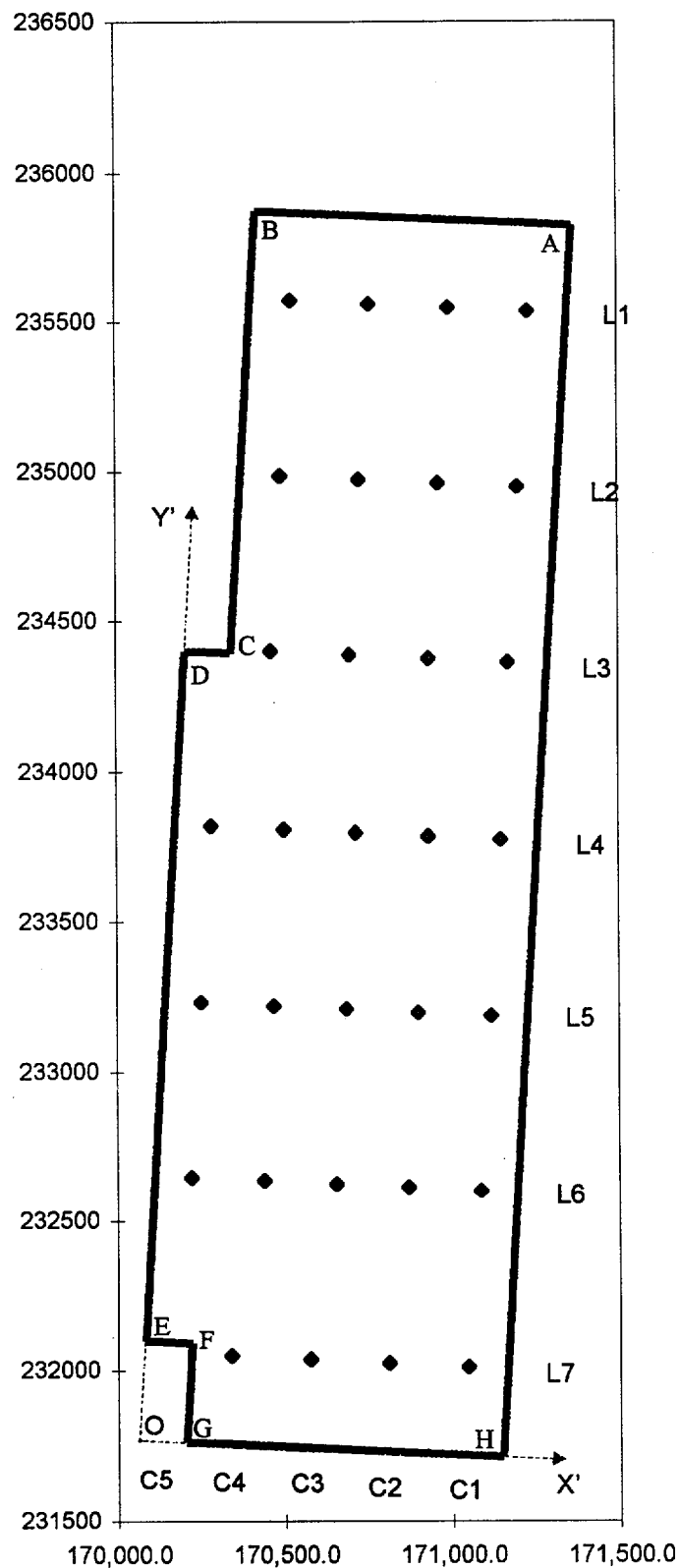
Figure II-1. Chimney Locations

ATTACHMENT III

VERIFICATION OF SOFTWARE ROUTINE CHIM_SURF_TP V1.1

VERIFICATION OF SOFTWARE ROUTINE CHIM_SURF_TP V1.1

ROUTINE IDENTIFICATION

Chim_Surf_TP V1.1, Initial issue of routine. The routine was developed and compiled using Fortran Version 77 SC4.2. The source code is *chim_surf_TP.f* (Attachment VIII).

ROUTINE PURPOSE AND VALIDATION

The purpose of this routine is to calculate the temperature and pressure at a given location using the inverse distance cubed method (Isaaks and Srivastava 1989, p. 258). The specific input files used for this calculation are: *tspa99_primary_mesh*, which is a renaming of *UZ99_3_3D.mesh* (see Figure 1), *bcs_99.dat*, and *column.data* (Attachment VIII). The inverse distance cubed function is:

$$V = \frac{\sum_{i=1}^{n} V_i \cdot \frac{1}{d_i^3}}{\sum_{i=1}^{n} \frac{1}{d_i^3}}$$

(Eq. III-1)

where:

V	-Value of interest at a given point
V_i	-Value at point i, d_i meters away
d_i	-Plan distance between points.
n	-Number of points in data set

Documentation of the accuracy of this routine is in the form of a test case. The test case is the interpolation of temperature at an arbitrary location (170000N, 230000E) given five temperatures at various locations. The hand calculation that verifies the accuracy of the test case is in Table III-1. Due to the reduction in file size and format minor changes were made to chim_surf_TP V1.1 in order to execute the test case. The modified source code (*chim_surf_bc_tst.f*) is in Attachment VIII and is used to execute the test case for *chim_surf_TP.f*. The input file for the test case is *chim_test* and the output file is *chim_out* (Attachment VIII).

Table III-1. Calculation of Temperature Using Inverse Distance Method

Northing	Easting	1/(distance^3)	Temperature	T_i / (distance^3)
169398.601	236623.643	3.39908E-12	14.27	4.85048E-11
172705.438	230904.031	4.30854E-11	18.62	8.0225E-10
168909.656	233244.625	2.49348E-11	17.00	4.23892E-10
171465.906	237975.359	1.87545E-12	16.89	3.16763E-11
172320.452	237217.733	2.29468E-12	17.53	4.02258E-11
	1/d^3 Sum:	7.55894E-11	T_i/d^3 Sum:	1.34655E-09
Estimated Temperature (T_i/d^3 Sum / 1/d^3 Sum):				17.8140

Note: The Northings and Eastings were randomly selected from *UZ99_3_3D.mesh* (Attachment VIII).
 The Temperatures were randomly selected from *bcs_99.dat* (Attachment VIII).
 The distance is between each point and the reference location.

The test case was run and the predicted temperature is 17.8140 °C (Attachment VIII, file *chim_out*). This documents the accuracy of this routine for predicting temperature and pressure at given points.

ATTACHMENT IV

VERIFICATION OF SOFTWARE ROUTINE COLUMNINFILTRATION V1.1

VERIFICATION OF SOFTWARE ROUTINE COLUMNINFILTRATION V1.1

ROUTINE IDENTIFICATION

ColumnInfiltration V1.1. Initial issue of routine. This routine was developed and compiled using C. The source code for this routine is *columninfiltration.c* (Attachment VIII).

ROUTINE PURPOSE AND VALIDATION

The purpose of this routine is to calculate the infiltration at a given location using Gaussian interpolation method (Isaaks and Srivastava 1989, p. 208 Kitanidis 1997, p. 54). The specific files used for this calculation are: *Glaciall.NV, Glacialm.NV, Glacialu.NV, Monsoonl.NV, Monsoonm.NV, Monsoonu.NV, Yml.NV, Ymm.NV, Ymu.NV,* and *column.data* (Attachment VIII). The Gaussian weighting function is:

$$I = \sum_{i=1}^{n} I_i \cdot W_i \qquad \text{(Eq. IV-1)}$$

where

$$W = e^{-\left[\left(\frac{D}{Scale}\right)^2\right]} \qquad \text{(Eq. IV-2)}$$

where
I	= Interpolated infiltration
I_i	= Value at point i, d meters away
D_i	= Plan distance between points.
n	= Number of points in data set
W	= Calculated weight assigned to each value (W=Wi)
Scale	= Effective radius of influence (Scale = 20ft).

Documentation of the accuracy of this routine is in the form of a test case. The test case involves the interpolation of the infiltration rate at an arbitrary reference location (242000N, 168000E) given infiltration rates at five various points. The input files for the test case are *columninfiltration_tst.NV* and *columninfiltration_tst.dat* (Attachment VIII). The output file from this test case is *columninfiltration_tst.out* (Attachment VIII). The hand calculation that verifies the accuracy of the test case is in Table IV-1.

Table IV-1. Calculation of Infiltration Using the Gaussian Method

Northing	Easting	Weight	Infiltration	W$_i$ * Infiltraiton$_i$
168192.021	242645.935	1.300E-79	1.94718	2.532E-79
168222.029	242645.830	9.530E-82	1.23309	1.17517E-81
168252.037	242645.725	3.399E-84	0.00	0
168282.045	242645.621	5.899E-87	0.45	2.67267E-87
168312.053	242645.516	4.981E-90	0.54	2.68959E-90
	Weight Sum:	1.30968E-79	W * Infiltration Sum:	2.54331E-79
Estimated Temperature (W * Infiltration Sum / Weight Sum):				1.941933

Note: The Northings, Eastings, and infiltration rates were selected from *Glaciall.NV* (Attachment VIII).
The weight is found using Equation IV-2.

The test case was run and the predicted infiltration rate is 1.941933 (Attachment VIII-*columninfiltration_tst.out*). This documents the accuracy of this routine for predicting infiltration rates at given points.

ATTACHMENT V

VERIFICATION OF SOFTWARE ROUTINE RME6 V1.1

VERIFICATION OF SOFTWARE ROUTINE RME6 V1.1

ROUTINE IDENTIFICATION

rme6 V1.1. Initial issue of routine. This routine was developed and compiled using C. The source code for this routine is *rme6.c* (Attachment VIII).

ROUTINE PURPOSE AND VALIDATION

The purpose of this routine is to reformat and combine the files *tspa99_primary_mesh* and *UZ99_3.grd* (Attachment VIII) to a format that is readable to YMESH V 1.53. As shown in Figure 1, *tspa99_primary_mesh* is a renaming of *UZ99_3_3D.mesh*. The output of this routine is the file *LBL99-YMESH* (Attachment VIII). This routine is verified by visually inspecting the file *LBL99-YMESH* file. The upper block of *LBL99-YMESH* is essentially the same as the mesh file *tspa99_primary_mesh* with the format modified. The lower block of *LBL99-YMESH* is the repetition of the vertices file *UZ99_3.grd* with modified format.

ATTACHMENT VI

CALCULATION OF THE NORMALIZED INFILTRATION RATES

CALCULATION OF THE NORMALIZED INFILTRATION RATES

The calculated infiltration rate in the modeled repository is different from the average infiltration rate in the actual repository. To offset this difference, the infiltration rates at the 31 locations are normalized (Table VI-1). The normalized infiltration rate is the product of the estimated infiltration rate and a normalization factor. The normalization factor is the quotient of the average normalized infiltration and the actual infiltration. The average normalized infiltration is the average of the estimated infiltration at the 31 block element locations (Attachment VIII, *.out). The average actual infiltration is included in the output from ConvertCoords V1.1 (files: *Glaciall_convert*, *Glacialm_convert*, *Glacialu_convert*, *Monsoonl_convert*, *Monsoonm_convert*, *Monsoonu_convert*, *Yml_convert*, *Ymm_convert*, and *Ymu_convert*).

Table VI-1. Interpolated and Normalized Infiltration Rates

	Interpolated									Normalized								
	Glacial			Monsoon			YM			Glacial			Monsoon			YM		
	Low	Mean	Hi	Low	Mean	Hi	Low	Mean	Hi	Low	Mean	Hi	Low	Mean	Hi	Low	Mean	Hi
I7c4	0.278	3.684	7.090	1.025	2.256	3.487	0.000	1.025	2.559	0.392	5.211	10.031	1.493	3.252	5.014	0.000	1.493	3.608
I7c3	1.511	13.020	24.530	3.212	7.432	11.651	0.006	3.212	7.559	2.131	18.418	34.705	4.677	10.710	16.751	0.010	4.677	10.657
I7c2	1.731	15.849	29.967	3.814	9.524	15.235	0.057	3.814	8.961	2.442	22.420	42.398	5.554	13.726	21.904	0.101	5.554	12.632
I7c1	0.848	4.958	9.067	1.168	3.184	5.200	0.030	1.168	3.839	1.196	7.013	12.829	1.700	4.588	7.476	0.053	1.700	5.413
I6c5	7.645	21.725	35.804	6.462	12.314	18.165	3.594	6.462	13.185	10.785	30.732	50.657	9.410	17.746	26.117	6.423	9.410	18.588
I6c4	1.476	33.842	66.208	7.761	22.656	37.551	0.000	7.761	19.471	2.082	47.872	93.674	11.302	32.651	53.989	0.000	11.302	27.449
I6c3	2.623	11.716	20.810	2.870	7.149	11.427	0.088	2.870	6.790	3.700	16.574	29.442	4.180	10.303	16.429	0.158	4.180	9.572
I6c2	1.824	7.766	13.708	2.161	4.970	7.780	0.333	2.161	4.950	2.573	10.986	19.395	3.147	7.163	11.186	0.596	3.147	6.978
I6c1	1.617	10.660	19.702	2.663	6.545	10.426	0.043	2.663	6.385	2.281	15.079	27.875	3.879	9.432	14.990	0.076	3.879	9.001
I5c5	6.474	21.117	35.760	5.787	11.980	18.172	1.947	5.787	12.368	9.134	29.872	50.594	8.428	17.265	26.127	3.479	8.428	17.436
I5c4	2.157	42.583	83.009	9.896	28.430	46.963	0.000	9.896	24.717	3.043	60.237	117.44	14.412	40.972	67.522	0.000	14.412	34.845
I5c3	4.065	14.103	24.140	3.900	9.104	14.308	0.690	3.900	8.635	5.735	19.949	34.154	5.680	13.120	20.571	1.233	5.680	12.173
I5c2	3.604	19.155	34.706	5.078	12.287	19.495	0.451	5.078	11.730	5.085	27.097	49.103	7.395	17.707	28.029	0.807	7.395	16.537
I5c1	0.084	0.577	1.071	0.455	0.303	0.150	0.000	0.455	1.302	0.118	0.816	1.515	0.663	0.436	0.216	0.000	0.663	1.835
I4c5	2.536	14.289	26.043	3.742	10.042	16.342	0.471	3.742	8.728	3.577	20.214	36.847	5.449	14.472	23.496	0.842	5.449	12.305
I4c4	1.412	29.690	57.967	6.957	20.036	33.115	0.000	6.957	17.227	1.992	41.998	82.014	10.132	28.876	47.611	0.000	10.132	24.286
I4c3	3.915	27.330	50.745	6.966	16.716	26.467	0.029	6.966	16.737	5.523	38.660	71.795	10.144	24.091	38.053	0.052	10.144	23.595
I4c2	1.910	19.740	37.570	4.744	11.727	18.710	0.001	4.744	11.278	2.694	27.923	53.155	6.909	16.900	26.900	0.003	6.909	15.899
I4c1	2.349	13.348	24.346	3.292	8.391	13.491	0.098	3.292	7.791	3.314	18.881	34.446	4.794	12.093	19.396	0.176	4.794	10.983
I3c4	3.505	45.970	88.435	10.902	30.526	50.151	0.000	10.902	26.916	4.944	65.028	125.12	15.877	43.993	72.104	0.000	15.877	37.945
I3c3	0.636	2.965	5.293	0.895	1.830	2.765	0.059	0.895	2.106	0.897	4.194	7.489	1.304	2.637	3.975	0.105	1.304	2.969
I3c2	0.163	0.899	1.634	0.333	0.341	0.350	0.006	0.333	0.836	0.230	1.271	2.312	0.485	0.492	0.503	0.012	0.485	1.179
I3c1	1.269	19.091	36.912	4.350	13.093	21.837	0.085	4.350	11.005	1.791	27.005	52.224	6.335	18.869	31.395	0.151	6.335	15.514
I2c4	6.417	41.445	76.473	10.985	29.341	47.696	1.105	10.985	25.800	9.052	58.627	108.19	15.998	42.285	68.574	1.974	15.998	36.372
I2c3	2.955	44.655	86.354	8.247	28.275	48.303	0.380	8.247	25.791	4.169	63.168	122.17	12.011	40.749	69.448	0.680	12.011	36.359
I2c2	0.054	16.541	33.029	0.973	6.352	11.731	0.000	0.973	6.517	0.076	23.399	46.730	1.416	9.154	16.866	0.001	1.416	9.188
I2c1	0.092	0.518	0.944	0.278	0.174	0.069	0.000	0.278	0.692	0.130	0.733	1.336	0.406	0.250	0.099	0.000	0.406	0.975
I1c4	0.174	13.472	26.770	2.071	8.032	13.993	0.001	2.071	7.583	0.245	19.057	37.875	3.015	11.575	20.119	0.002	3.015	10.690
I1c3	1.702	22.932	44.162	5.363	15.164	24.965	0.130	5.363	13.144	2.400	32.439	62.482	7.809	21.854	35.894	0.232	7.809	18.530
I1c2	0.390	1.506	2.622	0.602	0.652	0.703	0.119	0.602	1.419	0.550	2.130	3.709	0.877	0.940	1.010	0.212	0.877	2.001
I1c1	0.189	9.560	18.931	0.394	6.941	13.489	0.027	0.394	4.094	0.266	13.523	26.784	0.574	10.004	19.393	0.047	0.574	5.772
Avg Int.	2.116	17.571	33.026	4.108	11.154	18.200	0.315	4.108	10.326	2.985	24.856	46.726	5.982	16.074	26.166	0.562	5.982	14.558
Actual Avg	2.985	24.856	46.726	5.982	16.074	26.166	0.562	5.982	14.558	2.985	24.856	46.726	5.982	16.074	26.166	0.562	5.982	14.558

(Normalized value)=(Interpolated value * Actual avg/Avg of interpolated values)
Avg. Int. = Average of Interpolated values, or the average of each column.
Actual Avg = actual average of infiltration values that occur within the repository footprint. This value is included in the output files from *ConvertCoords V1.1*.

ATTACHMENT VII

CALCULATION OF THE LINEAR HEAT LOADING

CALCULATION OF THE LINEAR HEAT LOADING

The initial linear heat load for various type of spent nuclear fuel are calculated and listed in Table VII-1. An average initial linear heat load of 1.547 kW/m was calculated based on the total heat output and the total drift length. Thermal decay data listed in Table 10 of Section 4 were used to calculate the decay for all CSNF waste packages as presented in Table VII-2. The total heat of all CSNF WPs (7th column in Table VII-2) was calculated based on the individual spent fuel heat load and the number of WPs for each spent fuel as listed in Table VII-1. The linear heat load estimated for various times up to 100,000 years were calculated based on the initial linear heat load (1.547 kW/m) and the thermal decay percentage. The calculated linear heat loads for all packages are tabulated in Table VII-2.

Table VII-1. Estimate of Linear Heat Load along Emplacement Drift

Waste Package Type		Number of WPs	Fraction of Total	Length (m)	Heat Output Rate (KW)	Drift Length Required (meters)	Total Heat Output (kW)	Linear Heat Load (kW/m)
		Sec. 4.1.7.1		Sec. 4.1.7.1	Sec. 4.1.7.2	see Note 1	see Note 2	
21-PWR	Absorber	4279	0.429	5.305	11.3337	23128.00	48496.90	2.10
21-PWR	Control Rods	87	0.009	5.305	2.3709	470.24	206.27	0.44
12-PWR	Long	158	0.016	5.791	9.5402	930.78	1507.35	1.62
44-BWR	Absorber	2889	0.29	5.275	7.1346	15528.38	20611.86	1.33
24-BWR	Thick Plates	6	0.001	5.245	0.4910	32.07	2.95	0.09
5-DHLW		1249	0.125	3.73	4.0580	4783.67	5068.44	1.06
5-DHLW	Long	414	0.042	5.357	5.8280	2259.20	2412.79	1.07
Naval	Combined	285	0.029	5.888	7.1346 (see Note 2)	1706.58	2033.36	1.19
DOE/Other		598	0.06	5.57	0.7930	3390.66	474.21	0.14
Total		9965	1			52229.56	80814.14	
Average				5.141				1.5473

Note1: Total drift length required for a given type of WPs is determined using:
Total drift length = (Number of WPs)*(WP length + 0.1 m), where 0.1 m is the gap
between WPs (see Section 4.1.1, Table 5).

Note 2: Heat output for Naval packages is not available. Value listed was based on consideration
that the Naval package have the similar initial heat output of the 44-BWR packages
This consideration was documented in CRWMS M&O 1998b, Section 4.3.11.

Table VII-2. Decay of Linear Heat Load

Time (years)	21-PWR Absorber Plates	21-PWR Control Rods	12-PWR Long	44-BWR Absorber Plates	24-BWR Thick Absorber Plates	Total Heat of All CSNF WP (kW)	Percentage Decay of All CSNF WP (%)	All WP Linear Heat Load (kW/m)
	kW	kW	kW	kW	kW			
	(Sec 4.1.7.3)	(Sec 4.1.7.3)	(Sec 4.1.7.3)	(Sec 4.1.7.3)	(Sec 4.1.7.3)			
0.01	11.3337	2.3709	9.5402	7.1346	0.491	70825.33	100.00%	1.5473
0.5	11.1602	2.3495	9.4034	7.0215	0.487	69732.68	98.46%	1.5234
1	10.9954	2.3285	9.2722	6.9146	0.4829	68696.08	96.99%	1.5008
5	9.9653	2.1785	8.4286	6.2682	0.4445	62274.26	87.93%	1.3605
10	8.9956	2.0095	7.5901	5.6536	0.403	56201.90	79.35%	1.2278
15	8.1887	1.8547	6.8815	5.1467	0.3689	51159.11	72.23%	1.1176
20	7.5138	1.7241	6.3149	4.7102	0.3341	46909.07	66.23%	1.0248
25	6.9115	1.6038	5.8009	4.3098	0.3065	43083.23	60.83%	0.9412
26	6.8050	1.5819	5.7089	4.2419	0.3013	42414.93	59.89%	0.9266
30	6.3792	1.4942	5.3407	3.9701	0.2806	39741.73	56.11%	0.8682
35	5.9165	1.398	4.9411	3.6661	0.2578	36811.93	51.98%	0.8042
40	5.4984	1.3106	4.5868	3.3915	0.2369	34165.86	48.24%	0.7464
45	5.1192	1.2333	4.2517	3.1491	0.2182	31783.18	44.88%	0.6944
50	4.7912	1.1649	3.9792	2.9326	0.2033	29705.11	41.94%	0.6490
55	4.4921	1.1015	3.7277	2.7368	0.1889	27814.25	39.27%	0.6076
60	4.2229	1.0443	3.5026	2.5621	0.1754	26117.01	36.88%	0.5706
65	3.9776	0.9931	3.29	2.4046	0.1637	24574.24	34.70%	0.5369
70	3.7685	0.9479	3.1031	2.2625	0.1536	23235.45	32.81%	0.5076
75	3.5654	0.907	2.9482	2.1366	0.1445	21974.58	31.03%	0.4801
80	3.3915	0.8698	2.7908	2.0227	0.1361	20873.24	29.47%	0.4560
85	3.2288	0.8371	2.6476	1.9184	0.1289	19850.21	28.03%	0.4337
90	3.0866	0.807	2.5304	1.8264	0.1222	18954.78	26.76%	0.4141
95	2.949	0.7797	2.4047	1.7428	0.1164	18102.20	25.56%	0.3955
100	2.8314	0.7545	2.3024	1.6685	0.1111	17365.94	24.52%	0.3794
125	2.4552	0.6764	1.9895	1.4331	0.0955	15019.79	21.21%	0.3281
150	2.079	0.5983	1.6766	1.1977	0.0799	12673.63	17.89%	0.2769
200	1.7291	0.5244	1.3818	0.9878	0.0684	10516.93	14.85%	0.2298
250	1.5128	0.4796	1.2029	0.8725	0.0622	9226.08	13.03%	0.2016
300	1.3654	0.4452	1.0804	0.7889	0.0583	8331.46	11.76%	0.1820
400	1.1571	0.395	0.9118	0.6679	0.0528	7059.54	9.97%	0.1542
500	1.0046	0.3492	0.7901	0.5821	0.0485	6135.88	8.66%	0.1340
600	0.8839	0.3167	0.6928	0.5188	0.0449	5418.31	7.65%	0.1184
700	0.7888	0.2873	0.618	0.4629	0.0415	4835.48	6.83%	0.1056
800	0.7071	0.2629	0.5533	0.4202	0.0386	4350.16	6.14%	0.0950
900	0.6367	0.2415	0.4962	0.3832	0.0367	3931.13	5.55%	0.0859
1000	0.5804	0.2245	0.4538	0.3538	0.0346	3597.10	5.08%	0.0786
1500	0.3969	0.1653	0.3077	0.2477	0.0283	2477.11	3.50%	0.0541
2000	0.3093	0.1363	0.2395	0.1984	0.0247	1946.52	2.75%	0.0425
3000	0.2402	0.1134	0.182	0.1593	0.0221	1526.79	2.16%	0.0334
4000	0.2167	0.1042	0.1664	0.1421	0.0206	1373.27	1.94%	0.0300
5000	0.1995	0.0977	0.1529	0.1307	0.0194	1264.03	1.78%	0.0276
6000	0.1867	0.0916	0.1428	0.1214	0.0185	1180.26	1.67%	0.0258
7000	0.1728	0.0869	0.1315	0.1131	0.018	1094.60	1.55%	0.0239
8000	0.1619	0.0823	0.1236	0.106	0.017	1025.80	1.45%	0.0224
9000	0.1523	0.0781	0.1162	0.099	0.0158	962.95	1.36%	0.0210
10000	0.1432	0.0739	0.1088	0.0924	0.0154	903.41	1.28%	0.0197

Table VII-2. Decay of Linear Heat Load (continued)

Time (years)	21-PWR Absorber Plates	21-PWR Control Rods	12-PWR Long	44-BWR Absorber Plates	24-BWR Thick Absorber Plates	Total Heat of All CSNF WP (kW)	Percentage Decay of All CSNF WP (%)	All WP Linear Heat Load (kW/m)
	kW	kW	kW	kW	kW			
	(Sec 4.1.7.3)	(Sec 4.1.7.3)	(Sec 4.1.7.3)	(Sec 4.1.7.3)	(Sec 4.1.7.3)			
15000	0.1075	0.0582	0.0816	0.0686	0.0125	676.21	0.95%	0.0148
20000	0.084	0.0468	0.0635	0.0532	0.0103	527.30	0.74%	0.0115
25000	0.0674	0.0393	0.0506	0.0431	0.0089	424.39	0.60%	0.0093
30000	0.0554	0.0323	0.0416	0.0343	0.0077	345.58	0.49%	0.0075
35000	0.0466	0.0279	0.0352	0.0286	0.0067	290.06	0.41%	0.0063
40000	0.0399	0.0239	0.0299	0.0246	0.0058	248.64	0.35%	0.0054
45000	0.0349	0.0208	0.0263	0.0211	0.005	216.29	0.31%	0.0047
50000	0.0307	0.0183	0.023	0.0185	0.0046	190.07	0.27%	0.0042
55000	0.0267	0.0162	0.0202	0.0163	0.0041	165.97	0.23%	0.0036
60000	0.0242	0.0141	0.0185	0.0145	0.0036	149.61	0.21%	0.0033
65000	0.0212	0.0126	0.016	0.0128	0.0031	131.34	0.19%	0.0029
70000	0.0191	0.0111	0.0146	0.0119	0.0029	119.40	0.17%	0.0026
75000	0.0174	0.0101	0.0133	0.0106	0.0026	108.07	0.15%	0.0024
80000	0.0158	0.009	0.0121	0.0097	0.0024	98.34	0.14%	0.0021
85000	0.0145	0.0082	0.0112	0.0088	0.0022	89.96	0.13%	0.0020
90000	0.0134	0.0076	0.0103	0.0084	0.0019	83.91	0.12%	0.0018
95000	0.0126	0.0067	0.0096	0.0075	0.0019	77.69	0.11%	0.0017
100000	0.0118	0.0063	0.009	0.007	0.0019	72.70	0.10%	0.0016

ATTACHMENT VIII

COMPUTER FILES

COMPUTER FILES

This attachment provides a list of computer files for the water distribution and removal model. The files listed in Table VIII-1 are contained on the CD included with this attachment.

Table VIII-1. List of Computer Files

File Name	Directory	Brief description
Glaciall.inf	Source Data	Infiltration Input File for Glacial Lower Bound
Glacialm.inf		Infiltration Input File for Glacial Mean
Glacialu.inf		Infiltration Input File for Glacial Upper Bound
Monsoonl.inf		Infiltration Input File for Monsoon Lower Bound
Monsoonm.inf		Infiltration Input File for Monsoon Mean
Monsoonu.inf		Infiltration Input File for Monsoon Upper Bound
yml.inf		Infiltration Input File for Current Day Lower Bound
ymm.inf		Infiltration Input File for Current Day Mean
ymu.inf		Infiltration Input File for Current Day Upper Bound
bcs_99.dat		Pressure and Temperature Boundary Condition Files
Dft1.dat		Repository Drifts End Points Coordinates
UZ99_3_3D.mesh		UZ Model mesh File
UZ99_3.grd		UZ Model Grid File
Glaciall.NV	Intermediate Data Files	Converted Infiltration Data File for Glacial Lower Bound
Glacialm.NV		Converted Infiltration Data File for Glacial Mean
Glacialu.NV		Converted Infiltration Data File for Glacial Upper Bound
Monsoonl.NV		Converted Infiltration Data File for Monsoon Lower Bound
Monsoonm.NV		Converted Infiltration Data File for Monsoon Mean
Monsoonu.NV		Converted Infiltration Data File for Monsoon Upper Bound
yml.NV		Converted Infiltration Data File for Current Day Lower Bound
ymm.NV		Converted Infiltration Data File for Current Day Mean
ymu.NV		Converted Infiltration Data File for Current Day Upper Bound
Glaciall.out		Interpolated Infiltration at Chimneys for Glacial Lower Bound
Glacialm.out		Interpolated Infiltration at Chimneys for Glacial Mean
Glacialu.out		Interpolated Infiltration at Chimneys for Glacial Upper Bound
Monsoonl.out		Interpolated Infiltration at Chimneys for Monsoon Lower Bound
Monsoonm.out		Interpolated Infiltration at Chimneys for Monsoon Mean
Monsoonu.out		Interpolated Infiltration at Chimneys for Monsoon Upper Bound
yml.out		Interpolated Infiltration at Chimneys for Current Day Lower Bound
ymm.out		Interpolated Infiltration at Chimneys for Current Day Mean
ymu.out		Interpolated Infiltration at Chimneys for Current Day Upper Bound
Glaciall_convert		Actual Average Infiltration for Glacial Lower Bound
Glacialm_convert		Actual Average Infiltration for Glacial Mean
Glacialu_convert		Actual Average Infiltration for Glacial Upper Bound
Monsoonl_convert		Actual Average Infiltration for Monsoon Lower Bound
Monsoonm_convert		Actual Average Infiltration for Monsoon Mean
Monsoonu_convert		Actual Average Infiltration for Monsoon Upper Bound
yml_convert		Actual Average Infiltration for Current Day Lower Bound
ymm_convert		Actual Average Infiltration for Current Day Mean
ymu_convert		Actual Average Infiltration for Current Day Upper Bound
outpt		Pressure and Temperature at Ground Surface

Table VIII-1. List of Computer Files (Continued)

File Name	Directory	Brief description
outpt_wt	Intermediate Data Files	Pressure and Temperature at Water Table
shape1.dat		Block Model Corner Points Coordinates
Column.data		Coordinates for the 31 Chimney Locations
L4c4.dat		Coordinate for the L4C4 Chimney
LBL99-YMESH		Combined Files from UZ99_3.grd and UZ99_3_3D.mesh
L4c4.col.units		Stratigraphic Column for the L4C4 Chimney
repository_shape V1.0.xls		Calculation of the Coordinates of the Chimney Locations
Cover.m	Software Routine Source Codes and Verification Files	Source Code for Cover V1.1
Chim_Surf_TP.f		Source Code for Chim_Surf_TP V1.1
ColumnInfiltration.c		Source Code for ColumnInfiltration V1.1
rme6.c		Source Code for Rme6 V1.1
Chim_Surf_bc_tst.f		Modified Source Code for Chim_Surf_TP V1.1 for Verification
Chim_test		Verfication Input File for Chim_Surf_TP V1.1
Chim_out		Verfication output File for Chim_Surf_TP V1.1
columnInfiltration_tst.dat		Verfication Input File for ColumnInfiltration V1.1
columnInfiltration_tst.NV		Verfication Input File for ColumnInfiltration V1.1
columnInfiltration_tst.out		Verfication output File for ColumnInfiltration V1.1
1.in	NUFT Inputs	Input File for Case 1
2.in		Input File for Case 2
3wpmod.in		Input File for Case 3
4wpmod.in		Input File for Case 4
5.in		Input File for Case 5
6.in		Input File for Case 6
7.in		Input File for Case 7
8.in		Input File for Case 8
9.in		Input File for Case 9
9.1.in		Input File for Case 10
19.in		Input File for Case 11
20.in		Input File for Case 12
27.in		Input File for Case 13
dkm-afc-NBS-WDR		Material Properties File for the NBS
dkm-afc-NBS-Rev10-WDR		Material Properties File for the EBS
vtough.pkg		NUFT Accepted Data File
1.f.EBS.ext	NUFT Outputs	Fracture Output File for Case 1
1.m.EBS.ext		Matrix Output File for Case 1
2.f.EBS.ext		Fracture Output File for Case 2
2.m.EBS.ext		Matrix Output File for Case 2
3wpmod.f.EBS.ext		Fracture Output File for Case 3
3wpmod.m.EBS.ext		Matrix Output File for Case 3
4wpmod.f.EBS.ext		Fracture Output File for Case 4
4wpmod.m.EBS.ext		Matrix Output File for Case 4
5.f.ext		Fracture Output File for Case 5
5.m.ext		Matrix Output File for Case 5
6.f.ext		Fracture Output File for Case 6
6.m.ext		Matrix Output File for Case 6
7.f.ext		Fracture Output File for Case 7
7.m.ext		Matrix Output File for Case 7
8.f.ext		Fracture Output File for Case 8
8.m.ext		Matrix Output File for Case 8
9.f.ext		Fracture Output File for Case 9
9.m.ext		Matrix Output File for Case 9
9.1.f.ext		Fracture Output File for Case 10

Table VIII-1. List of Computer Files (Continued)

File Name	Directory	Brief description
9.1.m.ext	NUFT Outputs (Continued)	Matrix Output File for Case 10
19.f.EBS.ext		Fracture Output File for Case 11
19.m.EBS.ext		Matrix Output File for Case 11
20.f		Fracture Output File for Case 12
20.m		Matrix Output File for Case 12
27.f		Fracture Output File for Case 13
27.m		Matrix Output File for Case 13
Case1_Flux V1.0.mcd	Processed Outputs	Flow rate through the invert for Case 1
Case2_Flux V1.0.mcd		Flow rate through the invert for Case 2
Case3_Flux V1.0.mcd		Flow rate through the invert for Case 3
Case4_Flux V1.0.mcd		Flow rate through the invert for Case 4
Cases899.1_Flux V1.0.mcd		Flow rate through the invert for Cases 8, 9, and 10
Invert Fluxes Case 19 V1.0.mcd		Flow rate through the invert for Case 11
Invert Fluxes Case 20 V1.0.mcd		Flow rate through the invert for Case 12
Invert Fluxes Case 27 V1.0.mcd		Flow rate through the invert for Case 13
Case1 V1.0.mcd		Travel time through the invert for Case 1
Case2 V1.0.mcd		Travel time through the invert for Case 2
Case3 V1.0.mcd		Travel time through the invert for Case 3
Case4 V1.0.mcd		Travel time through the invert for Case 4
Case9 V1.0.mcd		Travel time through the invert for Case 9
Case9.1 V1.0.mcd		Travel time through the invert for Case 10
Case19 V1.0.mcd		Travel time through the invert for Case 11
Case20 V1.0.mcd		Travel time through the invert for Case 12
Case27 V1.0.mcd		Travel time through the invert for Case 13
Summary of travel time calculation V1.0.xls		Average pore water velocity through the invert for various cases

ATTACHMENT IX

COMPARISON OF NUFT FLUX RATES WITH A CLOSED FORM SOLUTION FOR FLOW NEAR A CYLINDRICAL INCLUSION

COMPARISON OF NUFT FLUX RATES WITH A CLOSED FORM SOLUTION FOR FLOW NEAR A CYLINDRICAL INCLUSION

IX.1 PURPOSE

The results of the NUFT calculations can be compared with a closed form solution for a single backfill. In this calculation, a closed form solution for the focusing effect of the backfilled drift is used. The calculation uses potential or field theory and is based upon a cylindrical geometry, and follows the example presented by Phillips (1991, pp. 67-69) for flow and reactions in permeable rocks.

The following calculation compares the results of two analyses. These analyses include the (1) closed form calculation based upon a cylindrical inclusion and a (2) two dimensional NUFT analysis for the base case (Section 6.3.1) based upon the active fracture concept for the water distribution and removal model. The following presents the calculation method used for the closed form solution, constitutive properties for the backfill, and surrounding rock media, the flux distribution across the repository drift horizon, and a comparison with the NUFT calculations.

IX.2 CALCULATION METHOD FOR THE CLOSED FORM SOLUTION

In this calculation, a closed form solution for the focusing effect of the backfilled drift is used. The calculation uses potential or field theory (Assumption 5.13) and is based upon a cylindrical geometry. The calculation follows the example presented by (Phillips 1991, pp. 67-69) for flow and reactions in permeable rocks.

IX.2.1 Closed Form Solution and Boundary Conditions

From Phillips (1991, pp. 67-69), a solution is presented for a spherical inclusion in a uniform flow field. A solution is developed below for a cylindrical geometry that corresponds to a backfilled tunnel. The solution presented satisfies the steady state flow Laplace equation presented by Phillips (1991, Equation 3.8.1, pp. 67 and 50). Consider the solution for a cylindrical geometry. The Laplace Operator for a cylindrical geometry for steady state flow (Sokolnikoff and Redheffer 1966, p. 417) is given by:

$$\text{del}^2 (u) = \frac{1}{r} \cdot \frac{d}{dr}\left(r \cdot \frac{d}{dr}u\right) + \frac{1}{r^2} \cdot \frac{d^2}{d\theta^2}u + \frac{d^2}{dz^2}u$$

$$(IX-1)$$

where

u = Field function,
r = Radius,
θ = Angle, and
z = Vertical coordinate.

Note that $\text{del}^2 = \nabla^2$

From Phillips (1991, p. 50), Laplace's Equation is satisfied for steady state flow:

$$\text{del}^2 (u) = 0$$

(IX-2)

Writing the Laplace Equation for two dimensional flow and noting that u is equivalent to pressure (u=p) for flow in a porous media:

$$\text{del}^2 (p) = \frac{1}{r}\cdot\frac{d}{dr}\left(r\cdot\frac{d}{dr}p\right) + \frac{1}{r^2}\cdot\frac{d^2}{d\theta^2}p + \frac{d^2}{dz^2}p$$

(IX-3)

Noting that for a two dimensional problem flow equals zero in the z direction,

$$\frac{d^2}{dz^2}p = 0$$

(IX-4)

$$\frac{d^2}{dr^2}p + \frac{1}{r}\cdot\frac{d}{dr}p + \frac{1}{r^2}\cdot\frac{d^2}{d\theta^2}p = 0$$

(IX-5)

The above equation is subject to the same conditions as the spherical inclusion (Phillips 1991, p. 68):

$$p_o = p_i \qquad r=a$$

(IX-6)

$$k_i\cdot\frac{d}{dr}p_i = k_o\cdot\frac{d}{dr}p_o \qquad r=a$$

(IX-7)

p_o approaches $-\omega x$ or $-\omega r\cos(\theta)$ as r approaches infinity

(IX-8)

where

p = Pressure,

r = Radius,

θ = Angle,

p_i = Internal pressure,

p_o = External pressure,

k_i = Permeability of the inclusion,

k_o = Permeability of the surrounding media,

ω = Field variable for a uniform flow field, and

x = Coordinate in the direction of the flow field.

In Bear (1988, p. 270) a definition for a well posed problem is provided. These include:

(a) The flow domain is defined at large distances from the inclusion with flow in the vertical direction,
(b) The flow problem can be stated mathematically by means of a dependent variable which in the present case is the pressure p,
(c) A partial differential equation can be specified for the dependent variable p, and
(d) The pressure p can be defined at infinity.

As Bear (1988, p. 271) states that for a well posed problem a solution exists that is unique and that continuously depends on the data. Therefore, if a solution is found that satisfies partial differential equation (Equation IX-5) subject to the boundary conditions (Equation IX-6) through (Equation IX-8), the solution is unique to the problem. The solution presented by Phillip (1991, p. 68) is expressible in spherical harmonics with two directions of curvature. Expressing a solution with one direction of curvature, p_i and p_o are obtained:

$$p_i = -\omega \cdot \frac{2 \cdot k_o}{k_i + k_o} \cdot r \cdot \cos(\theta) \quad r \leq a$$

(IX-9)

$$p_o = -\omega \cdot \left[1 - \frac{\left(k_i - k_o \right)}{k_i + k_o} \cdot \frac{a^2}{r^2} \right] \cdot r \cdot \cos(\theta) \quad r \geq a$$

(IX-10)

IX.2.2 Pressure Boundary Condition at the Radius of the Inclusion

Check the pressure boundary condition at r = a. The pressure p_i from (IX-9) is given by:

$$p_i = -\omega \cdot \frac{2 \cdot k_o}{k_i + k_o} \cdot a \cdot \cos(\theta)$$

(IX-11)

The pressure boundary condition from (IX-10) is given by:

$$p_o = -\omega \cdot \left[1 - \frac{(k_i - k_o)}{k_i + k_o} \cdot \frac{a^2}{a^2} \right] \cdot a \cdot \cos(\theta)$$

(IX-12)

which, after simplifying becomes:

$$p_o = -2 \cdot \omega \cdot \frac{k_o}{(k_i + k_o)} \cdot a \cdot \cos(\theta)$$

(IX-13)

The pressure at the boundary of the emplacement drift is satisfied ($p_o = p_i$) from the two relations (IX-11) and (IX-13).

IX.2.3 Gradient Boundary Condition at the Radius of the Inclusion

Check the gradient boundary condition at r = a. Considering the interior of the room, applying Darcy's Law to the left side of the expression from Equation (IX-7):

$$k_i \cdot \frac{d}{dr} p_i$$

(IX-14)

Substitute the expression on the right side of Equation IX-9 into Equation IX-14 yields:

$$k_i \cdot \left[\frac{d}{dr} \left(-\omega \cdot \frac{2 \cdot k_o}{k_i + k_o} \cdot r \cdot \cos(\theta) \right) \right]$$

(IX-15)

Taking the derivative to Equation IX-15 with respect to r and obtaining:

$$-2 \cdot k_i \cdot \omega \cdot \frac{k_o}{\left(k_i + k_o\right)} \cdot \cos(\theta)$$

(IX-16)

Apply the Darcy's Law for the exterior, and substitute in the expression on the right side of Equation IX-10 in similar fashion:

$$k_o \cdot \frac{d}{dr}\left[-\omega \cdot \left[1 - \frac{\left(k_i - k_o\right)}{k_i + k_o} \cdot \frac{a^2}{r^2}\right] \cdot r \cdot \cos(\theta)\right]$$

(IX-17)

Taking the derivative to Equation IX-17 with respect to r and obtaining:

$$k_o \cdot \left[-2 \cdot \omega \cdot \frac{\left(k_i - k_o\right)}{k_i + k_o} \cdot \frac{a^2}{r^2} \cdot \cos(\theta) - \omega \cdot \left[1 - \frac{\left(k_i - k_o\right)}{k_i + k_o} \cdot \frac{a^2}{r^2}\right] \cdot \cos(\theta)\right]$$

(IX-18)

Simplify the expression and substitute r = a at the boundary:

$$k_o \cdot \left[\omega \cdot \cos(\theta) \cdot \frac{\left(-a^2 \cdot k_i + a^2 \cdot k_o - r^2 \cdot k_i - r^2 \cdot k_o\right)}{\left[\left(k_i + k_o\right) \cdot r^2\right]}\right]$$

(IX-19)

Simplifying yields the expression:

$$-2 \cdot k_i \cdot \omega \cdot \frac{k_o}{\left(k_i + k_o\right)} \cdot \cos(\theta)$$

(IX-20)

The flux boundary condition in Equation IX-20 agrees with gradient boundary condition in Equation IX-16.

IX.2.4 Solution to the Partial Differential Equation Within the Drift

Check the solution to the partial differential equation inside the emplacement drift. Substituting the right side of Equation IX-9 into left side of Equation IX-5 yields the expression:

$$\frac{d^2}{dr^2}\left(-\omega\cdot\frac{2\cdot k_o}{k_i+k_o}\cdot r\cdot\cos(\theta)\right) + \left[\frac{1}{r}\cdot\frac{d}{dr}\left(-\omega\cdot\frac{2\cdot k_o}{k_i+k_o}\cdot r\cdot\cos(\theta)\right) + \frac{1}{r^2}\cdot\frac{d^2}{d\theta^2}\left(-\omega\cdot\frac{2\cdot k_o}{k_i+k_o}\cdot r\cdot\cos(\theta)\right)\right]$$

<div align="right">(IX-21)</div>

Evaluate the first term in the above expression by differentiating with respect to r twice:

$$\frac{d^2}{dr^2}\left(-\omega\cdot\frac{2\cdot k_o}{k_i+k_o}\cdot r\cdot\cos(\theta)\right) = 0$$

<div align="right">(IX-22)</div>

Evaluate the second term in Equation IX-21 by differentiating with respect to r once:

$$\frac{1}{r}\cdot\frac{d}{dr}\left(-\omega\cdot\frac{2\cdot k_o}{k_i+k_o}\cdot r\cdot\cos(\theta)\right) = \frac{-2}{r}\cdot\omega\cdot\frac{k_o}{\left(k_i+k_o\right)}\cdot\cos(\theta)$$

<div align="right">(IX-23)</div>

Evaluate the third term in Equation IX-21 by differentiating with respect to θ twice

$$\frac{1}{r^2}\cdot\frac{d^2}{d\theta^2}\left(-\omega\cdot\frac{2\cdot k_o}{k_i+k_o}\cdot r\cdot\cos(\theta)\right) = \frac{2}{r}\cdot\omega\cdot\frac{k_o}{\left(k_i+k_o\right)}\cdot\cos(\theta)$$

<div align="right">(IX-24)</div>

Zero is obtained by adding the right-hand side of Equations IX-22 through IX-24:

$$0 + \frac{-2}{r}\cdot\omega\cdot\frac{k_o}{\left(k_i+k_o\right)}\cdot\cos(\theta) + \frac{2}{r}\cdot\omega\cdot\frac{k_o}{\left(k_i+k_o\right)}\cdot\cos(\theta) = 0$$

<div align="right">(IX-25)</div>

The solution for pressure inside the drift satisfies the Partial Differential Equation (PDE) (Equation IX-5).

IX.2.5 Solution to the Partial Differential Equation Outside the Drift

Check the solution to the PDE outside the inclusion. Substituting the right hand side of Equation IX-10 into Equation IX-5, the following expression is obtained:

$$
\frac{d^2}{dr^2}\left[-\omega\cdot\left[1-\frac{k_i-k_o}{k_i+k_o}\cdot\frac{a^2}{r^2}\right]\cdot r\cdot\cos(\theta)\right] + \frac{1}{r}\cdot\left[\frac{d}{dr}\left[-\omega\cdot\left[1-\frac{k_i-k_o}{k_i+k_o}\cdot\frac{a^2}{r^2}\right]\cdot r\cdot\cos(\theta)\right]\right] \dots
$$

$$
+\frac{1}{r^2}\cdot\frac{d^2}{d\theta^2}\left[-\omega\cdot\left[1-\frac{k_i-k_o}{k_i+k_o}\cdot\frac{a^2}{r^2}\right]\cdot r\cdot\cos(\theta)\right]
$$

(IX-26)

Note that the symbol ". . ." signifies continuation of the expression on the next line.

Evaluate the first term in Equation IX-26 by differentiating the expression with respect to r twice:

$$
\frac{d^2}{dr^2}\left[-\omega\cdot\left[1-\frac{k_i-k_o}{k_i+k_o}\cdot\frac{a^2}{r^2}\right]\cdot r\cdot\cos(\theta)\right] = 2\cdot\omega\cdot\frac{k_i-k_o}{k_i+k_o}\cdot\frac{a^2}{r^3}\cdot\cos(\theta)
$$

(IX-27)

Evaluate the second term in Equation IX-26 by differentiating the expression with respect to r once:

$$
\frac{1}{r}\cdot\left[\frac{d}{dr}\left[-\omega\cdot\left[1-\frac{k_i-k_o}{k_i+k_o}\cdot\frac{a^2}{r^2}\right]\cdot r\cdot\cos(\theta)\right]\right] = \frac{-1}{r^3}\cdot\omega\cdot\cos(\theta)\cdot\frac{\left[a^2\cdot\left(k_i-k_o\right)+r^2\cdot\left(k_i+k_o\right)\right]}{\left(k_i+k_o\right)}
$$

(IX-28)

The expression above simplifies to:

$$\frac{-1}{r^3} \cdot \omega \cdot \cos(\theta) \cdot a^2 \cdot \frac{\left(k_i - k_o\right)}{\left(k_i + k_o\right)} - \frac{1}{r} \cdot \omega \cdot \cos(\theta) \cdot (1)$$

<div align="right">(IX-29)</div>

Evaluate the third term in Equation IX-26 by differentiating the expression with respect to θ twice:

$$\frac{1}{r^2} \cdot \frac{d^2}{d\theta^2}\left[-\omega \cdot \left[1 - \frac{\left(k_i - k_o\right)}{k_i + k_o} \cdot \frac{a^2}{r^2} \right] \cdot r \cdot \cos(\theta) \right] = \frac{1}{r} \cdot \omega \cdot \left[1 - \frac{\left(k_i - k_o\right)}{k_i + k_o} \cdot \frac{a^2}{r^2} \right] \cdot \cos(\theta)$$

<div align="right">(IX-30)</div>

This expression simplifies to:

$$\frac{1}{r} \cdot (\omega \cdot \cos(\theta)) - \frac{\left(k_i - k_o\right)}{\left(k_i + k_o\right)} \cdot \frac{a^2}{r^3} \cdot \omega \cdot \cos(\theta)$$

<div align="right">(IX-31)</div>

Combining Equations IX-27, IX-29, and IX-31:

$$2 \cdot \omega \cdot \frac{\left(k_i - k_o\right)}{\left(k_i + k_o\right)} \cdot \frac{a^2}{r^3} \cdot \cos(\theta) + \left[\frac{-1}{r^3} \cdot \omega \cdot \cos(\theta) \cdot a^2 \cdot \frac{\left(k_i - k_o\right)}{\left(k_i + k_o\right)} - \frac{1}{r} \cdot \omega \cdot \cos(\theta) \cdot (1) \right] \ldots$$
$$+ \frac{1}{r} \cdot (\omega \cdot \cos(\theta)) - \frac{\left(k_i - k_o\right)}{\left(k_i + k_o\right)} \cdot \frac{a^2}{r^3} \cdot \omega \cdot \cos(\theta)$$

<div align="right">(IX-32)</div>

All the terms presented above cancel out, and the Laplace Equation (Equation IX-5) is satisfied. The solution (Equation IX-5) for the potential function outside the inclusion satisfies the PDE.

IX2.6 Development of the Focusing Ratio

Phillips (1991, p. 68) develops focusing ratio for a spherical inclusion from the solution of the problem for a spherical inclusion. The following discussion develops a focusing ratio for a cylindrical inclusion. Consider the solution for the internal pressure from Equation IX-9. Substituting $x = r\cos(\theta)$, and Equation IX-9 into Darcy's Law gives the expression:

$$k_o \cdot \frac{d}{dx}(\omega \cdot x)$$

(IX-33)

Take the derivative with respect to x and noting that $x = r\cos(\theta)$:

$$\frac{d}{dx}p_i = -\omega \cdot \frac{2 \cdot k_o}{k_i + k_o}$$

(IX-34)

The water flux in the emplacement drift is given by substituting the expression on the right hand side of Equation IX-34 into Equation IX-14:

$$k_i \left(\frac{d}{dx}p_i \right) = k_i \left(\frac{-\omega \cdot 2 \cdot k_o}{k_i + k_o} \right)$$

(IX-35)

Consider the solution for the farfield pressure in Equation IX-10:

$$p_o = -\omega \cdot \left[1 - \frac{(k_i - k_o)}{k_i + k_o} \cdot \frac{a^2}{r^2} \right] \cdot r \cdot \cos(\theta)$$

(IX-36)

Taking the derivative with respect to x for Equation IX-35:

$$k_o \cdot -\omega$$

(IX-37)

The ratio of the fluxes is then:

$$\frac{(k_i) \cdot \left(\dfrac{-\omega \cdot 2 \cdot k_o}{k_i + k_o} \right)}{(k_o \cdot -\omega)}$$

(IX-38)

Which simplifies to:

$$2 \cdot \frac{k_i}{k_i + k_o}$$

(IX-39)

This formula can be used to bound the flow through the backfill and the effects of percolation rate at the repository horizon. Figure IX-1 presents relationship for the focusing ratio for the cylindrical inclusion (Equation IX-39) as a function of the ratio of the conductivities (k_i/k_o). This solution is compared to the solution presented by Phillips (1991, p. 69) for a spherical inclusion. For low (k_i/k_o) ratios, the focusing ratio is small while for large ratios, the focusing ratio approaches three for the spherical case and two for the cylindrical case.

IX.3 CONSTITUTIVE PROPERTIES FOR THE BACKFILL AND SURROUNDING ROCK MEDIA

The moisture potential versus unsaturated hydraulic conductivity for the surrounding tuff is used to determine the moisture potential or moisture potential over the range of infiltration rates under the assumption that the percolation rate under steady state conditions equals the unsaturated hydraulic conductivity (Section 5.14). Steady state conditions are defined as the conditions in which the flow rate is constant or is not changing with time.
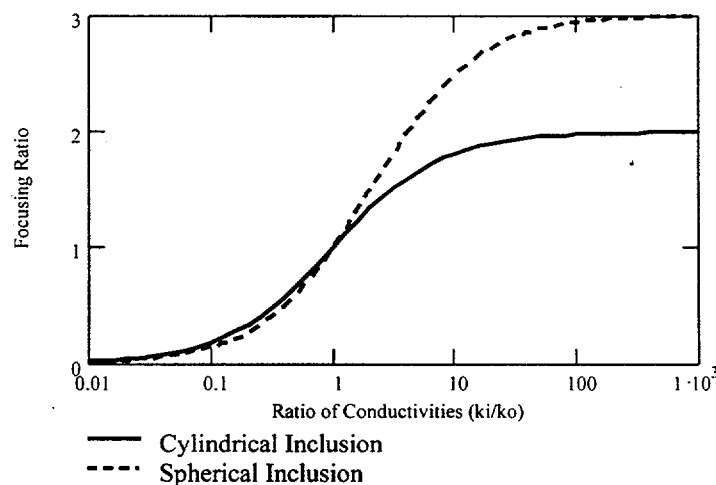

Figure XI-1. The Focusing Raio or Velocity Ratio for a Sphere of Permeability k_i in a Matrix of Permeability k_o

The van Genuchten constitutive relation given by Fetter (1993, p. 182) for the unsaturated hydraulic conductivity for the several media are presented in Figure IX-2. The van Genuchten constitutive relation for the unsaturated hydraulic conductivity at ambient temperature is given by:

$$K(\alpha,n,\psi,K_s) := K_s \cdot \frac{\left[1 - (|\alpha \cdot \psi|)^{(n-1)} \cdot \left[1 + (|\alpha \cdot \psi|)^n \right]^{\left(-1+\frac{1}{n}\right)} \right]^2}{\left[1 + (|\alpha \cdot \psi|)^n \right]^{\left[\frac{1}{2} - \frac{1}{(2 \cdot n)}\right]}}$$

(IX-40)

For the active fracture model at the repository horizon, the constitutive relation as a function of saturation S_e is given by Equation 6:

$$K_{af}(S_e,\gamma,m) := S_e^{\frac{(1+\gamma)}{2}} \cdot \left[1 - \left[1 - S_e^{\frac{(1-\gamma)}{m}} \right]^m \right]^2 \cdot K_f$$

(IX-41)

For the active fracture model, for the retention relationship for the active fracture model is given by Equation 5:

$$P_c(S_e,\alpha,\gamma,m) := \frac{1}{\alpha} \cdot \left[S_e^{\frac{(\gamma-1)}{m}} - 1 \right]^{\frac{1}{\frac{-1}{(m-1)}}}$$

(IX-42)

Equations IX-41 and IX-42 can be combined together resulting in the relationship of K_{af} as function of the capillary pressure.

For a deep water table in an isotropic medium, the seepage flux downwards establishes a moisture potential equilibrium level in which (Jury et al. 1991, p. 127):

$$J_w = -K(\theta)$$

(IX-43)

This can be expressed through the unsaturated hydraulic conductivity relationship (Equation IX-40):

$$J_w = -K(\psi)$$

(IX-44)

Equation IX-44 can be applied to estimate the moisture potential within the surrounding media. In the water distribution and removal model for the glacial climate for the column chimney L4C4, the estimated seepage flux (J_w) is 42 mm per year ($1.331 *10^{-6}$ kg/(m^2-sec) (Section 6.2.5). This estimated seepage rate corresponded to an unsaturated hydraulic conductivity of $1.3* 10^{-7}$ cm/s with the moisture potential of 42 cm (4100 Pa).

IX.4   FLUX DISTRIBUTION ACROSS THE REPOSITORY DRIFT HORIZON

The following analysis develops the flux distribution across the repository drift horizon for comparison to the NUFT calculations in Section IX.5. If Darcy's Law is applied to the closed form solution at the mid plane of the inclusion, expressions for the flow focusing can be derived in which the unsaturated hydraulic conductivities are estimated from Figure IX-2 for a particular percolation rate. Within the entry, the flux is uniform, and equals the value given by Equation IX-35. The following analysis develops the solution outside the inclusion (r>=a) through use of the closed form solution from Equation IX-9.

Equation IX-9 presents the solution in cylindrical coordinates. The following analysis develops the gradient in the x direction using a coordinate transformation from cylindrical coordinates to rectangular coordinates. The chain rule is invoked the flux distribution.

From the *CRC Standard Mathematical Tables* (Beyer 1987, p. 205), the coordinate transformation is given by

$$\theta = atan\left(\frac{y}{x}\right) \quad r = \sqrt{x^2 + y^2}$$

(IX-45)

Define a variable u for application of the chain rule:

$$u = \frac{y}{x}$$

(IX-46)

Take the derivative of u with respect to x:

$$\frac{d}{dx}u = \frac{-y}{x^2}$$

(IX-47)

Consider the inverse tangent function:
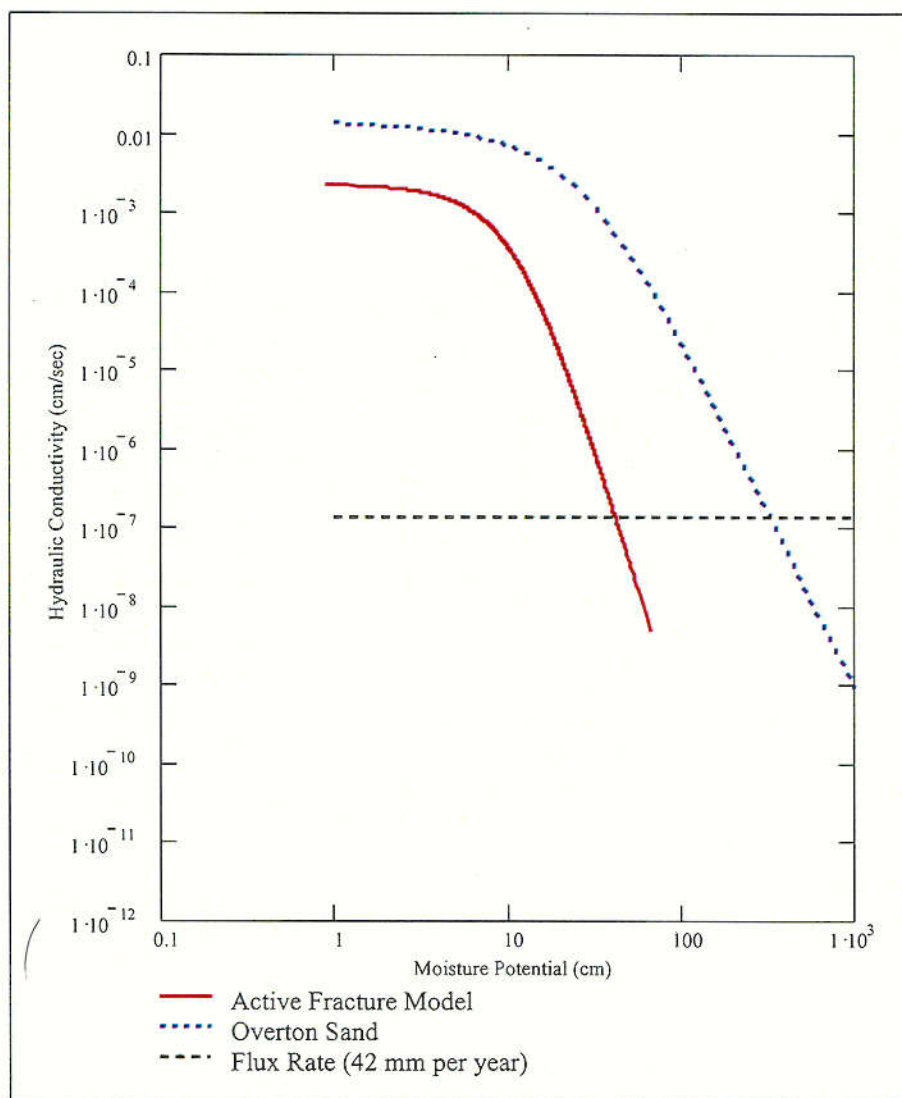
$$\theta = atan(u)$$

(IX-48)

Figure IX-2. Constitutive Properties for the Active Fracture Model, and the Overton Sand

C/7

From the *CRC Standard Mathematical Tables* (Beyer 1987, p. 231), the derivative is given by

$$\frac{d}{dx}\theta = \frac{1}{1+u^2} \cdot \frac{d}{dx}u$$

(IX-49)

Applying the chain rule, the following derivative is obtained:

$$\frac{d}{dx}\theta = \frac{-y}{\left(x^2+y^2\right)}$$

(IX-50)

Take the derivative with respect to the radius:

$$r = \sqrt{x^2+y^2}$$

(IX-51)

$$\frac{d}{dx}r = \frac{1}{\left(x^2+y^2\right)^{\left(\frac{1}{2}\right)}} \cdot x$$

(IX-52)

For the case inside the inclusion, the derivative is trivial from Equation IX-9:

$$\frac{d}{dx}p_i = -\omega \cdot \frac{2 \cdot k_o}{k_i + k_o} \cdot 1$$

(IX-53)

For the case outside the inclusion using the chain rule

$$\frac{d}{dx}p_o = -\omega \cdot \left[1 + \frac{(k_i - k_o)}{(k_i + k_o)} \cdot \frac{a^2}{r^2}\right] \cdot \frac{x}{\sqrt{x^2+y^2}} \cdot \cos(\theta) - \omega \cdot \left[r - \frac{(k_i - k_o)}{k_i + k_o} \cdot \frac{a^2}{r}\right] \cdot -\sin(\theta) \cdot \frac{-y}{\left(x^2+y^2\right)}$$

(IX-54)

Substitute the definitions for sin(θ) and cos (θ)

$$\frac{d}{dx}p_o = -\omega \cdot \left[1 + \frac{(k_i - k_o)}{(k_i + k_o)} \cdot \frac{a^2}{r^2}\right] \cdot \frac{x}{\sqrt{x^2+y^2}} \cdot \frac{x}{r} - \omega \cdot \left[r - \frac{(k_i - k_o)}{k_i + k_o} \cdot \frac{a^2}{r}\right] \cdot \frac{-y}{r} \cdot \frac{-y}{\left(x^2+y^2\right)}$$

(IX-55)

Simplifying the expression:

$$\frac{d}{dx}p_o = -\omega \cdot \left[1 + \frac{(k_i - k_o)}{(k_i + k_o)} \cdot \frac{a^2}{r^2} \right] \cdot \frac{x^2}{r^2} - \omega \cdot \left[1 - \frac{(k_i - k_o)}{k_i + k_o} \cdot \frac{a^2}{r^2} \right] \cdot \frac{y^2}{r^2}$$

(IX-56)

Noting that x = 0 along the drift centerline:

$$\frac{d}{dx}p_o = -\omega \cdot \left[1 - \frac{(k_i - k_o)}{k_i + k_o} \cdot \frac{a^2}{r^2} \right] \cdot \frac{y^2}{r^2}$$

(IX-57)

Applying Darcy's Law Inside the inclusion, the flux is

$$-\omega \cdot \frac{2 \cdot k_o}{k_i + k_o} \cdot k_i$$

(IX-58)

Applying Darcy's Law outside the inclusion along the y axis

$$k_o \cdot \left[\omega \cdot \left[1 - \frac{(k_i - k_o)}{k_i + k_o} \cdot \frac{a^2}{r^2} \right] \cdot \frac{y^2}{r^2} \right]$$

(IX-59)

IX.5 COMPARISON WITH NUFT CALCULATIONS

These expressions can be compared to the results of NUFT calculations from the water distribution and removal model for the Overton sand for the percolation rate of 42 mm per year. From Figure IX-2, the ratio of the unsaturated hydraulic conductivities of the Overton sand to the active fracture hydraulic conductivity is approximately a factor 3700. From Equation IX-53, the ratio of fluxes nearly equals the theoretical maximum ratio of 2. The flux distributions are compared in Figure IX-3. The calculations are in qualitative agreement in showing an increase in flux within the drift, and a decrease in flux rate outside the drift.

Note that within the drift, the drip shield acts to exclude water, which increases the flux in the drip lobe that forms adjacent to the drip shield. The maximum flux rate from the water distribution model is 145 mm per year (4.6 * 10^{-6} kg/(m^2-sec)). The peak flux rate from the simple ratio of the diameters of the drift diameter to the drip shield is approximately 200 mm per year (Figure 11).
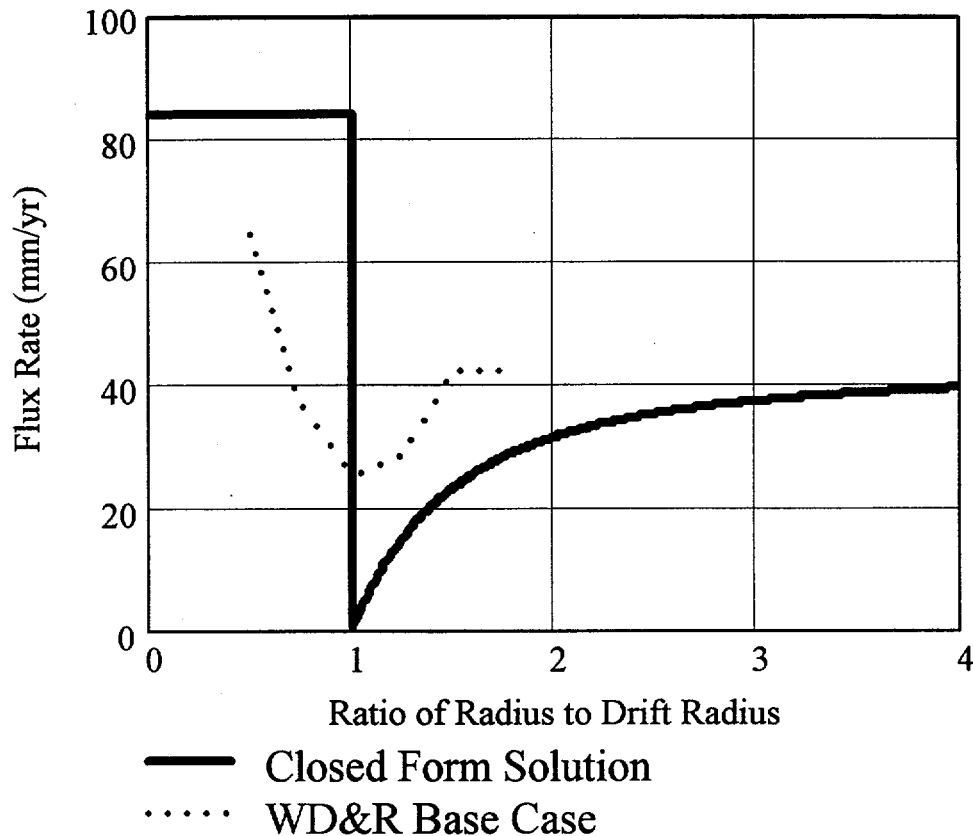
Figure IX-3. Comparison of the NUFT WD&R Model Calculations to the Closed Form Solution

IX.6   CONCLUSIONS

Comparisons were made between the NUFT calculations for the base case of the water distribution and removal model, and a closed form solution for steady state flow for a fine Overton sand backfill. The unsaturated hydraulic conductivity for the backfill was compared to the unsaturated hydraulic conductivity for the active fracture model. It was found that the Overton sand unsaturated hydraulic conductivity is a factor of 3700 higher than the surrounding host rock at a percolation rate of 42 mm per year. The water distribution and removal model predicts that the flux rate through the backfill will be higher than percolation rate through the host rock by some factor ranging from 1.5 to 5 affected by flow exclusion of the drip shield. These results are in general agreement with the results of hand calculations based upon a closed form solution for flow in and around a cylindrical inclusion.